Template Assisted Calcium Based Drug Carriers for Efficient Oral Delivery Applications

THESIS SUBMITTED TO

DELHI TECHNOLOGICAL UNIVERSITY

FOR THE AWARD OF THE DEGREE OF

DOCTOR OF PHILOSOPHY

SUBMITTED BY

MEENAKSHI GAUTAM

2K15/PhD/AC/01

UNDER THE GUIDANCE OF

DR. DEENAN SANTHIYA

DEPARTMENT OF APPLIED CHEMISTRY

DELHI TECHNOLOGICAL UNIVERSITY

SHAHBAD DAULATPUR, MAIN BAWANA ROAD,

DELHI 110042, INDIA

July 2020

Dedicated

to

My Family

Department of Applied Chemistry

Delhi Technological University

Shahbad-Daulatpur, Bawana Road

Delhi-110042, India

DECLARATION

This is to certify that the work presented in this thesis entitled **"Template Assisted Calcium Based Drug Carriers for Efficient Oral Delivery Applications"** is original and has been carried out by me for the degree of **Doctor of Philosophy** under the supervision of **Dr. Deenan Santhiya**, Assistant Professor, Department of Applied Chemistry. This thesis is a contribution of my original research work. Wherever research contributions of others are involved, every effort has been made to clearly indicate the same. To the best of my knowledge, this research work has not been submitted in part or full for the award of any degree or diploma of **Delhi Technological University** or any other university/Institution.

Meenakshi Gautam

(Candidate)

Department of Applied Chemistry
Delhi Technological University
Shahbad-Daulatpur, Bawana Road
Delhi-110042, India

CERTIFICATE

This is to certify that the Ph.D. thesis entitled **"Template Assisted Calcium Based Drug Carriers for Efficient Oral Delivery Applications"** submitted to the Delhi Technological University, Delhi-110042, India in fulfillment of the requirements for the award of the degree of **Doctor of Philosophy** has been carried out by the candidate **Meenakshi Gautam** under the supervision of **Dr. Deenan Santhiya,** Assistant Professor, Department of Applied Chemistry. It is further certified that the work embodied in this thesis has neither partially nor fully submitted to any other university or Institution for the award of any degree or diploma.

Dr. Deenan Santhiya
Assistant Professor
Department of Applied Chemistry
Delhi Technological University
Shahbad Daulatpur
Bawana, Delhi-110042
India

Prof. S. G. Warkar
Head of Department,
Department of Applied Chemistry
Delhi Technological University
Shahbad Daulatpur
Bawana, Delhi-110042
India

ACKNOWLEDGMENT

I would like to express my heartfelt gratitude to my supervisor **Dr. Deenan Santhiya,** Assistant Professor, Department of Applied Chemistry, Delhi Technological University, for her valuable discussion and advice. Who suggested me to the wonderful topic of my research area of drug delivery. Her unconditional support and invaluable guidance made it easy to cross every obstacle came across during my work. She provided me persistence, motivation, freedom and helped me to release my stress throughout my Ph.D. years. I would like to thank her for encouraging me and completing my work. She helped me to develop intellectual thoughts as well as conceptual ideas in me and always stood by my side. Her vision and perspectives are encouraging. She instructed me to discover things for myself at every stage of this journey that made me strong and confident. Without her advice, enthusiasm and insightful guidance, my Ph.D. work would never have been completed. It was a pleasant experience worked with her.

I am thankful to Prof. S.G. Warkar, Head of the Department, Delhi Technological university, for his providing the necessary help in my research work. Also, my gratitude extends to Prof. Archna Rani and for her support in my doctoral studies at Delhi Technological University.

I am also thankful to Prof. Yogesh Singh, the vice-chancellor, Delhi Technological University, for providing all the facilities and necessary help to carry out this investigation.

I would like to express my sincere thanks to Dr. Munia Ganguli for allowing me to perform cell culture studies at her lab in CSIR-IGIB, Delhi.

I thank all my lab mates, especially Mr. Himansh Goel, for his affection and time to time support in my research work. My sincere thanks goes to other supporting staff members of the Applied Chemistry Department for providing their appropriate assistance.

I would like to express my heartiest thanks to my loving husband, **Dr. Rajveer Singh**. Who morally supported and helped me to keep things under control. He has always been my motivation by guiding me in all my activities. My Ph.D. journey would have never been possible without his love, care and Patience. Thank you so much for standing by my side as a helping hand when time gets more laborious. I appreciate his contribution to my research work and affection showed during my Ph.D. journey.

Finally, I would like to special thanks all my friends and well-wisher who helped me directly or indirectly during my research work.

Meenakshi Gautam

Overview of thesis

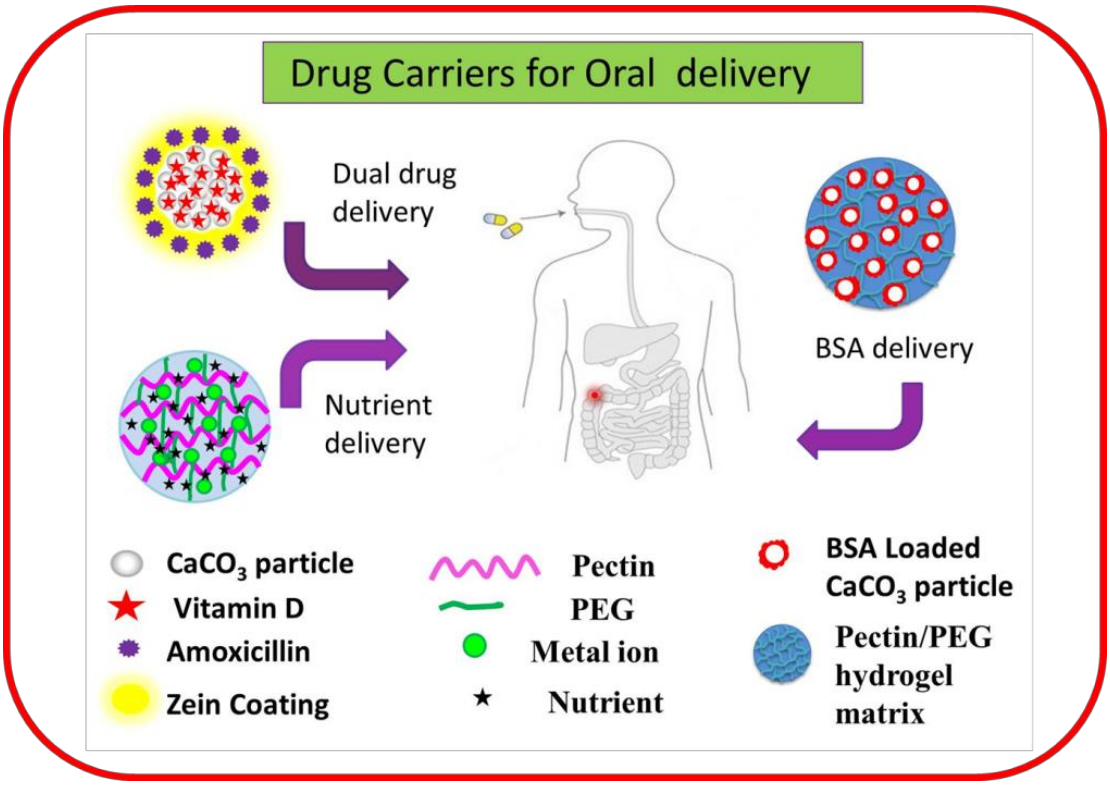

Abstract

Among the various routes of drug administration, oral administration is the most widely used and common delivery system associated with the gastrointestinal (GI) tract. It is easily accessible, self-administered and having high potential for the reduction of side effects of the drug dosages. It also provides several challenges for the researchers; for instance, variation in pH of the GI tract, to protect the drug from the harsh environment in the stomach, intestine motility and finally, mucus barrier. To overcome these obstacles, it is necessary to design a new strategy with the colon-specific delivery system. A colon is the ideal delivery site where a drug can be protected from the attack of numerous proteases.

$CaCO_3$ nanoparticles due to their properties such as biodegradability and biocompatibility have significant priority in the biomedical field. $CaCO_3$ nanoparticles are highly porous in nature and show high drug loading capacity owing to their high surface area to volume ratio. They can be easily synthesized and are cost-effective. Moreover, surface modification is easily possible with the $CaCO_3$ nanoparticles by which these nanoparticles have been considered as a great carrier in the targeted delivery of drug. $CaCO_3$ nanoparticles are naturally present in the human body and show stability in the biological matrix. They have pH dependent solubility, and nontoxic material approved by FDA.

Food grade oral delivery vehicles for the targeted delivery of nutrients are currently fabricated by adapting pharmaceutical approaches to promote human health. Food grade delivery systems contain nutritional value along with appreciable functionality.

These may be protein, carbohydrate and lipid-based systems. Food grade oral delivery systems have been reported as appropriate and safer vehicles as approved by the FDA. Moreover, these food grade approaches are used as a matrix for the synthesis of nanoparticles since they have ability to control the size of the nanoparticles and also enhance the functionality of the delivery system. They are cost-effective approaches to the prevention and treatment of various diseases.

Interestingly, pectin a naturally occurring edible polymer has been used as a drug carrier in the biomedical field. Pectin shows an excellent gelling property therefore used in the formation of hydrogel that can be used for oral delivery. Besides, pectin exhibited various properties such as pH sensitive, biodegradability, mucoadhesive. Hence, Pectin based drug carriers are considered as a colon specific delivery system as they exhibit prolonged retention and completely degraded by the bacteria present in the colon.

In this thesis, considering the huge consequences of $CaCO_3$ as well as pectin for targeted oral delivery, synthesis and characterization of $CaCO_3$ nanoparticles was focused. Subsequently, to avoid the aggregation of the nanoparticles, pectin based hydrogel was introduced and an attempt has been made for *in-situ* mineralized $CaCO_3$ particles in pectin based hydrogel matrix. This thesis has been summarized in five chapters.

Chapter 1 discusses a brief introduction of oral drug delivery, attributes of the colon specific drug vehicles, and $CaCO_3$ nanoparticles along with their biomedical applications. A brief introduction of edible hydrogel and the importance of pectin, zein and PEG polymer are also mentioned.

Chapter 2 provides the details of instruments used for the characterization of the material and their working principle are also discussed.

Chapter 3 involves the synthesis of $CaCO_3$ nanoparticles using gelatin as a template through a novel bio-inspired method for the sequential delivery of vitamin D and amoxicillin. The synthesized $CaCO_3$ nanoparticles were characterized using Transmission electron microscopy (TEM), X-ray diffraction (XRD), Fourier transform infrared spectroscopy (FTIR), Thermogravimetric analysis (TGA) and Brunauer-Emmett-Teller (BET). XRD and TEM confirmed nanocrystalline nature of $CaCO_3$ in size range of 10-15 nm. Further, $CaCO_3$ nanoparticles encapsulated with vitamin D, coated with zein and finally loaded with amoxicillin as a model drug. The release study of vitamin D and amoxicillin was performed in the simulated gastric fluid (SGF) (pH 1.2) and simulated intestinal fluid (SIF) (pH 6.8) and (pH 7.4) at 37 °C temperature. The encapsulation of hydrophobic vitamin D in $CaCO_3$ nanoparticles with an external zein coating approach enhances their controlled and sustained release property at the target site. The role of gelatin molecule in the synthesis of nano-sized $CaCO_3$ was demonstrated using CD spectroscopy. MTT assay was performed on zein coated $CaCO_3$ nanoparticles at varying concentrations on kidney (HEK) and liver (Hep G_2) cell lines after 24 hours exposure to ensure its biocompatibility.

In **chapter 4**, Ca^{2+} with vitamin D / Fe^{2+} with vitamin C were entrapped in edible pectin/PEG polymer blend matrix to obtain hydrogels namely PPCaD and PPFeC. Thermogravimetric analysis (TGA) and Fourier transform infrared spectroscopy (FTIR) analysis of pectin based hydrogels confirmed the existence of metal ion

content in the hydrogel matrix and their corresponding interaction with the pectin matrix through electrostatic and hydrogen bonding. Rheological measurements revealed a higher elastic nature of PPCaD compared to PPFeC and were in good agreement with the swelling studies. *In-vitro* release studies concluded that the lowest release of metal ion and vitamin from the corresponding hydrogel samples in simulated gastric fluid (SGF) was observed at pH 1.2 for 3 h. It indicated that protection of nutrients from the gastric environment was conferred by the hydrogels. The release studies carried out in the next 3 h in simulated intestinal fluid (SIF) at pH 6.8 indicated not only the highest swelling of the hydrogel samples but also the highest co-release of nutrients at the intestinal site.

In **Chapter 5** $CaCO_3$ microparticles were *in-situ* mineralized in pectin/poly(ethylene glycol) (PEG) hydrogel blend to protect and release protein drug at the colon site. Further, bovine serum albumin (BSA) as a model drug was loaded during the fabrication of pectin/PEG blend containing *in-situ* mineralized $CaCO_3$ particles. The interaction of loaded BSA with $CaCO_3$ by physical forces was evidenced by FTIR analysis. BSA could also be visualized around the mineralized $CaCO_3$ by TEM throughout the hydrogel matrix. Rheological studies on the oral delivery vehicle revealed dynamic nature of the hydrogel, an essential property required for drug carriers for its interaction with the target site. *In-vitro* swelling and protein release studies of pectin based hydrogel indicated the potentiality of the drug carrier in releasing protein at the colon site. The conformational stability of the released BSA from the hydrogel blend (PPCB) was confirmed by SDS-PAGE and CD spectropolarimetry.

Contents

List of Figures

CHAPTER 4 Pectin/PEG food grade hydrogel blend for the targeted oral co-delivery of nutrients

List of Tables

List of Abbreviations and Symbols

AMX	Amoxicillin
$CaCl_2$	Calcium chloride
$Ca(OH)_2$	Calcium hydroxide
$Ca(NO_3)_2$	Calcium nitrate
CC	Calcium carbonate
CCD	Vitamin D loaded calcium carbonate
CCDZ	Zein coated vitamin D loaded calcium carbonate
CCDZA	Zein coated vitamin D and amoxicillin loaded calcium carbonate
DNA	Deoxyribonucleic acid
FDA	Food and drug administration
GIT	Gastrointestinal tract
IUPAC	International Union of Pure and Applied Chemistry
JCPDS	Joint Committee on Powder Diffraction Standard
Na_2CO_3	Sodium carbonate
MTT	3-(4,5-Dimethylthiazol-2-yl)-2,5-diphenyltetrazolium bromide
PP	Pectin-Polyethylene glycol hydrogel blend
PPB	Pectin-Polyethylene glycol hydrogel blend

	containing BSA
PPC	*In situ* mineralization of calcium carbonate in Pectin-Polyethylene glycol
PPCB	BSA loaded *in-situ* mineralized calcium carbonate in Pectin-Polyethylene glycol hydrogel blend
PPCaD	Pectin-Polyethylene glycol hydrogel blend containing Ca^{2+} ions with vitamin D
PPFeC	Pectin-Polyethylene glycol hydrogel blend containing Fe^{2+} ions with vitamin C
RNA	Ribonucleic acid
SGF	Simulated gastric fluid
SIF	Simulated intestinal fluid
RF	Radio frequency
G′	Storage modulous
G″	Loss modulous
tan δ	Loss tangent
Pa	Pascal
θ	Diffraction angle
d	Inter-planar spacing
λ	X - ray wavelength
β	Full width and half maxima
kD	Kilo dalton

%	Percentage
wt.	Weight
mL	millilitre
M	Molar
mM	Millimolar
gm	Gram
mg	Milligram
***μ*g**	Microgram
K	Kelvin
MW	Molecular weight
KJ	Kilojoule
^{o}C	Degree celsius
min	Minutes
mA	Milliampere
Å	Angstrom
MHz	Megahertz
Hz	Hertz
emu	Electromagnetic unit
***μ*m**	Micrometre
nm	Nanometer
cm	Centimeter
cc	Cubic centimeter
mm	Millimeter

kV	Kilo Volts
eV	Electron-volt
h	Hour
Fe^{2+}	Iron (II) ion
Ca^{2+}	Calcium ion

Chapter 1

Introduction

1.1. Oral drug delivery

Oral administration is one of the most preferred wide-spread drug delivery routes because of its various advantages, which include patient acceptability due to its well-established convenient dosing as well as handling and compliance. Oral drug delivery has prolonged retention and a high possibility of drug absorption due to the increased surface area of the gastrointestinal (GI) tract.[1,2] GI tract comprises mouth, stomach, small intestine and large intestine, as shown in Fig. 1.1. The therapeutic efficacy of the drug is enhanced by the oral route since this non-invasive route avoids the pain of injections and the oral formulations are also cheaper to produce.[3,4,5] Despite the advantages, some challenges also have been seen in oral administration; for example, the pH range of the GI tract is acidic to basic. In detail, stomach lies at pH 1.0-2.0, small intestine between pH 6.0-7.4 and colon lies at pH 5.5-7.0.[6] Such variation in the pH of the stomach prevents drug absorption.

Further, mucus plays an important role in the GI tract that contains carbohydrates, proteins, lipids, some salts, bacteria and antibodies. Mucin is the major protein component of mucus, secreted throughout the GI tract. It provides the lubricating property and inhibits the interaction of epithelial cells with the ingested foreign particles. Thus, mucus creates a significant barrier for the nanoparticles and prevents drug penetration[7,8] and helps in determining the absorption and bioavailability of orally administered drugs.[3]

1.2. Colon Specific drug vehicle

For the oral route of drug delivery, colon is the most suitable delivery site. In the colon, drugs are free from the attack of numerous proteases and shown to be an ideal location to direct drug into the bloodstream and the immune system. Colon-specific oral drug vehicles need to remain intact till they reach GI tract to protect the incorporated drug from the chemical and enzymatic degradation and also should release the drug immediately upon entering the colon segment of the lower GI tract.

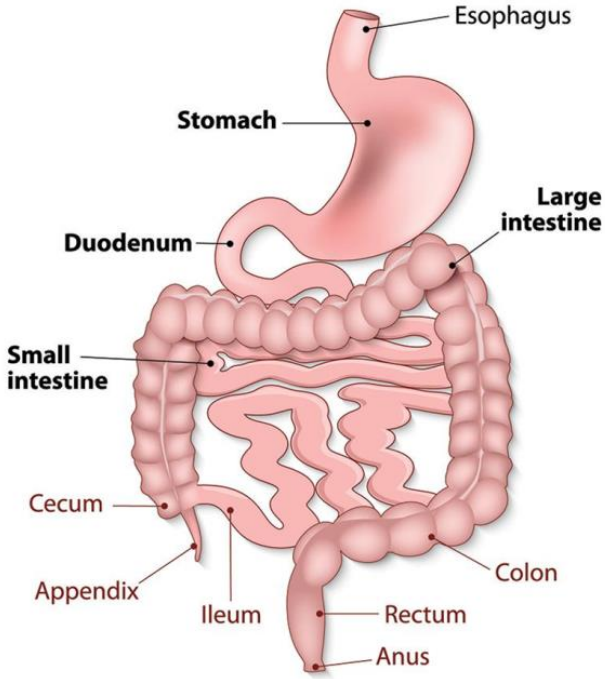

Fig. 1.1: Gastrointestinal tract

Colon reduces the side effects caused by a high dose.[5,6,9,10] Hence, the vehicle used in the oral drug delivery should be biodegradable for the avoidance of its accumulation in the body for prolonged use and it also shields the drug from the gastric environment.[9]

1.3. Biomedical applications of $CaCO_3$ nanoparticles

Over recent years, biocompatible and biodegradable nanoparticles have attracted much attention in the biomedical field. $CaCO_3$ nanoparticles are not only a perfect biomaterial used in cosmetics, toothpaste but also used in the paper industry, food industries, environmental applications and drug delivery applications.[11] Various biomedical applications of $CaCO_3$ nanoparticles are depicted in Fig. 1.2. Calcium based nanoparticles like $CaCO_3$ are all the way biocompatible and biodegradable than any other nanoparticles.

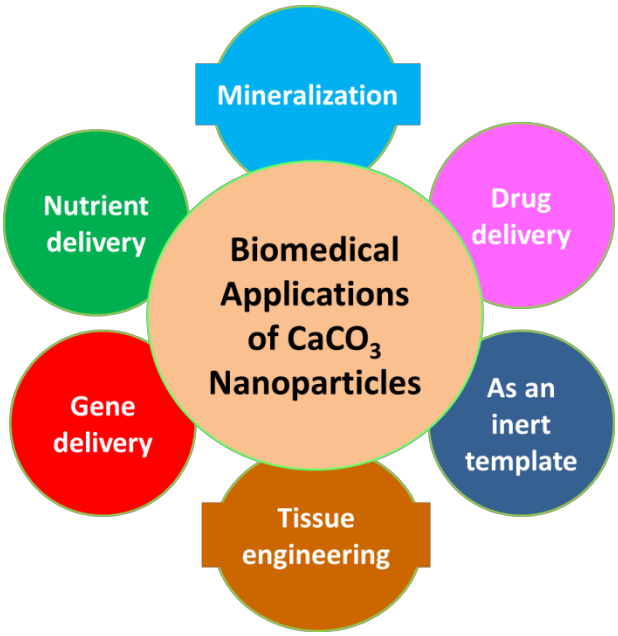

Fig. 1.2: Biomedical applications of $CaCO_3$ nanoparticles[13]

There are four polymorphs of $CaCO_3$: calcite, aragonite, vaterite and amorphous calcium carbonate (ACC). Calcite is thermodynamically most stable among all polymorphs.[12] $CaCO_3$ nanoparticles are also present inside the human body owing to their *in-vivo* stability. It is pertinent to mention that the pH-dependent solubility and stimuli-

responsive behavior of $CaCO_3$ nanoparticles make the material a suitable carrier for the tumor treatment. Porous $CaCO_3$ nanoparticles tend to retain the drug for a prolonged period after administration since they have longer biodegradation time. This property also further helps in diffusion-controlled kinetics. Currently, targeted delivery is more focused as well as uniformly effective since it increases the concentration of drug at the desired body part along with reduces the frequency of the drug dosages. Surface modification is easily possible in the $CaCO_3$ nanoparticles with lipids and polymer molecules that not only intensifies its physical stabilization but also furnishes the binding site for drug vehicles. Thus, surface modification makes $CaCO_3$ nanoparticles more worthy of the targeted delivery of drug. Besides, the synthesis of $CaCO_3$ nanoparticles is facile and cost-effective. $CaCO_3$ nanoparticles have the capacity of loading both hydrophobic and hydrophilic drug molecules.[13]

Moreover, $CaCO_3$ is extensively used as a dietary additive in the food industry since calcium is vitally required for various biological functions in the body like contraction of muscles, nervous system, blood clotting, intracellular cell-signaling, hormonal secretion including healthy bones and teeth.[5,14] It has been reported that calcium from their salts is principally absorbed in the colon.[15] This unique property makes $CaCO_3$ a fantastic vehicle for oral delivery since particles present in the nano range and there is no particle agglomeration in the colon. Apart from this, in colon targeted oral delivery, it is essential to protect $CaCO_3$ particles from dissolution in the stomach at pH 1-2. Therefore, in the present study, a protective coating was given to the $CaCO_3$ using food grade polymer itself or in the form of hydrogel.

1.4. Edible hydrogel

Hydrogels are crosslinked hydrophilic polymers having high water-absorbing capacity and contain pores in their network.[16] The stability of hydrogels mostly depends upon the chemical/physical interaction of their molecular content.[17] It is essential to highlight that natural polymers such as Alginate, Xanthan, Dextran, Chitosan, Guar gum, Okra gum, and Locust gum, soya protein and Pectin etc., are known to form edible hydrogels with the suitable cross-linkers.[16,18] Hence, edible hydrogels are widely used as a gelling agent for different types of food and pharmaceutical products.[19] Hydrogels have also been used for various other applications such as domestic, environmental, biosensor and biomedical.[16] In the biomedical field, researchers have a keen interest in hydrogel materials in the field of regenerative medicine, tissue engineering, cosmetology, drug delivery and nutrient delivery.[20] Interestingly, hydrogels are the best 3D scaffold materials, that can be used as an injectable liquid material for *in-situ* gelation inside the body. Hence, edible hydrogels are the most attractive for the biomedical field, due to their favorable and eco-friendly properties like biocompatibility, biodegradability and non-toxicity.[17] Although edible hydrogels show some drawbacks such as poor mechanical strength, low flexibility, and polymer diffusion problem, that can be overcome by blend formation and chemical modification[21]. In addition, hydrogels are known to protect the cells, easy to modify and have good transport properties.[22] Some of the biomedical applications of hydrogels are shown in Fig.1.3.

In this study, various pectin based hydrogels were synthesized by blending with poly ethylene glycol (PEG) in order to protect $CaCO_3$ particles carrying nutrient/drug.

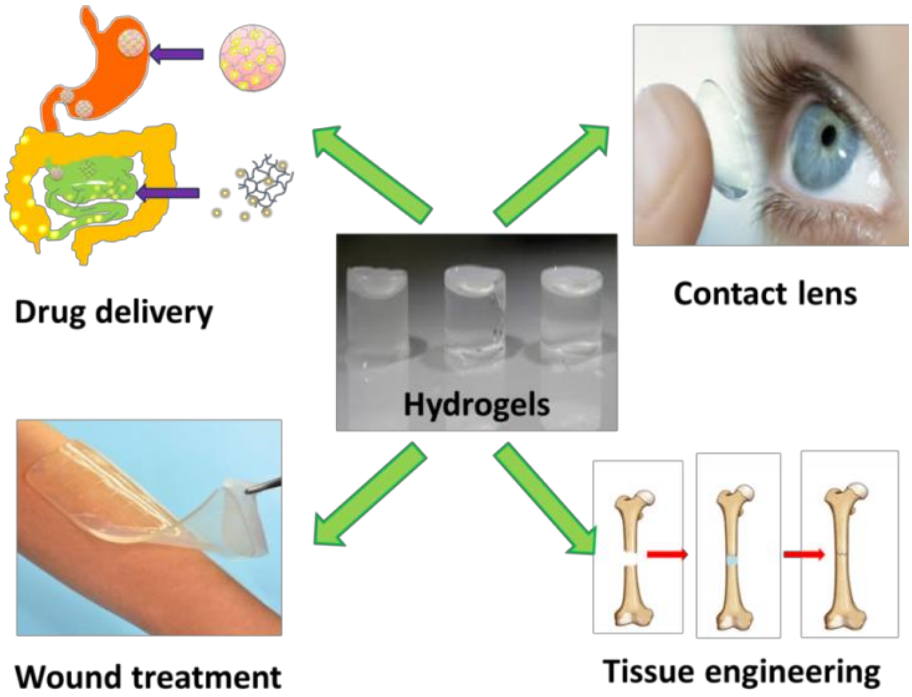

Fig. 1.3: Biomedical Applications of hydrogels

1.5. Pectin

Pectin is a natural polymer found in the plant cell wall. It is essential, water-soluble, non-toxic, linear edible polysaccharide having good biodegradability and biocompatibility. The main component of pectin is poly α 1– 4-galacturonic acids.[23,24] The structure of the pectin is shown in Fig. 1.4. Pectin is widely used as a thickening and gelling agent in the food industry for making hydrogel, which has wide-spread applications in the various fields; among them, drug delivery is well known.[25] Interestingly, pectin based drug delivery systems are considered to be more reliable and reproducible, especially for colon-specific drug delivery systems due to their pH sensitivity as well as film-forming ability.[26] Hence, for colon-specific oral delivery of protein drugs, it becomes essential to

retaining the vehicle intact as it reaches intestine from mouth not only to protect the loaded drug from proteolysis but also to release it instantly at the colon site.[1,3,6]

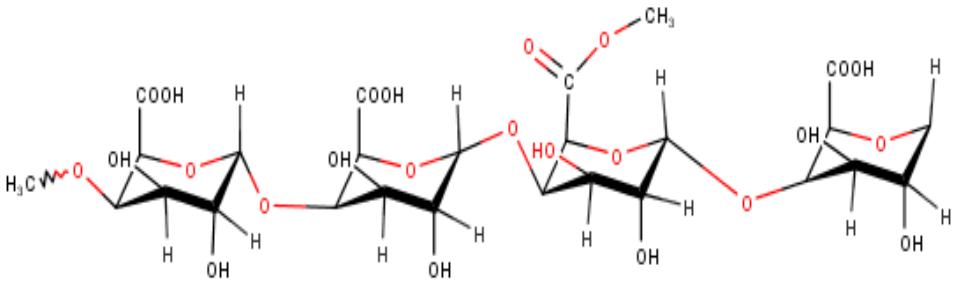

Fig. 1.4: Structure of pectin

1.6. Polyethylene glycol (PEG)

PEG is a neutral synthetic polymer approved by FDA having good water solubility as well as biocompatibility.[27] It is an efficient plasticizer for biopolymers and nano-composite. It has been used for various biomedical and pharmaceutical applications as an additive owing to its non-toxic and bio-adhesive nature.[28-30] The structure of the PEG is shown in Fig. 1.5.

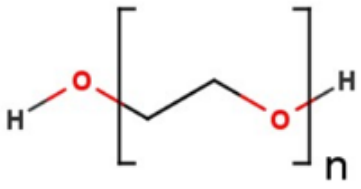

Fig. 1.5: Structure of Polyethylene glycol

1.7. Zein Protein

Zein is a natural storage corn protein having excellent biocompatibility and biodegradability.[31] Zein is water insoluble and non-toxic protein approved by the FDA.[32] This water-insoluble property is owing to the presence of some hydrophobic amino acids such as alanine, phenylalanine, leucine, and proline are accountable for its water-insoluble property. It has been used as a packaging material as well as a moisture impervious barrier in the food industry and also shows a good tensile property. Zein has slower digestibility in the gastric environment. Hence it is an ideal candidate for oral drug delivery.[33] Zein helps to encapsulate hydrophobic drug and its controlled release in the targeted area.[34,35] Zein has been considered as a food biopolymer for nutrient delivery.[33] In the present work, zein was used as a coating material to protect nanoparticles containing nutrients from the stomach environment and release it in the intestine.

In this investigation, considering the importance of calcium-based drug carriers for targeted oral delivery, the following major objectives are proposed.

1.8. Major Objectives of the Thesis

The following are the major objectives of the thesis.

- To fabricate target-specific oral delivery vehicles for the controlled delivery of nutrients/drugs by bioinspired method.
- To delineate the mechanisms involved in the fabrication of the drug carriers by green method.
- To understand *in-vitro* swelling studies of the drug carriers in simulated gastric fluid (SGF at pH 1.2) as well as simulated intestinal fluid (SIF) of two different

pH values (pH 6.0 and pH 6.8) and their corresponding degradability and drug delivery mechanisms.

1.9. Outline of the Thesis

The summary of the chapters included in the thesis is as follows.

Chapter II involves different characterization techniques, used in the present study accompanying with their working principle.

Chapter III discusses the synthesis of zein coated $CaCO_3$ nanoparticles using gelatin as a template. The synthesis was done under ambient conditions for the targeted sequential delivery of vitamin D and amoxicillin across the intestine**.**

Chapter IV involves the fabrication of Pectin /PEG food grade hydrogel blends with the encapsulation of nutrients. In this chapter, different Characterizations were carried out to study morphology, the structural and rheological property of the hydrogel. The protection of the nutrients through the edible hydrogels was demonstrated in the gastric environment. The targeted *in-vitro* co-release of nutrients was successfully shown at the intestinal site.

Chapter V discusses *in-situ* mineralized calcium carbonate microparticles in pectin/PEG hydrogel blend and then loaded with BSA as a model protein drug. The loaded BSA was successfully released at colon site by maintaining its structural stability is also discussed in detail.

References:

[1] Y. Yun, Y.W. Cho, K. Park, Nanoparticles for oral delivery: Targeted nanoparticles with peptidic ligands for oral protein delivery, Adv. Drug Deliv. Rev. 65 (2013) 822-832.

[2] K. Modi, M. Modi, D. Mishra, P. Mittal, U. Sorathiya, P. shelat, Oral controlled release drug delivery system: an overview, Int. Res. J. Pharm. 4 (2013) 70-76.

[3] N.N. Salama, N.D. Eddington, A. Fasano, Tight junction modulation and its relationship to drug delivery, Adv. Drug Deliv. Rev. 58 (2006) 15-28.

[4] H. Gupta, D. Bhandari, A. Sharma, Recent trends in oral drug delivery: a review, recent patents on drug delivery & formulation. 3 (2009) 162-173.

[5] D. Render, T. Samuel, H. King, M. Vig, S. Jeelani, J.B. Ramapuram, V. Rangari, Biomaterial-derived calcium carbonate nanoparticles for enteric drug delivery, J. Nanomater. (2016) 1-8.

[6] T.F. Vandamme, A. Lenourry, C. Charrueau, J.C. Chaumeil, The use of polysaccharides to target drugs to the colon, Carbohydr. Polym. 48 (2002) 219-231.

[7] L.M. Ensign, R. Cone, J. Hanes, Oral drug delivery with polymeric nanoparticles: the gastrointestinal mucus barriers, Adv. Drug Deliv. Rev. 64 (2012) 557-570.

[8] A.M. Hillery, A.W. Lloyd, J. Swarbrick, Drug delivery and targeting for pharmacists and pharmaceutical, in: H.L. Vincent, Johnny Lee, J. Yang (Eds.), Oral drug delivery, Taylor & Francis e-Library, New York, 2005, pp. 131-167.

[9] V.R. Sinha, R. Kumria, Polysaccharides in colon-specific drug delivery, Int. J. Pharm. 224 (2001) 19-38.

[10] J.A. Fix, Oral controlled release technology for peptides: status and future prospects, Pharm. Res. (New York) 13 (1996) 1760-1763.

[11] W. Wei, G.H. Ma, G. Hu, D. Yu, T. Mcleish, Z.G. Su, Z.Y. Shen, Preparation of hierarchical hollow $CaCO_3$ particles and the application as anticancer drug carrier, J. Am. Chem. Soc. 130 (2008) 15808-15810.

[12] Y. Boyjoo, V.K. Pareek, J. Liu, Synthesis of micro and nano-sized calcium carbonate particles and their applications, J**.** Mater. Chem. A 2 (2014) 14270-14288.

[13] S. Sharma, A. Verma, B.V. Tej, G. Pandey, N. Mittapelly, R. Trivedi, P.R. Mishra, An insight into functionalized calcium based inorganic nanomaterials in biomedicine: trends and transitions, Colloids Surf. B Biointerfaces 133 (2015) 120-139.

[14] J. Alee, M.K. Kim, H.M. Kim, J.K. Lee, J. Jeong, Y.R. Kim, J.M. Oh, S.J. Choi, The fate of calcium carbonate nanoparticles administered by oral route: absorption and their interaction with biological matrices, Int. J. Nanomed. 10 (2015) 2273-2293.

[15] R.A. Ohta, S. Baba, M. Ohtsuki, T. Takizawa, T. Adachi, H. Hara, *In-vivo* absorption of calcium carbonate and magnesium oxide from the large intestine in the rats, J. Nutr. Sci. Vitaminol. 43 (1997) 35-46.

[16] Anamica, P.P. Pande, Polymer hydrogels and their applications**,** Int. J. Mater. Sci. 12 (2017) 11-14.

[17] A.S. Hoffman, Hydrogels for biomedical applications, Adv. Drug Deliv. Rev. 64 (2012) 18-23.

[18] J.P. Gleeson, S.M. Ryan, D.J. Brayden, Oral delivery strategies for nutraceuticals: delivery vehicles and absorption enhancers, Trends Food Sci. Technol. 53 (2016) 90-101.

[19] S. Banerjee, S. Bhattacharya, Food gels: gelling process and new applications, Crit. Rev. Food Sci. Nutr. 52 (2012) 334-346.

[20] J. Jagur-Grodzinski, Polymeric gels and hydrogels for biomedical and pharmaceutical applications, Polym. Adv. Technol. 21 (2010) 27-47.

[21] A. Ali, S. Ahmed, Recent advances in edible polymer based hydrogels as a sustainable alternative to conventional polymers, J. Agric. Food Chem. 66 (2018) 6940-6967.

[22] S.P. Nagam, A. Nagajyothi, J. Poojitha, A. Santhosh, R.R. Nadendla, A comprehensive review on hydrogels, Int. J. Curr. Pharm. Res. 8 (2016) 19-23.

[23] B.R. Thakur, R.K. Singh, A.K. Handa, Chemistry and uses of pectin - a review**,** Crit. Rev. Food Sci. Nutr. 37 (1997) 47-73.

[24] F. Munarin, M.C. Tanzi, P. Petrini, Advances in biomedical applications of pectin gels, Int. J. Biol. Macromol. 51 (2012) 681- 689.

[25] M. Sadeghi, Pectin-based biodegradable hydrogels with potential biomedical applications as drug delivery systems, J. Biomater. Nanobiotechnol. 2 (2011) 36-40.

[26] A. Noreen, Z.I.H. Nazli, J. Akram, I. Rasul, A. Mansha, N. Yaqoob, R. Iqbal, S. Tabasum, M. Zuber, K.M. Zia, Pectins functionalized biomaterials; a new viable approach for biomedical applications: A review, Int. J. Biol Macromol. 101 (2017) 254-272.

[27] G. Cavallaro, G. Lazzara, S. Milioto, Sustainable nanocomposites based on halloysite nanotubes and pectin/polyethylene glycol blend, Polym. Degrad. 98 (2013) 2529-2536.

[28] N. Bhattarai, H.R. Ramay, J. Gunn, F.A. Matsen, M. Zhang, PEG-grafted chitosan as an injectable thermosensitive hydrogel for sustained protein release, J. Control. Release. 103 (2005) 609-624.

[29] H.S. Mansur, R.L. Orefice, A.A.P. Mansur, Characterization of poly(vinyl alcohol)/poly(ethylene glycol) hydrogels and PVA-derived hybrids by small-angle X-ray scattering and FTIR spectroscopy, Polymer. 45 (2004) 7193-7202.

[30] S.D.P. Cabello, E.A. Takara, J. Marchese, N.A. Ochoa, Influence of plasticizers in pectin films: microstructural changes, Mater. Chem. Physics. 162 (2015) 491-497.

[31] T. Lin, C. Lu, L. Zhu, T. Lu, The biodegradation of zein *in-vitro* and *in-vivo* and its application in implants, AAPS Pharm. Sci. Tech. 12 (2011) 172-176.

[32] P. Franco, E. Reverchon, I.D. Marco, Production of zein/antibiotic microparticles by supercritical antisolvent coprecipitation, J. Supercrit. Fluids. 145 (2018) 31-38.

[33] N. Sharif, M.J. Fabra, A. Lopez-Rubio, Nanostructures of zein for encapsulation of food ingredients, Biopolymer nanostructures for food encapsulation purposes, elsevier (2019) pp. 217-245.

[34] M.S. Alqahtani, M.S. Islam, S. Podaralla, R.S. Kaushik, J. Reineke, T. Woyengo, O. Perumal, Food protein based core-shell nanocarriers for oral drug delivery: effect of shell composition on *in-vitro* and *in-vivo* functional performance of zein nanocarriers, Mol. Pharmaceutics. 14 (2017) 757-769.

[35] T. Yoshino, S. Isobe, T. Maekawa, Influence of preparation conditions on the physical properties of zein films, J. Am. oil chem. Soc. 79 (2002) 345-349.

Chapter 2

Characterization Techniques

2.1. For structural determination

2.1.1. X-ray Diffraction Technique (XRD)[1-3]

X-ray diffraction is one of the best techniques to identify the crystalline or amorphous phase of the materials and various structural properties. X-ray diffraction works on the principle of Bragg's law. When a beam of X-ray having the energy (1-100 keV) is incident on the crystal planes of the material, it is scattered by atoms in all directions. These scattered X-rays can interfere constructively and destructively.

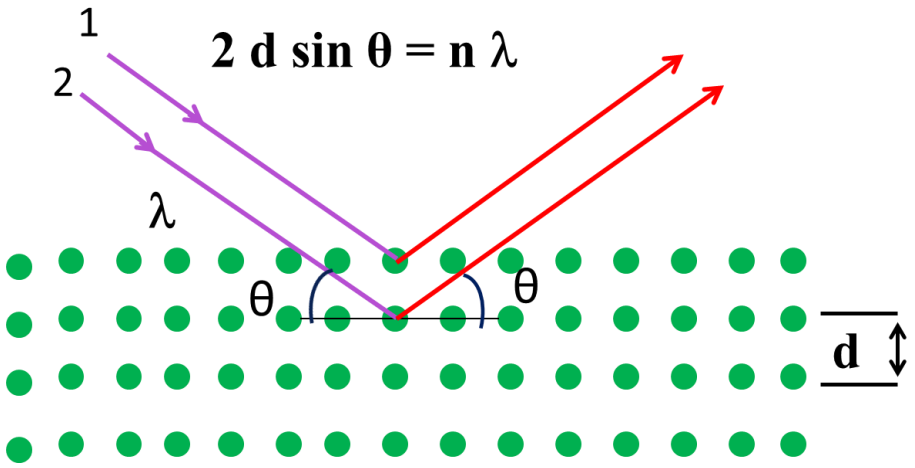

Fig. 2.1: Schematic diagram of X-ray diffraction[3]

The constructive interference occurs if the angle of incidence is equal to the angle of diffraction and the path difference between the scattered X-ray is an integral multiple of wavelength (λ). i.e. path difference = $n\lambda$. The path difference between scattered X-rays

for destructive interference will be ($2n\pm \lambda/2$), where n is an integer. The schematic diagram of X-ray diffraction is shown in Fig. 2.1.

Two X-ray beams are incident on crystal planes with inter-planar spacing '*d*' of the sample at angle θ. The ray 1 and 2 gets reflected from the upper and lower atomic planes respectively, at an angle θ equal to the incidence angle. The path difference between the two rays is $2d \sin \theta$, represented by equation 2.1, known as Bragg's law for X-ray diffraction.

$$2d \sin\theta = n\lambda \qquad (2.1)$$

where *n* is an integer λ is the wavelength of the radiation, *d* is the interplanar spacing, and θ is the incident angle relative to the plane of atoms. The average crystallite size (D) of the sample can be calculated by Scherrer formula defined as:

$$D = \frac{k\,\lambda}{\beta \cos\theta} \qquad (2.2)$$

where *k* is a constant whose value is 0.94 in most of the cases and β is the full width and half maxima (FWHM); and λ and θ have their usual meanings. Generally, X-ray diffraction provides information about long-range order structure, phase composition, crystallinity, crystal size, shape, micro-stress, and strain.

2.1.2. Fourier Transform Infrared spectroscopy (FTIR)[4-6]

This technique used to identify the unknown material, the amount of component in a mixture and functional group in the organic compound. The infrared spectroscopy follows the principle that governs the molecule tends to absorb infrared region frequencies. In a molecule, all bonds do not absorb infrared radiation. Only those bonds

which show change in dipole moment absorb infrared radiation and are called an infrared active molecule. The main objective of the infrared spectroscopy is to make out the identity of the two compounds under similar conditions in the fingerprint region (below 1500 cm^{-1}). This fingerprint region contains a huge number of absorption bands due to bending and stretching vibration of the molecules. Hence some molecules show similar absorption above 1500 cm^{-1} but different in absorption in fingerprint region and can be identified easily.

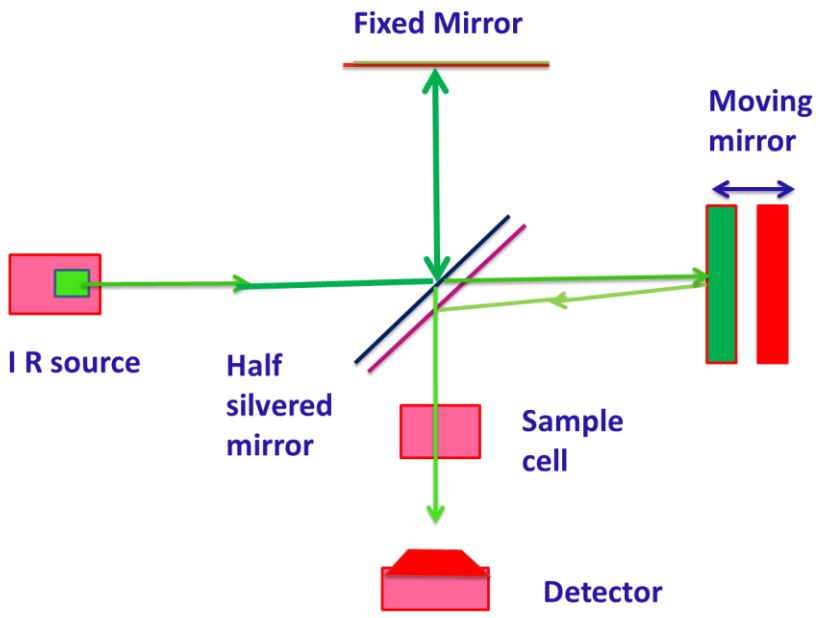

Fig. 2.2: Schematic diagram of interferometer[5]

When infrared radiation is passed through the sample, some part of the radiation is absorbed and some is transmitted. The resulting spectrum creates a molecular fingerprint for that sample. By absorbing the infrared radiation (less than 100 cm^{-1}), molecular rotation takes place and discrete lines are formed in the spectrum. When more energetic radiation (10^4 to 10^2 cm^{-1}) is passed through the sample, molecular vibration takes place.

These absorptions cause rotation and vibration in the infrared region and they are quantized. An organic compound molecule will show a number of peaks in the infra-red region. Infrared spectroscopy gives sufficient structural information of the compound.

Fourier transform is a preferable method of infrared spectroscopy. It is associated with a simple optical device called interferometer. The Schematic diagram of the interferometer is shown in Fig. 2.2. This creates a signal called interferogram, which is converted in the desired spectrum that contains information of every molecule.

2.1.3. Thermogravimetric Analysis (TGA)[7-9]

TGA is an analytical technique used to evaluate the thermal stability of the compound. In this analysis, the weight loss of the sample is measured over time as a function of temperature.

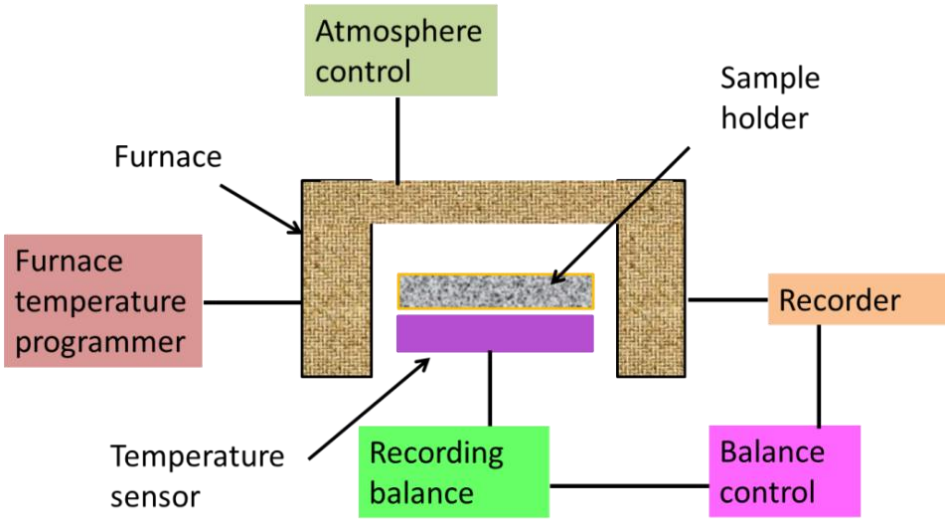

Fig. 2.3: Block diagram of TGA (Modified)[8]

Block diagram of thermogravimetric analysis is shown in Fig. 2.3. This method also gives information about absorption, adsorption, desorption and thermal decomposition.

The instrument used in TGA called thermogravimetric analyzer that consists of a precision balance with a sample holder located inside the furnace. Generally, the temperature is increased with the constant rate and weight percentage is measured. In TGA, the temperature normally reaches to 1000 °C during the thermal reaction carried out under inert atmosphere, especially N_2 gas. In addition, TGA provides a curve between mass percentage and temperature. If the material is thermally stable, the mass change will not be observed and no slope in the TGA trace. This technique is also used to evaluate the thermal stability of the polymers.

2.1.4. Brunauer Emmett Teller (BET)[10-13]

BET is the best method to evaluate the surface area and the porosity of the materials. This method is based on the adsorption of the gas molecules on the solid surface. It is an expansion of Langmuir's theory. Langmuir theory explains the monolayer molecular adsorption while BET applies to the multilayers molecular adsorption with the following postulates, such as Gas molecules adsorbed on the solid surface in the form of layers infinitely. These gas molecules interact with the adjacent layer only. Langmuir's theory can be applied to each layer of the gas molecules. In BET method, Nitrogen gas is used as an adsorbate due to its chemically inert behavior for measuring the surface area of the material. In the IUPAC classification, Pores of solid material are roughly classified into three categories based on their pore diameter. (i) Macroporous (greater than 50 nm), (ii) mesoporous (2-50 nm) and (iii) Microporous (less than 2 nm). Fig. 2.4 represents different types of nitrogen adsorption-desorption isotherm and hysteresis loop.

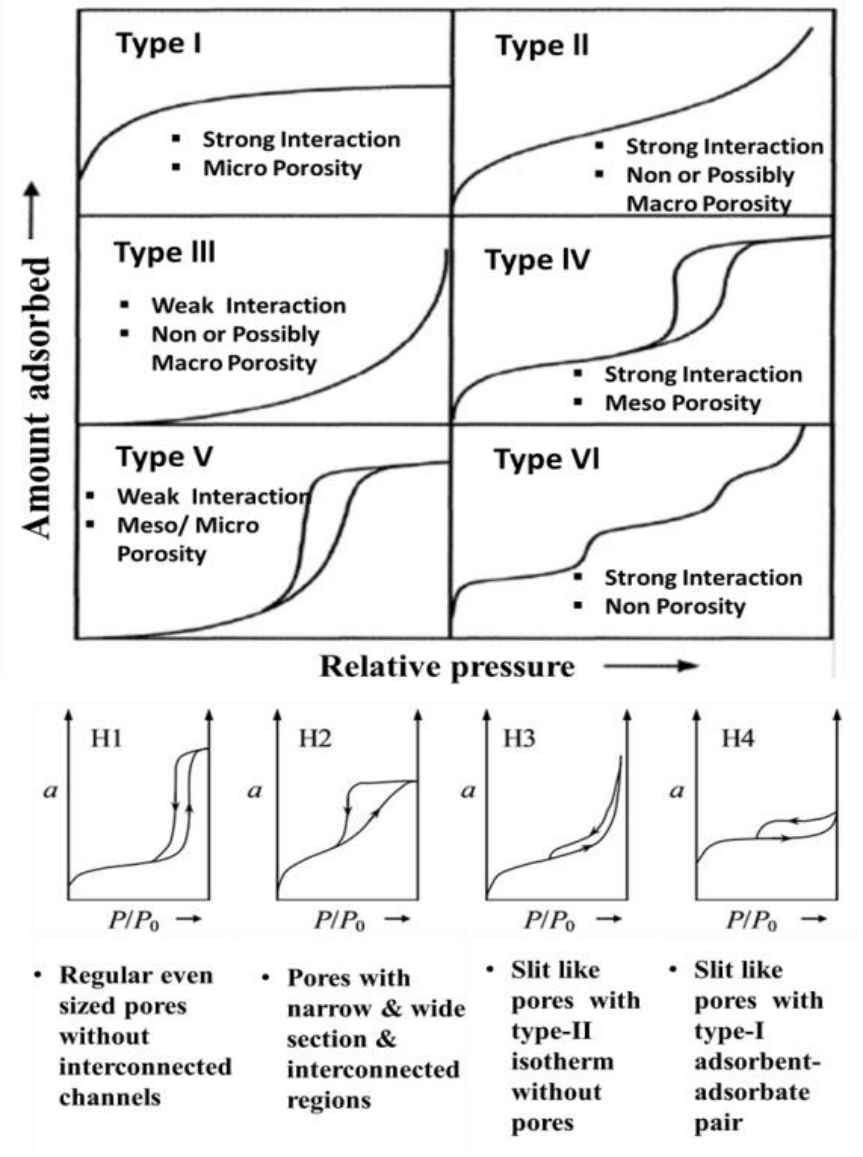

Fig. 2.4: (a) Nitrogen adsorption-desorption isotherm (b) hysteresis loop

2.1.5. Zetasizer[14]

Zetasizer is an instrument used to measure particle or molecular size and zeta potential of the colloidal dispersion, nanoparticles and protein. The principle behind the measurement of the particles is molecules that are in Brownian motion, diffuse at speed related to their size. Zetasizer system measures the particle using dynamic light scattering (DLS),

electrophoretic light scattering (ELS) and static light scattering (SLS). DLS is a non–invasive method used to measure size and size distribution of the molecules or particles less than a nanometer. ELS is used to measure the zeta potential and electrophoretic mobility of the particles in the liquid medium. SLS is used to measure the average molecular weight of the polymer.

2.2. For morphological and elemental analysis

2.2.1. Electron Microscopy[15-20]

Electron microscopes are used to examine objects on a very fine scale. Electron microscopes make use of energetic electrons instead of light as in optical microscopes. There are two types of electron microscopes: Transmission Electron Microscope (TEM) and Scanning Electron Microscope (SEM).

Transmission Electron Microscope (TEM)

TEM is a powerful tool used for the imaging of the material. In this technique, an electron beam is transmitted through the sample to produce images. A high energy electron (upto 300 kV) is required to operate this instrument. TEM determines the highly magnified view of the Particle size, shape, size distribution density of the sample. TEM can be used for higher resolution.

It works on the same principle as a normal light microscope, but in this technique, electrons are used instead of light. When electron beam is passed through a material to be characterized, electrons are scattered and focused by the electromagnetic lens into an image. This instrument is composed of various components shown in Fig. 2.5.

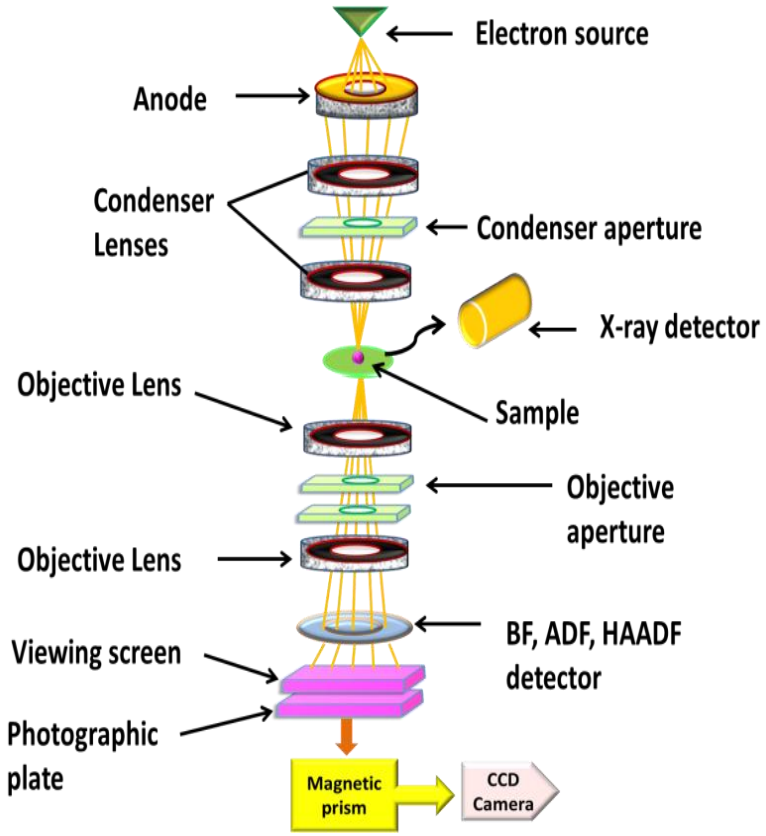

Fig. 2.5: Schematic diagram of the core component of TEM (Modified)[18]

The images, produced by TEM, depend upon the mode of operations and these modes reveal the various insights about the sample as follows.

- Imaging mode provides the highly magnified view of the sample.
- High resolution imaging mode gives a piece of information about the atomic rearrangements.
- The diffraction mode determines accurate information about the structure.
- The nano-analytical mode tells about the element present in the volume of the material.

Scanning Electron Microscope (SEM)

SEM is a strong technique, which gives information about a specimen's morphology, topography, crystallographic information. It generates a Two-dimensional image of the material. For mounting the sample, it should be dried and an electrically conducted sample is used since this technique is based on the electron beam. Therefore, a very thin layer gold coating is done by sputtering on the surface of non-coating material to make it electrically conducting for imaging. These are the following core components of SEM shown in Fig. 2.6. In SEM thermionic emission gun is used to produce the free electron and these electrons are converted into a fine beam by the magnetic lens.

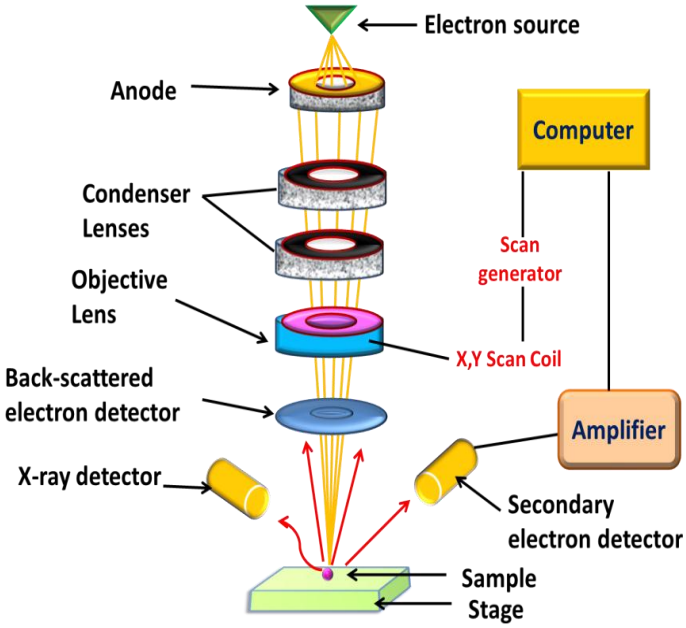

Fig. 2.6: Schematic diagram of the core components of an SEM microscope (modified)[18]

When this accelerated beam strikes the sample, image is developed by rastering the beam. Various type of signal is produced such as secondary electrons, back-scattered electrons, auger electrons and x-ray, which give the information about the topography,

topography as well as atomic number, sensitivity and composition of the surface respectively. In the SEM, only secondary electrons are detected and the image is created, which displays the topography of the surface of the sample.

Energy Dispersive X-ray spectroscopy (EDX) is a technique that provides information about the abundance of elements and its distribution present in the material.

2.2.2. Inductively coupled plasma atomic emission spectroscopy (ICP-AES) [21-23]

ICP-AES is a technique used for trace element detection. It is also used the elemental composition and its concentration present in the sample. It gives precise results. It is similar to emission spectroscopy in which inductively coupled plasma is used, which causes excited atom and ion that emit electromagnetic radiation, which attributes to the wavelength of that particle corresponding element. A schematic diagram of ICP-AES is depicted in Fig. 2.7. Each element emits energy at a different wavelength, but in ICP-AES a particular wavelength of the element is selected.

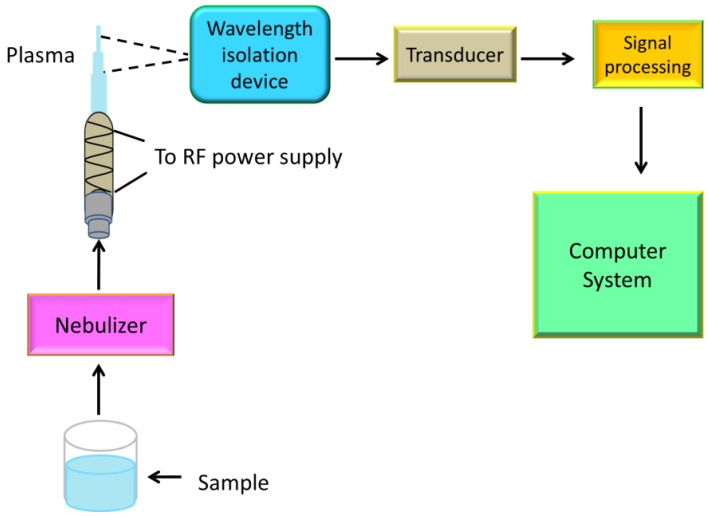

Fig. 2.7: Schematic diagram of ICP-AES[21]

The intensity of the emitted energy at a particular wavelength is proportional to the concentration of the element present in the sample. Hence element composition of the sample can be measured by determining the intensity of the wavelength. In ICP-AES , Argon gas is mainly used to dissociate the ion.

2.3. For Mechanical Properties

Rheometer[24,25]

Rheometer is a laboratory instrument, which is used to measure the rheology of the sample. Sample can be in the form of liquid, suspension and slurry. Viscosity and viscoelastic properties can be measured through the rheometer.

Rheometers are of two types as follows; (i) Rotational rheometer that controls the applied shear stress and shear strain. (ii) Extensional rheometer that applies extensional stress and strain. Rotational rheometer is usually designed as strain-controlled and stress-controlled as shown in Fig. 2.8.

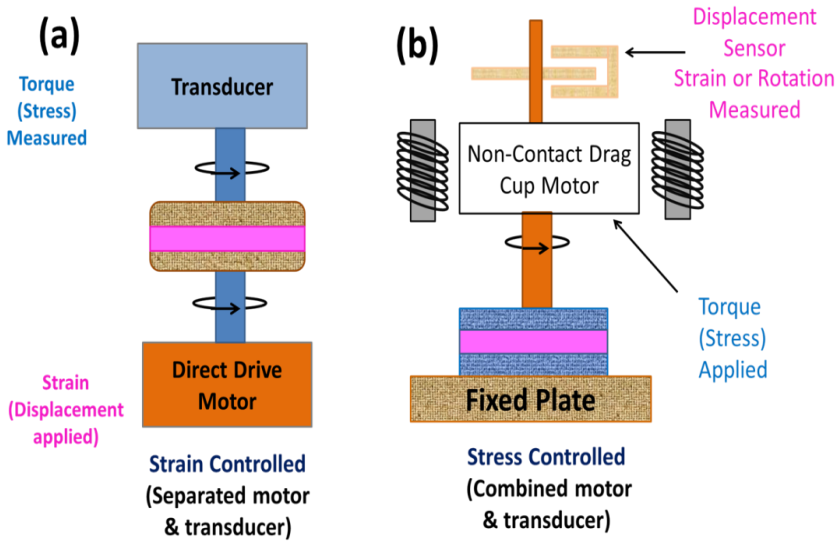

Fig. 2.8: Stain and stress controlled Rheometer (Modified)[25]

In the case of controlled strain rheometer (most common), sample is placed between the two plates and strain (deformation) is applied by the help of direct drive motor, sample determines how much amount of torque (stress) is transmitted. By altering the frequency or the shear rate, viscosity is measured as a function of frequency. In the controlled stress rheometer, stress is applied, sample responds by deforming (strain) that can be measured.

2.4. Biophysical studies

2.4.1. Circular Dichroism[26]

CD is a powerful technique to determine the differential absorption of left and right-handed circular polarized light when interacting with the chiral molecule, as shown in Fig 2.9. Basically, in circular dichroism, linear polarized light is converted into left and right-handed circular polarized light when passed through the Photo Elastic Modulator. This circular polarized light is absorbed by the optically active molecule and detected by the photomultiplier tube.

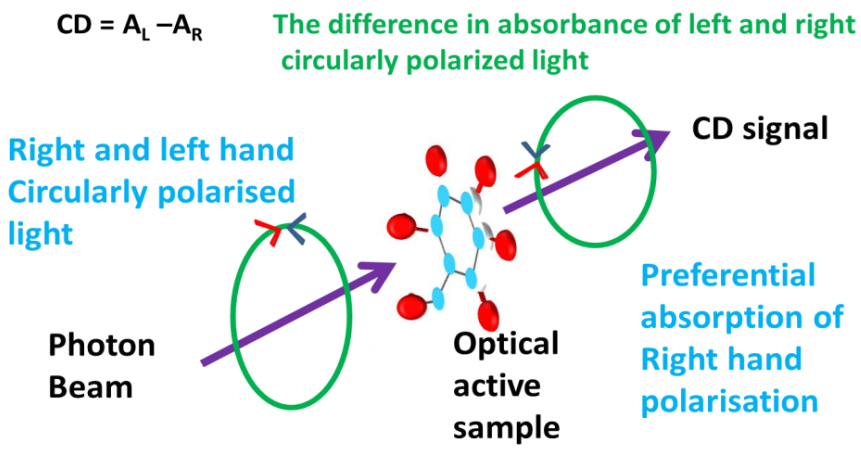

Fig. 2.9: Principle of Circular Dichroism spectroscopy[26]

CD spectroscopy is associated with an advanced technique known as optical rotatory dispersion (ORD). CD is measured in or near the absorption band of the molecule whereas ORD is measured far the absorption bands. The Far-UV CD spectrum gives information about the secondary structure of the protein, while the near-UV CD spectrum reveals the knowledge of the tertiary structure of protein molecule. Near-UV CD spectrum gives the signals above the 250 nm.

In general, CD is used to explore the structural information of small organic molecules like DNA and Protein. The primary use of CD spectroscopy is to analyze the secondary structure of macromolecule, particularly proteins and its interaction with the other molecule. Since the secondary structure is too sensitivity to the environment, temperature and pH conditions so this technique can be used to observe the changes in the structure at the above conditions.

2.4.2. Gel Electrophoresis[27,28]

Gel electrophoresis is widely used analytical method for the separation of macromolecules (DNA, RNA, and proteins) by their size and charge. Polyacrylamide gel is used for the separation of protein since they have high resolution capacity compare to agarose, starch and cellulose acetate. Polyacrylamide gel separates protein with the size range from 5-2000 kD. Different components of polyacrylamide gel electrophoresis are displayed in Fig. 2.10. The following reagents are used in the gel electrophoresis.

Acrylamide and N, N'-methylene bisacrylamide, Sodium dodecylsulphate (SDS), Tris buffer, TEMED (N,N,N'-N'-tetramethylethylene-diamine), Ammonium persulphate (AP), Tris glycine electrophoresis buffer (TGEB).

Preparation of gel

Stacking gel: Stacking gel was prepared by mixing of 30% acrylamide mixture, 1 M Tris at pH 6.8, 10% SDS, 10% ammonium persulphate and then TEMED in deionized water as per the required amount. This gel contains larger pores and lower ionic strength.

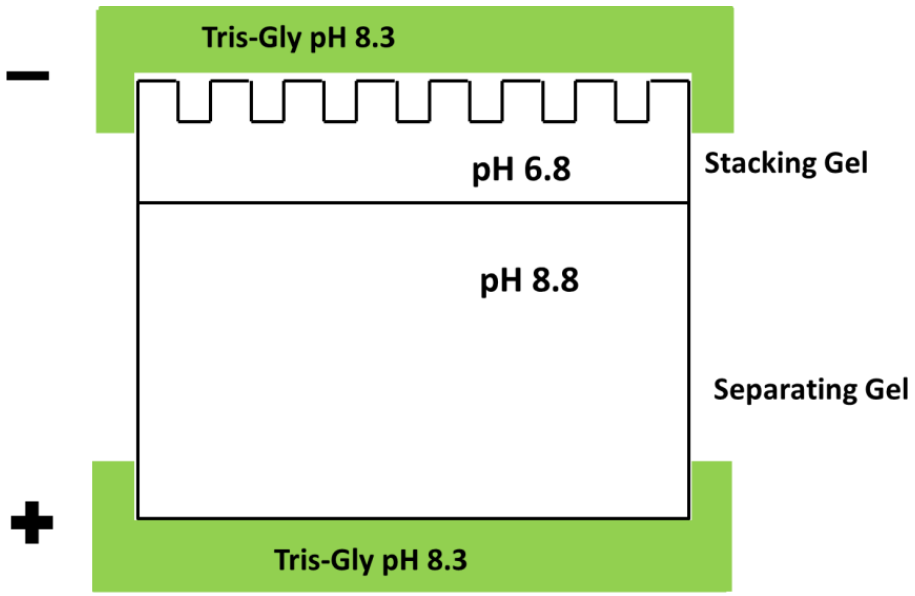

Fig. 2.10: Component of polyacrylamide gel electrophoresis

Separating gel: This gel was prepared by mixing 30 % acrylamide mixture, 1.5 M Tris at pH at 8.8, 10 % SDS and 10% ammonium sulphate, in deionized water. This gel contains smaller pores and higher ionic strength.

Sample preparation

Protein sample, to be analyzed was mixed with the following sample solubilization solution.

Sample solubilization solution: 1gm of SDS, 2ml of glycerol, 2ml of bromophenol blue tracking dye (0.1% (w/v) solution in distilled water), 1.25 ml of 1M tris HCl of pH 6.8, 2 ml of 2-mercaptoethanol was mixed and the volume made upto 10 ml with distilled water.

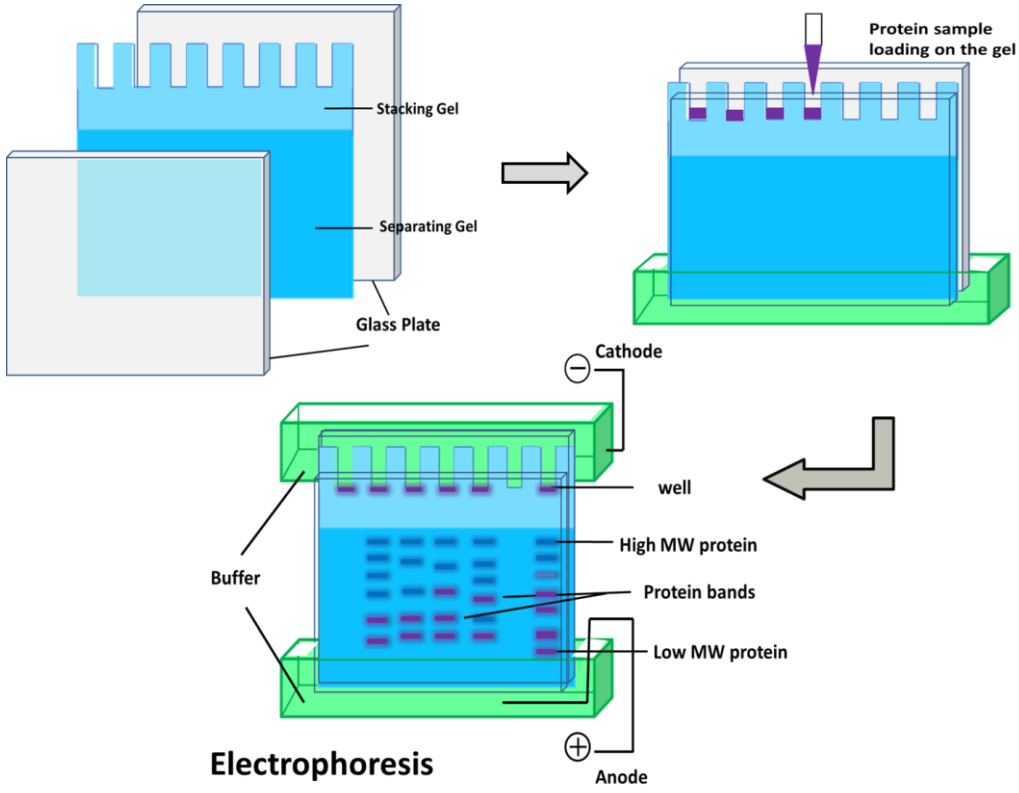

Fig. 2.11: Different steps involved in gel electrophoresis[28]

In gel electrophoresis, protein samples are applied in the wells present in stacking gel. When an electric current is applied to the buffer solution, macromolecules travel to their oppositely charged end according to their molecular weight. The negatively charged DNA and RNA go to the positively charged end of the gel. Whereas in the case of protein, sodium dodecyl sulfate as a surfactant is mixed with the protein to make it

negatively charged. This allows the protein to travel towards the positively charged end of the gel shown in Fig. 2.11. The traveling distance of macromolecules through gel pores is inversely proportional to their length. This is done by molecular sieving effect based on the size of the macromolecules.

References:

[1] F.H. Chung, D.K. Smith, Industrial application of x-ray diffraction, Marcel Dekker, New York, 2000.

[2] C.R. Bundle, C.A. Evans, Jr. S. Wilson, Encyclopedia of materials characterization, Manning Publications Co. Greenwich, 1992.

[3] C. Suranarayana, M.G. Nortan, X-ray diffraction: a practical approach, plenum Press, New York, 1998.

[4] A.L. Smith, Applied infrared spectroscopy: fundamentals, techniques and analytical problem solving, John Wiley & Sons, Ltd, 1979.

[5] P.R. Griffiths, C. Holmes, Handbook of vibrational spectroscopy, Chichester: John Wiley and Sons, 2002.

[6] D.L. Pavia, G.M. Lampman, G.S. Kriz, Introduction to spectroscopy, Thomson Learning, Inc., 3rd ed., 2001.

[7] H.H. Willard, L.L. Merritt and J.A. Dean, Instrumental Methods of Analysis, Princeton, 1958.

[8] T. Hatakeyama and Z. Liu, Handbook of thermal analysis, John Willey & Sons, New York, USA, 1998.

[9] A.W. Coats, J.P. Redfern, Thermogravimetric analysis: a review, Analyst. 88 (1963) 906–924.

[10] S.J. Gregg, K.S.W. Sing, Adsorption, surface area and porosity, Academic Press, C.A. San Diego, 1995.

[11] I. Langmuir, The constitution and fundamental properties of solids and liquids. Part 1. Solids, J. Am. Chem. Soc. 38 (1916) 2221–2295.

[12] S. Brunauer, P.H. Emmett and E. Teller, J. Am. Chem. Soc. 60 (1938) 309–319.

[13] A.W. Adamson, A.P. Gast, Physical chemistry of surfaces, 6th ed.,Wiley, 1997.

[14] Zetasizer nano series user manual, Malvern Instruments Ltd., 2013.

[15] R.F. Egerton, Physical principle of electron microscopy; an introduction to TEM, SEM, and AFM, Springer New York, 2006.

[16] D.B. Williams and C.B. Carter, Transmission electron microscopy: a textbook for materials science, Springer New York, 1996.

[17] L. Reimer, Scanning electron microscopy: physics of image formation and microanalysis, Springer-Verlag, Berlin Heidelberg, Germany, 1985.

[18] B.J. Inkson, 2 - scanning electron microscopy (SEM) and transmission electron microscopy (TEM) for materials characterization using nondestructive evaluation (NDE) methods, (2016) 17-43.

[19] G. Dhem, J.M. howe, J. zweck, *In-situ* electron microscopy: application in physics, chemistry and material science, willey-VCH Verlag & co. KGaA, 2012.

[20] T.G. Rochow, E.G. Rochow, An introduction to microscopy by means of light, electron, x-rays , or ultrasound, Plenum Press, New York and London, 1978.

[21] G.L. Moore, Introduction to inductively coupled plasma atomic emission spectrometry, Elsevier Science Publishers B.V., The Netherlands, 1989.

[22] M. Aceto, O. Abollino, M.C. Bruzzoniti, E. Mentasti, C. Sarzanini, M. Malandrino, Determination of metals in wine with atomic spectroscopy (flame-AAS, GF-AAS and ICP-AES); a review, Food Addi. Contam. 19 (2010) 126-133.

[23] D. Harvey, in Analytical chemistry 2.0, McGraw-Hill, 1999, pp. 543–666.

[24] T.G. Mezger, Applied rheology: with joe flow on rheology road, Anton Paar GmbH, 1 st., 2015.

[25] J. Gotto, Rheology of thermosets part 2: rheometers.

[26] R.A. Scott and C.M. Lukehart, Eds., Applications of physical methods to inorganic and bioinorganic chemistry, John Wiley & Sons, Ltd, 2007.

[27] S. Magdeldin, Ed., Gel electrophoresis – principles and basics, In Tech Croatia, 2012.

[28] G. Buyukkoroglu, D.D. Dora, F. Ozdemir, C. Hizel, Techniques for protein analysis, Omics Technologies and Bio-Engineering, Academic Press, 2018, pp. 317-351.

Chapter 3

Zein coated calcium carbonate nanoparticles for the targeted controlled release of model antibiotic and nutrient across the intestine

3.1. Introduction

Oral administration of vitamin D has been long explored as a dietary supplement for calcium homeostasis and bone remineralization.[1,2] Apart from these, vitamin D has also been found to be effective in a plethora of conditions, including cancer.[3,4] However, unregulated dietary intake can be detrimental due to the risk of hypercalcemia.[5] Since the appropriate dosage of vitamin D is difficult to achieve through dietary intake, the risk of overdosing the vitamin becomes difficult to prevent, especially for chronic intake.[6] Further, the lipophilic, as well as acid-labile nature of vitamin D, makes it susceptible in Gastrointestinal (GI) Fluid, thus adding to its limited oral bioavailability.[7,8] Interestingly, vitamin D analogues have been explored to outperform vitamin D activity in intestine and have shown to be effective in limiting disorders related to calcium deficiency.[9,10] Among various approaches, followed for improving oral bioavailability of vitamin D,[11,12] an effective choice is to directly deliver vitamin D to the source of absorption through nanocarriers.[12,13,14] Currently, a variety of nanocarriers such as liposomes, polymeric nanoparticles, lipid nanoparticles, micelles and inorganic nanoparticles are being used for vitamin D delivery.[14] For example, Luo *et al*. prepared carboxymethyl chitosan (CMC) hydrogel beads to deliver vitamin D3 and observed its release in simulated

gastrointestinal conditions.[15] Besides, zein nanoparticles coated with carboxymethyl chitosan has also been designed for encapsulation and controlled release of vitamin D3.[16] Similarly, lipid-based carriers of vitamin D have been explored in the delivery of vitamin D.[17-19] Bothiraja *et al*. used a commercially available nanoparticle-based novel drug delivery system (Arachitol Nano^{TM}) to deliver vitamin D3 and showed its absorption in the intestine.[20] Even though polymeric and lipid-based nanocarriers are commonly used in drug delivery, a major challenge towards the safety of its *in-vivo* application is due to the use of organic solvents during synthesis.[21,22] Apart from this, low solubility, short half-life and high production cost further add up to the above limitation.[22] Nanocarriers like phospholipids may undergo oxidation; for instance, FDA approved PLGA produces acidic molecules during degradation and in several cases, leakage of encapsulated drugs with lower molecular weights has been reported.[23,24] Inorganic nanocarriers address these limitations by a certain extent and can successfully deliver drug molecules at the target site.[25]

In this investigation, $CaCO_3$ nanoparticles loaded with vitamin D were used mainly to couple vitamin D and calcium components together to obtain a synergistic outcome. Calcium and vitamin D supplementation are a common prescription for healthy bone growth where the former is absorbed with the aid of the latter, particularly in the intestine.[26] Interestingly, previous reports have shown increased bioavailability of $CaCO_3$ nanoparticles when compared to direct oral administration of $CaCO_3$.[27,28] The $CaCO_3$ nanoparticles on account of their size and stability in GI fluid (through coating) are expected to increase the serum level of vitamin D, which, once converted by the kidney to its active form calcitriol, can help in increasing calcium uptake from the intestine.[29,30] The approach is mainly to overcome the limitations related to suboptimal dosing that are

otherwise encountered by direct oral intake of the components. Herein, we expect that zein coated nano-sized $CaCO_3$ particles should help in increasing oral bioavailability of vitamin D, which would, in turn, help in increased calcium absorption from the intestine. The $CaCO_3$ nanoparticles utilized as carriers, in this case, can contribute to calcium homeostasis through vitamin D. We believe that $CaCO_3$ nanoparticles loaded with vitamin D can perform at comparatively lower doses than that administered orally for treatment related to its deficiency. Also, it can be effective for a longer period due to controlled release at colon site. This can help in avoiding the risk of hypercalcemia that is heavily associated with unregulated vitamin D intake.[31]

There are several methods for the synthesis of $CaCO_3$ using organic substrates as a template,[25] but to our knowledge, the synthesis of around 10 nm sized $CaCO_3$ nanoparticles using gelatin as a template has not been reported yet. So far, $CaCO_3$ nanoparticles synthesized through nanotechnological approaches have been mostly reported to be having a particle size range of 80 nm or above. It has been reported that oral absorption of $CaCO_3$ is very low (only 4 %).[32] Strategies to overcome this limitation is under investigation. The purpose of the present study is mainly to develop an efficient nano-sized delivery vehicle for the sequential delivery of vitamin D and amoxicillin (Fig. 3.1). We report the preparation of gelatin templated $CaCO_3$ nanoparticles through the bio-inspired method.[33] The obtained particles were estimated to be in the range of 10-15 nm as observed from the XRD and TEM data. The nano-sized $CaCO_3$ particles are able to persist in the gastrointestinal tract (GIT) for a longer period, provided it can delay its dissolution by the strong acidic pH of the stomach. Hence, $CaCO_3$ nanoparticles prepared in our case are coated with zein, a hydrophobic corn protein to protect the particles from dissolution in acidic pH so as to increase its intestinal presence. Once vitamin D was

loaded on the nanoparticles, zein coating not only helped in encapsulation of the second cargo amoxicillin but also contributed towards its controlled release.[34] Herein, amoxicillin has been chosen as the other cargo because of its opposite polarity and it being a GIT relevant antibiotic.[35]

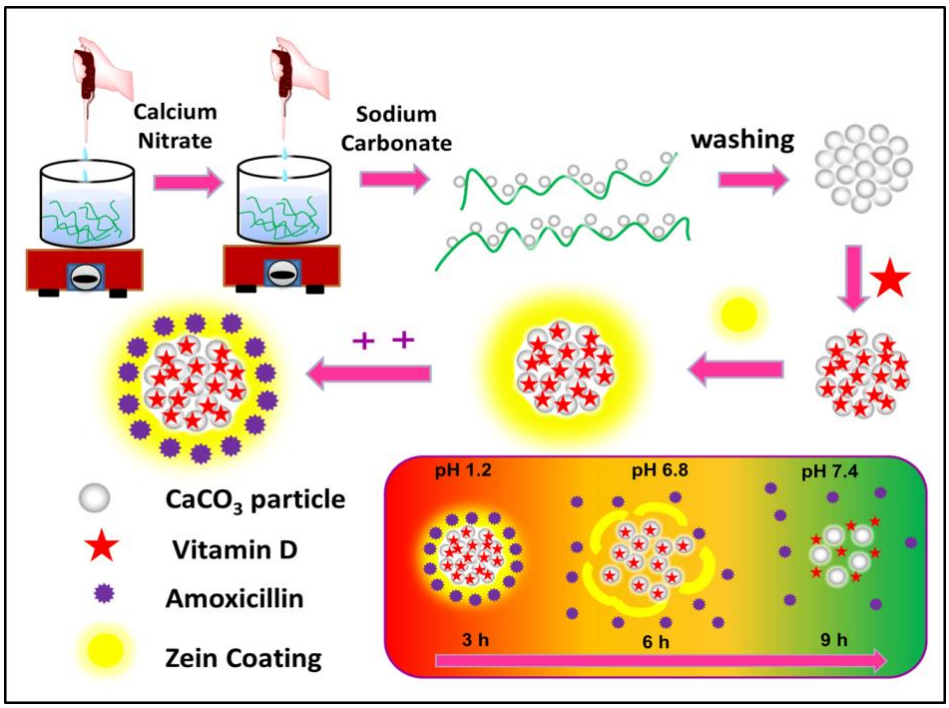

Fig. 3.1: Schematic diagram of the synthesis of $CaCO_3$ nanoparticles and the targeted sequential delivery of vitamin D and amoxicillin in the different pH conditions of the gastrointestinal tract.

3.2. Experimental Section

3.2.1. Materials

Calcium nitrate, zein and vitamin D were purchased from Sigma-Aldrich. Sodium carbonate was obtained from Qualigens Fine Chemicals, India. Gelatin was obtained from Loba chemie, India. Amoxicillin was procured from Titan Media Ltd., India. Milli-

Q water was used for all the experimental work. All the reagents were of analytical grade.

3.2.2. Methods

3.2.2.1. Preparation of $CaCO_3$ nanoparticles (CC)

1 % gelatin solution was prepared in 10 mM Trizma buffer solutions at pH 8.5. Once the gelatin was fully dissolved, a required amount of $Ca(NO_3)_2$ and Na_2CO_3 solutions were added sequentially to obtain 30 mM concentration of each under continuous stirring for 24 h at room temperature. After 24 h, centrifugation was carried out at 12000 rpm. The resultant white precipitate was washed with water and finally dried in an oven at 50 °C. A schematic illustration for the preparation of calcium carbonate nanoparticles (CC) is displayed in Fig. 3.2.

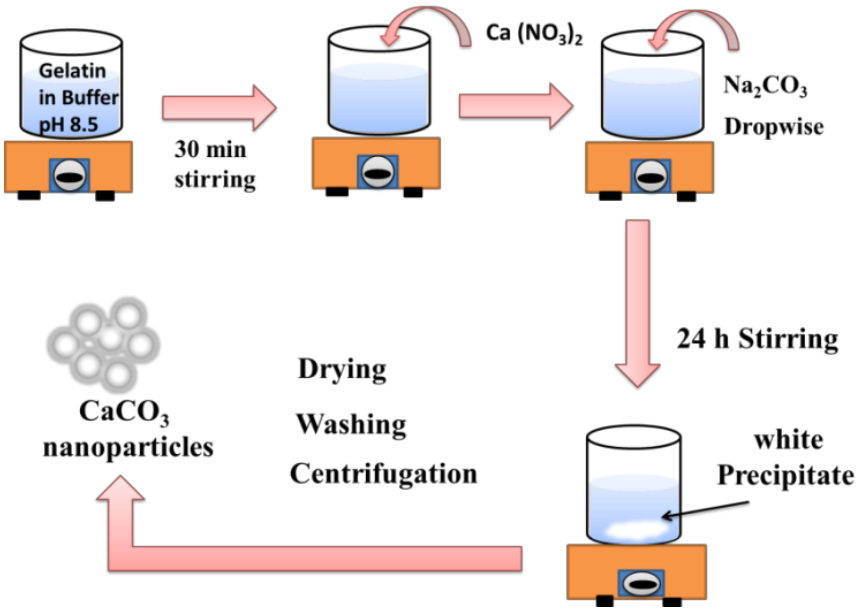

Fig. 3.2: A schematic illustration for the preparation of calcium carbonate nanoparticles (CC)

3.2.2.2. Circular Dichroism (CD) Spectropolarimetry

CD spectra of the template gelatin were recorded using a Jasco spectropolarimeter (model J-815) equipped with a Peltier thermostat controlled cell holder at 37 °C and a cuvette with a path length of 1 cm at pH 8.5 before and after sequential addition of each precursor used ($Ca(NO_3)_2$ and Na_2CO_3).

3.2.2.3. Vitamin D Encapsulation

As prepared 100 mg of the $CaCO_3$ nanoparticles were suspended in 10 mL of vitamin D (1 mg/mL) in ethanol, kept in water bath shaker at 37°C and stirred at 120 rpm. At an interval of every 1 h vitamin D encapsulation efficiency was determined till 24 h using UV-vis spectrophotometer (UV-1800 Shimadzu spectrophotometer) at wavelength 271 nm.[36] The encapsulation efficiency of vitamin D was calculated by the following equation.

$$\text{Encapsulation efficiency (EE)} = \frac{W_T - W_F}{W_T} \times 100 \qquad (3.1)$$

Where, W_T and W_F are the total weight of drug fed and non-encapsulated free drug, respectively. Herein, the time point of maximum vitamin D encapsulation was determined and the suspension was centrifuged at that time point to obtain the residue (CCD), washed with water and dried.

3.2.2.4. Zein coating on CCD

1 % (w/v) zein solution (prepared in 70% ethanol solution) was added drop-wise into the 20 mL suspension containing 100 mg of CCD under mild stirring carried out for 1 h.

Further, the suspension was centrifuged at 8000 rpm for 10 min. The obtained precipitate (CCDZ) was collected and dried in an oven at 50 °C.

3.2.2.5. Amoxicillin Encapsulation

100 mg of CCDZ nanoparticles were dispersed in 10 mL amoxicillin solution (10 mg/mL) in water and kept in a water bath shaker at 37 °C and 120 rpm. Here again, the time point of maximum amoxicillin encapsulation was determined using UV-vis spectrophotometer at wavelength 351 nm as explained in section 3.2.2.3. Further, amoxicillin encapsulated CCDZ suspension was centrifuged at the time point of maximum drug encapsulation to obtain CCDZA and dried.

3.2.3. Characterization of $CaCO_3$ nanoparticles

3.2.3.1. FTIR

The FTIR spectra of various $CaCO_3$ samples were recorded after pelletizing with KBr using NICOLET 380 FTIR spectrophotometer operating in the range of 4000-400 cm^{-1}.

3.2.3.2. XRD

Rigaku Miniflex-II operating at 20 kV and 10 mA using Cu-Kα radiation was used to record the XRD pattern of various $CaCO_3$ samples under investigation at room temperature in the 2θ range of 10° to 70° degree with a scan rate of 2°/min.

3.2.3.3. TGA

Thermogravimetric analysis of dried powders was carried out using Parkin Elmer TGA 4000. The powdered samples were heated from room temperature to 800 °C at a heating rate of 10 °C min^{-1} and a nitrogen flow of 20 mL min^{-1}.

3.2.3.4. BET

The porosity of the $CaCO_3$ nanoparticles was determined by nitrogen adsorption–desorption analysis at -196 °C using a Quantachrome Autosorb-1C TCD analyzer (Model ASICX- TCD6) and with nitrogen as adsorptive gas (N2, cross sectional area 0.162 nm^2). As per the standard BET protocol, before analysis, the sample was degassed under vacuum at 200 °C for 6 h. The surface area was determined using the Brunauer–Emmett–Teller (BET) equation on the nitrogen adsorption data obtained. The pore-size distribution was determined by the Barret-Joyner–Halenda (BJH) method applied to the desorption branch of the isotherm.

3.2.3.5. TEM

The morphology of the samples was characterized by Transmission electron microscope (JEOL JEM-1400) with an acceleration voltage of 120 kV. Powdered samples were suspended in methanol and the suspension was briefly sonicated for 15 min to ensure proper dispersion and to avoid aggregate formation.

3.2.3.6. Particle size and Zeta potential measurement

The particle size at a fixed angle of 173° and zeta potential of $CaCO_3$ nanoparticles was measured at each stage of $CaCO_3$ fabrication by Zetasizer Nano ZS (Malvern Instrument, UK) at 25° C. Water was used as a dispersant to record the zeta values. In addition, during *in-vitro* drug release also $CaCO_3$ nanoparticles were subjected to size analysis. Herein, for each sample zeta size and charge measurements were carried out in triplicates and averaged.

3.2.3.7. Erosion of zein coating

Erosion of zein protein was determined in SGF (pH 1.2) for 3 h and then in SIF (pH 6.8) for next 3 h and finally in SIF (pH 7.4) for 3 h at 37 °C. 100 mg of the zein coated $CaCO_3$ sample (CCDZA) was submerged in 20 mL of required simulated solutions at each time interval of 1 h. The suspension was centrifuged at 8000 rpm and the obtained residue was dried in oven and finally weighed. This procedure was performed in triplicates and their average was taken to calculate the erosion percentage according to the following equation:

$$\text{Erosion rate (\%)} = \frac{(\text{Wi}-\text{Wr})}{\text{Wi}} \times 100 \qquad (3.2)$$

Where, W_i is the initial weight and W_r is the remaining weight after dried.

3.2.3.8. MTT assay

The cytotoxicity of all $CaCO_3$ samples were examined by MTT assay as per the procedure described elsewhere.[37-40] The cell lines were maintained in cell culture facility in DMEM with high glucose content for Hep G2 and DMEM F12 media for HEK cell line. Both media were constituted with 10 % heat-inactivated fetal bovine serum and 0.1% penicillin/streptomycin at 37 °C with 5 % CO_2. The cells were seeded into 96 well plates at 10^4 cells per well and were incubated under standard culturing conditions. Once around 60 % confluency was achieved in the wells, the particles were added at a varying concentration ranging from 10 μg/mL to 1 mg/mL. Cells were incubated in their presence for 24 h after which they were subjected to MTT assay. MTT assay measures the reduction of the tetrazolium component (MTT) into formazan crystals by viable cells. Therefore, the level of reduction of MTT into formazan crystals can reflect the level of

cell metabolism. In order to carry out the assay, initially, 10 % MTT reagent was added along with Opti-MEM and incubated for 2 h at 37 °C under cell culture conditions. After two hours the plate was taken out and 100 μL of DMSO was added in each well to dissolve formazan crystals. After incubation, absorbance was taken at 570 nm using a TECAN multimode plate reader. The cell viability was calculated as described by Mishra *et al.*[41]

3.2.3.9. Release study

Release study of vitamin D and amoxicillin was carried out simultaneously using simulated solutions (SGF/SIF) at various pH values for 9 h. For this, a known weight of CCDZA was suspended in 20 mL of desired pH of simulated solutions and kept in water shaker bath for required time at 120 rpm. 1 mL solution was withdrawn from the release system at regular time intervals and subjected to quantitative analysis of vitamin D and amoxicillin using UV-vis spectrophotometer at wavelength 271 nm and 351 nm, respectively. The withdrawn 1 mL solution for quantitative analysis at every time was replaced by fresh solution. This procedure was carried out initially for 3 h in SGF at pH 1.2. Thereafter, the sample under investigation was centrifuged and resuspended in SIF at pH 6.8 for the next 3 h followed by in SIF at pH 7.4 for the last 3 h.

3.2.3.10. Drug release kinetics

In order to investigate the release kinetics, drug release data for vitamin D and amoxicillin were analyzed using various models (zero order, first order, Higuchi and Korsmeyer-Peppas). But the best-fitted data was found for Korsmeyar-Peppas model according to the following equation:

$$\frac{M_t}{M_\infty} = Kt^n \quad (3.3)$$

Where, M_t / M_∞ is the fraction of drug release at the time t. K is the kinetic constant and n is the release exponent, which describes the drug release mechanism.

3.3. Result and discussion

3.3.1. FTIR

The FTIR spectra of various $CaCO_3$ samples were shown in Fig. 3.3(a). In the case of CC, the characteristic peak at 1404 cm^{-1} was due to symmetrical $–COO^–$ stretching of carbonate ions and peaks at 872 cm^{-1} and 713 cm^{-1} correspond to the v_2 *and* v_3 $CO_3^{2–}$ absorption bands of calcite.[42,43] This observation confirmed the presence of carbonate ions in CC. In the spectrum of CCD, two new peaks observed at 3300 cm^{-1} and 1063 cm^{-1} corresponds to –OH stretching[16] and asymmetric –C–O vibration of encapsulated vitamin D, respectively. Interestingly, a significant shift in symmetrical $–COO^–$ stretching of carbonate ions from 1404 cm^{-1} to 1428 cm^{-1} was reported for CCD, which indicates an interaction between carbonate groups and vitamin D molecules through physical forces. In the case of CCDZ, the peaks observed at 3401 cm^{-1}, 2854 cm^{-1}, 1647 cm^{-1} are attributed to –O–H stretching, –C–H stretching and an overlap of –O–H bending and amide I band, respectively.

The intensified amide I band in CCDZ confirmed the coating of zein protein around $CaCO_3$ nanoparticles compared to CCD. Herein, other peaks due to carbonate ions at 1428 cm^{-1}, 1063 cm^{-1} and 872 cm^{-1} were retained as seen in CCD. It is noteworthy that in the case of CCDZA, peaks correspond to –O–H stretching, and overlap of –O–H bending and amide I band were shifted to higher wavenumbers at 3443 cm^{-1} and 1686 cm^{-1}, respectively, compared to CCDZ. –C=O stretching peak at 1775 cm^{-1} appeared at lower

wavenumber compared to CCDZ. These observations indicate the physical interaction of loaded amoxicillin with coated zein molecules in CCDZA.[44]

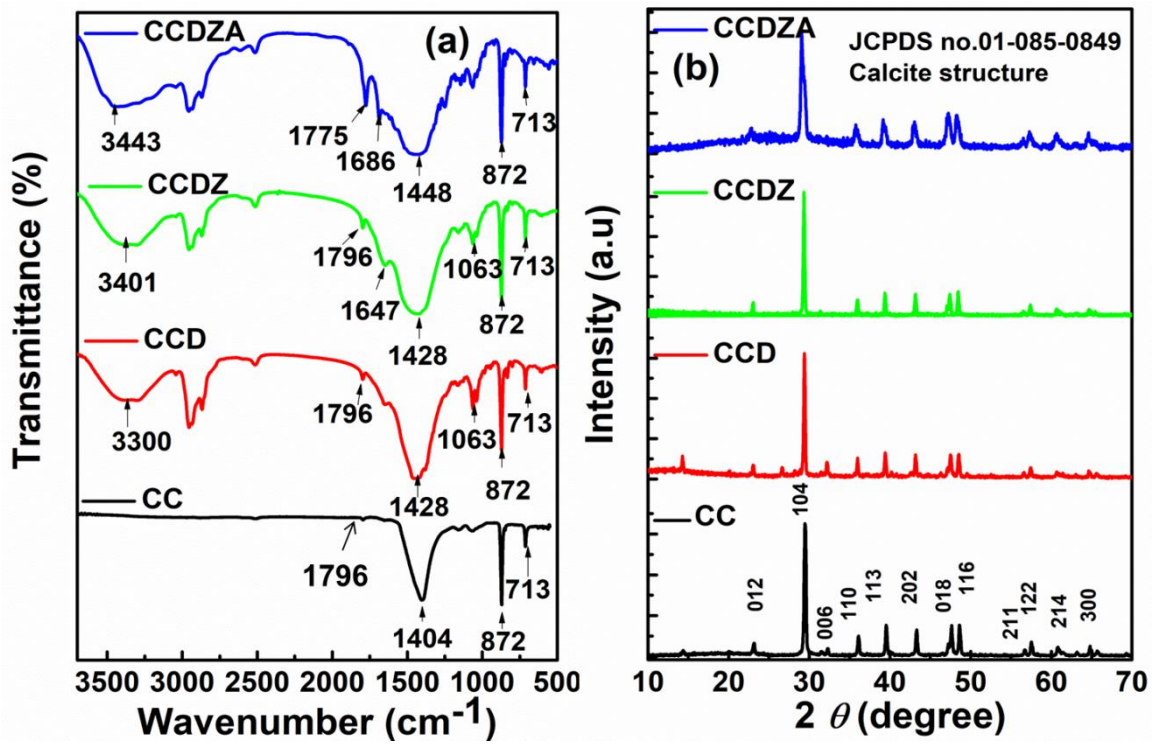

Fig. 3.3: (a) FTIR spectra and (b) XRD patterns of CC, CCD, CCDZ and CCDZA.

3.3.2. XRD

Fig. 3.3(b) depicts XRD spectrum of various $CaCO_3$ samples. For pure $CaCO_3$ (CC), a series of characteristic peaks (23.1°, 29.5°, 32.3°, 36.1°, 39.5°, 43.3°, 47.7°, 48.6°, 57.5°, 60.8° and 64.8°) was observed and it can be assigned as (012), (104), (006), (110), (113), (202). (018), (116), (122), (214) and (300), respectively. These peaks are consistent with the standard pattern JCPDS no 01-085-0849, which indicates that $CaCO_3$ nanoparticles

are of pure calcite crystals with rhombohedral crystal system.[45,46] After loading vitamin D (CCD), followed by zein coating (CCDZ) and finally encapsulating with amoxicillin (CCDZA), the crystal structure of $CaCO_3$ remains same as the rhombohedral crystal system. The mean crystallite size (D) of various $CaCO_3$ nanoparticles was calculated by the Debye-Scherrer equation.[47]

$$D(nm) = \frac{K\lambda}{\beta \cos\theta} \qquad (3.4)$$

Where, K is a constant (K= 0.9 for Cu-K_α), λ is a wavelength (0.15406 nm), β is the full width of half-maximum (FWHM) and θ is the diffraction angle (Table 3.1). It is clear from the Table 1 that the crystallite size of CC (15.7 nm) changes with vitamin D loading (17.4 nm), zein coating (22.5 nm), and encapsulating with amoxicillin (25.7 nm), where an increase in the crystallite size was observed. It is possible that subsequent steps of loading vitamin D, coating zein and loading of the second cargo (amoxicillin) encapsulation might have led to growth of smaller sized CC into larger crystallite sizes.

Table 3.1: Data obtained from XRD analysis of various $CaCO_3$ nanoparticles using the Debye-Scherrer equation[47]

Parameters	**CC**	**CCD**	**CCDZ**	**CCDZA**
FWHM (β)	0.48931	0.44983	0.36454	0.31136
Crystallite size (*D*) (nm)	15.69	17.4	22.5	25.74

3.3.3. TGA

The TGA thermograms of non-zein coated (CC and CCD) and zein coated (CCDZ and CCDZA) $CaCO_3$ particles are depicted in Fig. 3.4(a). In the case of CC, the first decomposition was seen at 170 °C due to water evaporation, second decomposition began at 337 °C and ended at about 730 °C, with 31 % weight loss due to the decomposition of $CaCO_3$ to calcium oxide accompanied by loss of carbon dioxide.[45] For CCD, first decomposition was reported around 357 °C with weight loss of 10%, indicating the presence of vitamin D molecules and was found to be in good agreement with the thermogram of pure vitamin D (data not shown).

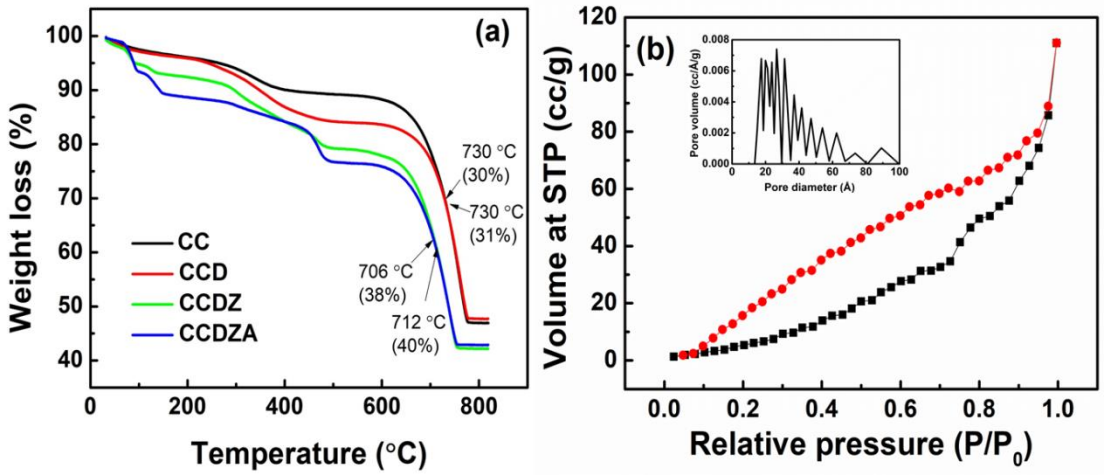

Fig. 3.4: (a) TGA thermograms of CC, CCD, CCDZ and CCDZA (b) Nitrogen adsorption-desorption isotherm of $CaCO_3$ nanoparticles inset shows pore size distribution.

This was followed by decomposition of $CaCO_3$ at 730 °C with 30 % weight loss. Herein, it is noteworthy that water loss was not reported due to the encapsulation of vitamin D in ethanol. In the case of zein coated samples CCDZ and CCDZA, the initial weight loss was observed of about 8 % at the temperature 101 °C for CCDZ and at 105 °C for

CCDZA due to loss of water. In comparison to thermograms of pure vitamin D and zein (data not shown), decomposition of vitamin D, as well as depolymerization of zein, was reported at 337 °C with 13 % weight loss in case of CCDZ, followed by further degradation of the polymer at 437 °C with 18 % weight loss and finally decomposition of $CaCO_3$ was seen at 706 °C with 38 % weight loss. The decomposition of CCDZA was also found to be more or less similar to CCDZ with three decomposition steps at 326 °C (14 wt %), 453°C (19 wt %) and 712 °C (40 wt %), respectively. Herein, the decomposition of amoxicillin was not specifically noticed. At 706 °C, 26 % weight loss for non-coated $CaCO_3$ and 38 % for zein coated $CaCO_3$ was observed. From the observation, it can be concluded that non coated $CaCO_3$ nanoparticles were of high thermal stability compared to zein coated $CaCO_3$ nanoparticles. Differences observed in the thermograms of CC, CCD, CCDZ and CCDZA confirm the existence of zein and vitamin D in the corresponding samples.

3.3.4. BET

The N_2 adsorption-desorption isotherm analysis on CC was investigated by BET method and results indicated that the sample exhibited an IUPAC type V isotherm pattern with hysteresis loop 4 (Fig. 3.4(b)). The reported isotherm pattern and the hysteresis loop revealed that CC particles consist of slit-like meso as well as micro-sized pores (Fig. 3.4 (b)). The pore size distribution analysis carried out by BJH method further confirms the existence of multi-sized (micro and meso) pores with the diameter ranging from 1.8 to 6.0 nm (inset Fig. 3.4(b)) and pore volume 0.28 cc/g. The obtained pore diameter range further revealed that CC consisted of a small number of micro and a large number of mesopores. The calculated surface area for CC using BET was found to be 296 m^2/g,

which is very high compared to the commercial $CaCO_3$ powder (19.27 m^2/g),[48] indicating very small particle size of CC.

3.3.5. TEM

The surface morphology of CC and CCDZA samples were shown in Fig. 3.5(a) and 3.5(c). TEM images of CC and CCDZA both samples exhibited nanosize range and were observed to be agglomerated. The average particle size was determined using ImageJ-analysis (data not shown) to be in the range of 10-15 nm for CC and 20-25 nm for CCDZA.

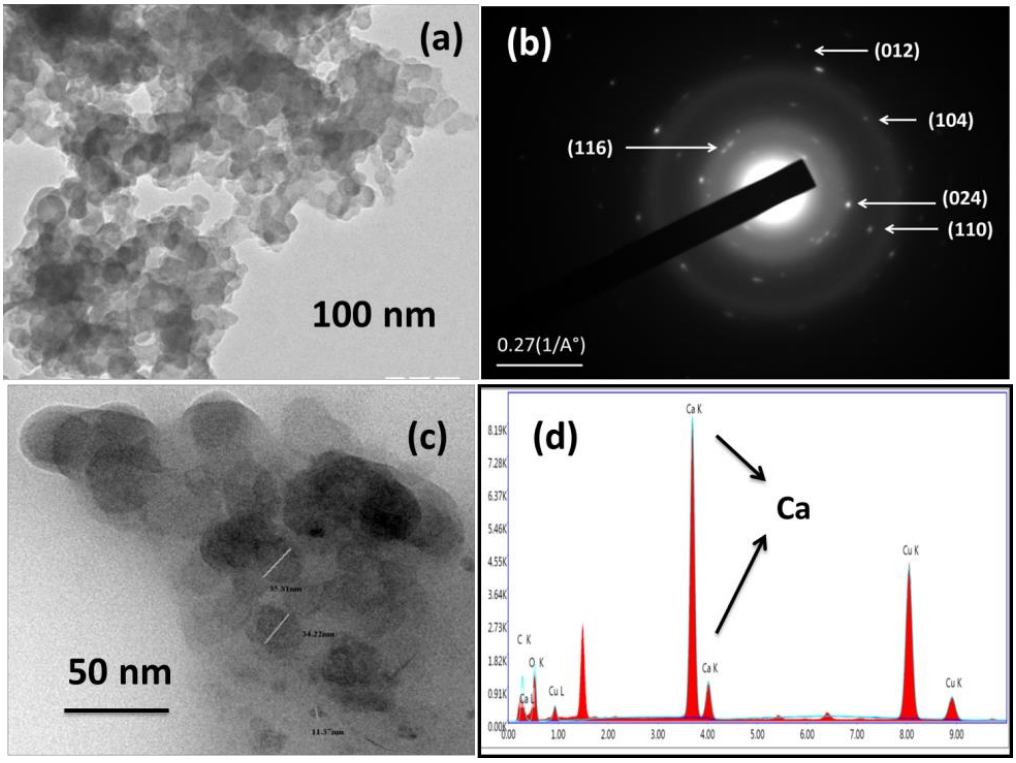

Fig. 3.5: TEM images (a) CC and (c) CCDZA (b) SAED pattern of CC and (d) EDX analysis on CC.

The observed size ranges by TEM of CC and CCDZA are in good agreement with the corresponding estimated average crystallite size using XRD data (Table 3.1, Section 3.3.2). The reported SAED pattern and EDX analysis of CC (Fig. 3.5(b) and 3.5(d)) confirmed the existence of characteristic (024), (012), (104), (110) and (116) planes of pure calcite crystals with rhombohedral crystal system as observed by XRD analysis (Fig. 3.3(b), CC).

3.3.6. Encapsulation efficiency

Vitamin D encapsulation (Fig. 3.6(a)) on CC was observed to be 62.6 % at 4 h and remained almost similar till 24 h. Similarly, from 5 h to 24 h, amoxicillin encapsulation was observed to attain saturation around 89.4 % (Fig. 3.6(a)).

3.3.7. Plausible mechanisms for $CaCO_3$ nanoparticles synthesis and following surface modifications

In this investigation, nano-sized $CaCO_3$ particles were synthesized through a bio-inspired route using gelatin as a template at pH 8.5. $Ca(NO_3)_2$ and Na_2CO_3 precursor solutions were added sequentially to the gelatin solution at pH 8.5 for the reaction to take place (Section 3.2.2.1 and Fig. 3.2). In order to elucidate the molecular interaction or the nature of modulation of the gelatin conformational changes occurring during the sequential addition of precursors, gelatin CD signatures were recorded at each step (Fig. 3.6(b)). As reported, gelatin at pH 7.0 is known to have a negative peak at 205 nm suggesting a random coil conformation and a positive peak at 222 nm suggesting triple-helical conformation.[49,50] In this study, the gelatin at pH 8.5 was showing similar negative peak at around 205 nm and a comparatively slightly negative at around 220 nm at 37 °C due to thermal denaturation[51] (Fig. 3.6(b)). This suggests that the overall conformation of

gelatin may have undergone a slight alteration at pH 8.5.[52] When $Ca(NO_3)_2$ was added to the gelatin solution, the obtained CD signal indicates a distortion possibly due to the addition of the salt. The obtained CD signature by the addition of Na_2CO_3 to the gelatin-$Ca(NO_3)_2$ matrix was found to be considerably smoothened and registered the signature negative peak of gelatin molecule at a higher wavelength with significant lower amplitude. Also, the peak at 220 nm underwent an increase in its amplitude and shifted to a slightly shorter wavelength. Since the isoelectric point of gelatin has been reported around 4.88,[53] the positively charged residues of the gelatin molecule are expected to interact with the excess negative charged counter ions at pH 8.5. The overall charge of gelatin should be more negative at pH 8.5. This can cause a shift in conformation from random coil towards a more ordered structure. Based on this, it is hypothesized that the addition of $Ca(NO_3)_2$ to the gelatin matrix opens up more number of nucleation sites for the interaction of hydroxylated calcium ions[53] (Fig. 3.6(c)). Following this, the addition of Na_2CO_3 in the gelatin-$Ca(OH)_2$ matrix results in the formation of nano sized calcium carbonate by hetero nucleation on the gelatin chains. Herein, the added calcium ions on gelatin chain cause a distortion of CD signature in the alkaline surrounding. Further, the addition of Na_2CO_3 led to the formation of $CaCO_3$ at the sites of gelatin-$Ca(OH)_2$ interaction. Consequently, the distortion observed in the CD spectrum on adding Na_2CO_3 was reduced.[54] As evidenced by FTIR analysis during the sequential addition of precursors (data not shown), the interaction of the hydroxylated Ca^{2+} is mostly through amide I and carboxylate anions of gelatin molecules. Nucleation of $CaCO_3$ was taken place at the interaction sites of Ca^{2+} on gelatin upon the addition of Na_2CO_3 solution.

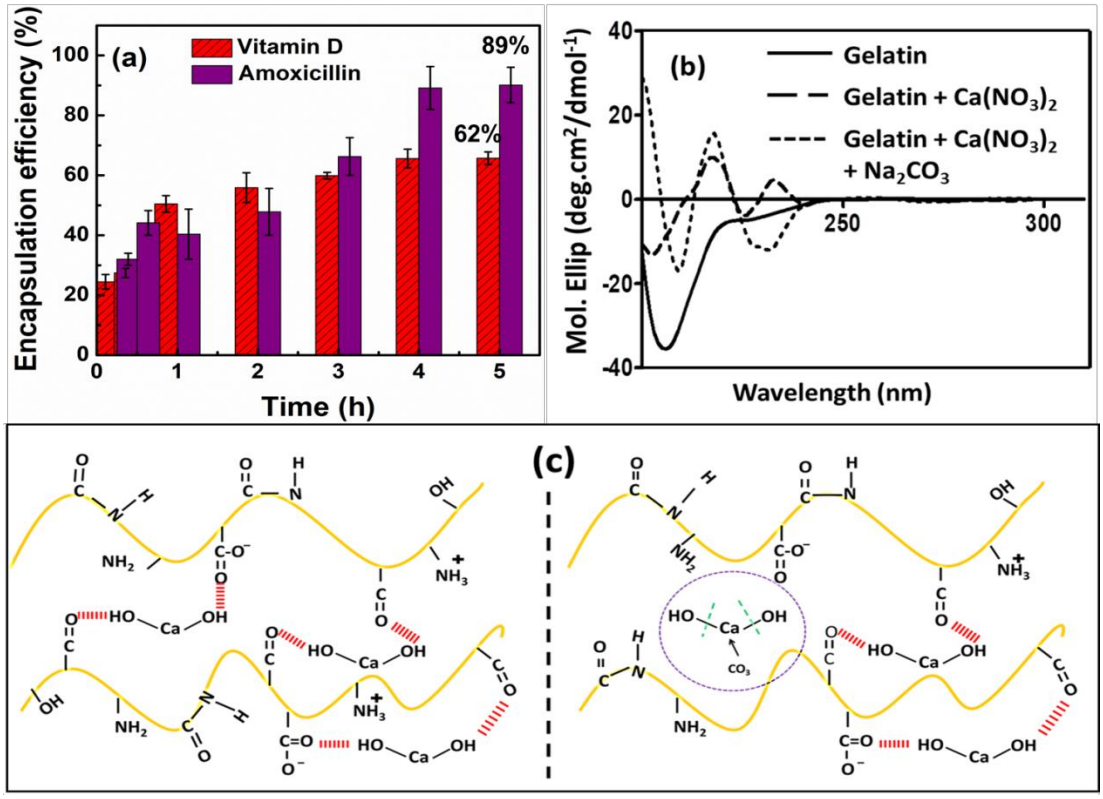

Fig. 3.6: (a) Encapsulation efficiency of vitamin D and amoxicillin, (b) gelatin CD signatures at pH 8.5 (c) Schematic diagram showing nucleation of $CaCO_3$ nanoparticles.

The resulted porous nanoparticles (CC) were subjected to zeta potential measurements (Fig. 3.7(a)) and the corresponding surface charge was determined as -21.8 mV. Change in zeta potential value of $CaCO_3$ after vitamin D encapsulation (-0.01) further confirms the corresponding interaction as observed in FTIR studies (section 3.3.1). Zeta potential of CCDZ (-2.72 mV) and CCDZA (0.367 mV) is more or less same, which indicate interaction of CCD with zein and CCDZ with amoxicillin is only through hydrogen bonding and Van der Waals forces (Fig. 3.3(a)). Interestingly, hydrodynamic particle size (Fig. 3.7(b)) of various $CaCO_3$ particles determined in water by Malvern zetasizer was in the order of CC (335 nm) ≈ CCD (355.2 nm) < CCDZA (463.5 nm) << CCDZ (877.9

nm). The observed hydrodynamic size of zein coated CCD was due to well-known chain and loop conformation of adsorbed polymer on inorganic particles. On the other hand, coated zein molecules were compacted by amoxicillin due to their corresponding physical interaction, as observed by FTIR spectroscopy (Fig. 3.3(a)). Besides, Fig. 3.7(c) and 3.7(d), portray zeta size of $CaCO_3$ particles at various pH conditions before and after coating with zein, respectively.

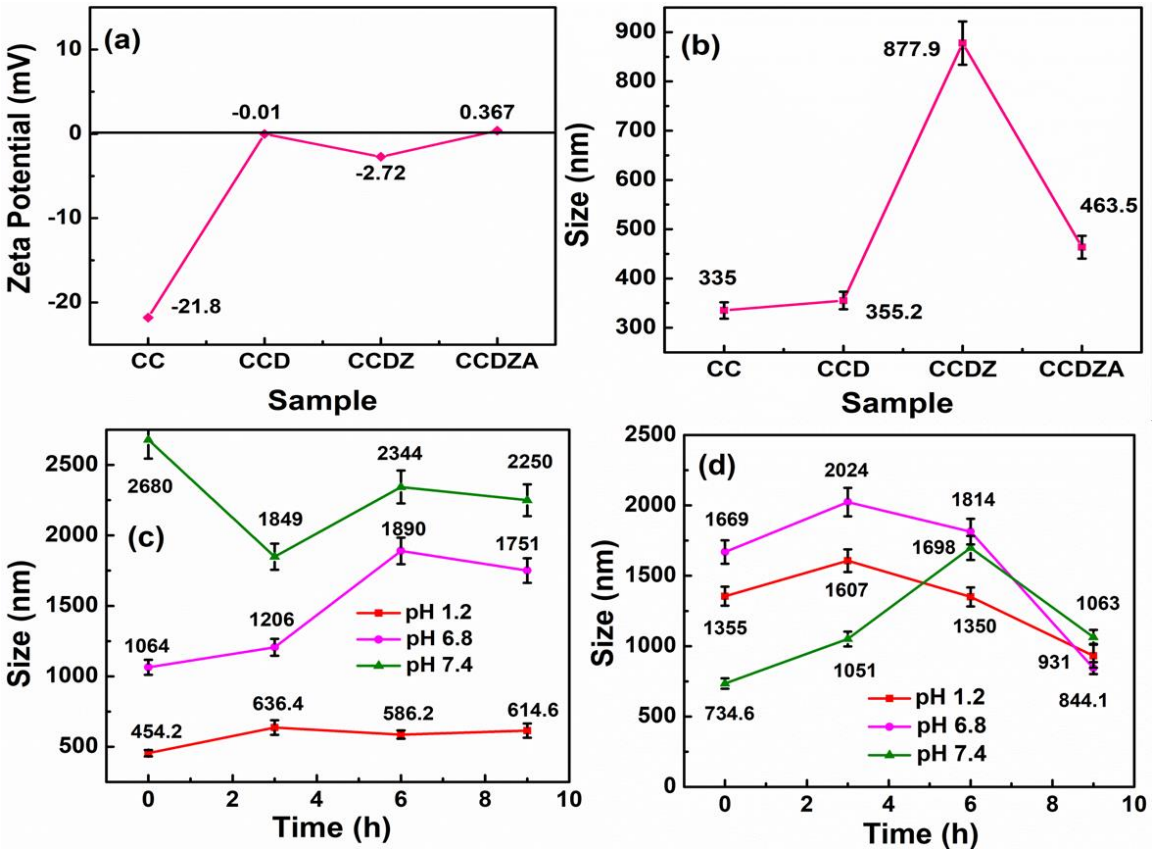

Fig. 3.7: (a) Zeta potential (b) Size distribution of as synthesized CC, CCD, CCDZ and CCDZA (c) without coated nanoparticles (d) coated nanoparticles at various pH conditions.

The size of the non-coated particles was observed to be increased due to surface hydroxylation. On the other hand, zeta size of zein coated $CaCO_3$ particles was slightly increased upto 6 h in the reported pH conditions and, after that, decreased due to the erosion of zein coating.

3.3.8. Erosion of zein coating

As shown in Fig. 3.8(b), erosion of zein coating was feeble in the initial 2 h (10 %). However in the next 6 h, it was observed that the erosion of zein increased to 70 %. After 6 h erosion continued and reached 100 % at 8 h.[55]

3.3.9. In-vitro targeted control release study

During initial phase of the release study shown in (Fig. 3.8(a)), in SGF at pH 1.2, a feeble amoxicillin release was reported in the first 3 h but vitamin D release was not observed. This observation confirmed that zein coating on $CaCO_3$ particles were intact upto 3 h due to the insoluble nature of zein in water. Further, due to the hydrophobic nature of zein, amoxicillin release remained hindered during this period. However, post 3 h in SIF solution at pH 6.8, a burst release of amoxicillin (80 %) was reported and release was maintained at around 80 % up to 6 h and at pH 7.4 from 6 h to 9 h. The burst drug release post 3 h from zein coated particles indicates the erosion of the water insoluble protein layer. It is noteworthy that a feeble amount of vitamin D was released (10 % to 20 %) from 3 h to 5 h. At 6 h, the release of vitamin D was found to have been initiated. Thereafter, the release continued gradually to till 9 h. By 9 h, 90 % vitamin D was found to be released from the nanoparticles. The gradual and controlled release of vitamin D molecule might be attributed to the porous structure of $CaCO_3$ nanoparticles as observed through BET analysis.

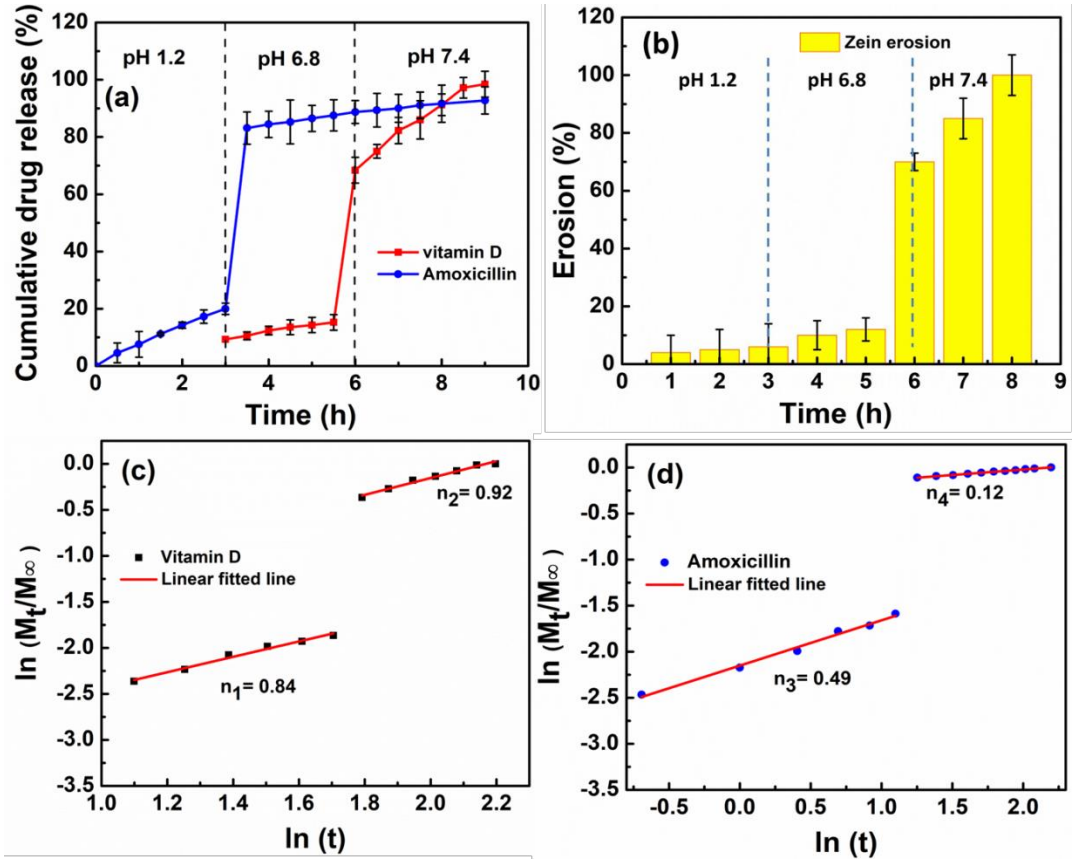

Fig. 3.8: (a) Cumulative release % with different time intervals at pH 1.2, 6.8 and 7.4 (b) Erosion of zein at different time intervals (c) and (d) Korsmeyer- peppas model by plotting ln (Mt/M∞) versus ln (t) for vitamin D and amoxicillin.

3.3.10. Kinetic modelling

The drug release kinetics data of vitamin D and amoxicillin as shown in Fig. (3.8(c) and 3.8(d)), were fitted with different kinetic models (Table 3.2). The correlation coefficient (r^2) was calculated and release exponent (n) was estimated from the slope of the plot of ln (M_t/M_∞) versus ln (t) and their values were indicated in the plot. The highest value of (r^2) for both vitamin D and amoxicillin in SGF and SIF was observed for Korsmeyer-Peppas model.

Table 3.2: Correlation coefficients (r^2) of different Models in SGF and SIF Solutions.

Model	Vitamin D		Amoxicillin	
	SGF	SIF	SGF	SIF
Zero order	0.9852	0.9871	0.9828	0.9774
First order	0.9482	0.9778	0.9614	0.9489
Higuchi	0.9563	0.9854	0.9776	0.9415
Peppas	**0.9899**	**0.9882**	**0.9915**	**0.9978**

The value of n in this model determines the release mechanism. In this study, the calculated n value for amoxicillin in SGF and SIF was 0.4 and 0.1, respectively, indicating Fickian diffusion mechanism. Whereas, in the case of vitamin D, the value of n was found to be 0.8 in SGF and 0.9 in SIF confirming the non-Fickian transport and super case II transport mechanism, respectively.[56]

3.3.11. MTT assay

One of the main objectives of the study was to assess the biocompatibility of the $CaCO_3$ nanoparticles on liver and kidney cell. As the aim is to orally deliver the $CaCO_3$ along with vitamin D and other components, it becomes imperative that once in the body the nanoparticles will be exposed to liver and kidney. The high vascularity as well as the first pass metabolism makes it important that the particles and its constituents does not have any detrimental effect on the organs. Also the vitamin D is activated by a two-step process, first by the liver and then by the kidneys. As such to assess if the exposure does not cause any significant toxicity to the liver and kidney, MTT assay was performed on

CCDZA sample at varying concentrations on kidney (HEK cell line) and liver (Hep G_2 cell line). The assay was carried out post 24 h exposure of the samples to the cell lines and results were displayed in Fig. 3.9. From the Figure, it was evident that viability of both the cell lines was observed above 90 % for the concentration range 10 μg/mL to 1000 μg/mL. The results revealed that CCDZA is a safe candidate for oral delivery.

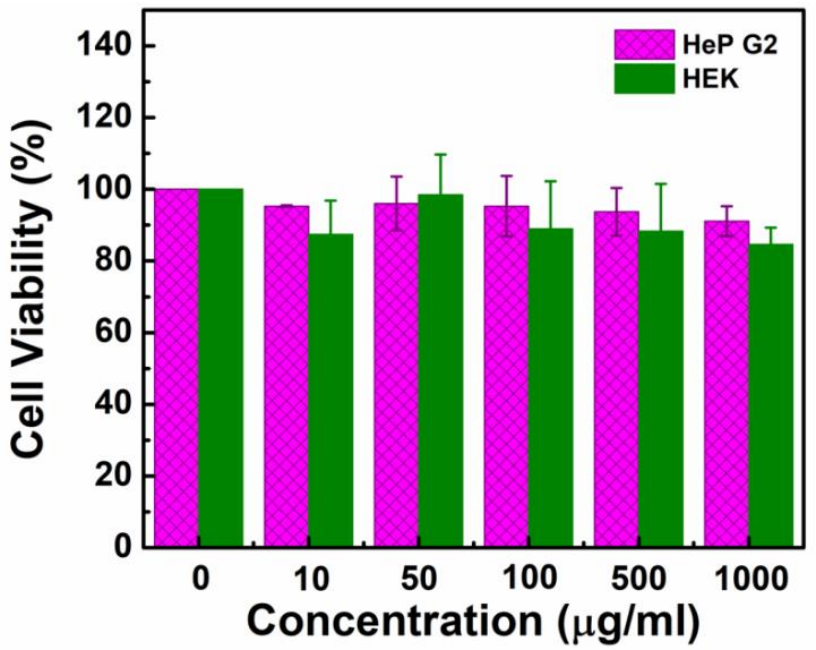

Fig. 3.9: Cytotoxicity test of CCDZA at different concentrations using HepG2 and HEK.

3.4. Conclusion

The study shows that similar to calcium and vitamin D supplementation, $CaCO_3$ nanoparticles can act as a viable GIT delivery vehicle coupled to vitamin D delivery to the intestine. Specific coatings like zein on nanoparticles would help to resist the

corrosive environment of the GIT while facilitating a second cargo loading. Further, the coating can render controlled release for both cargoes. Overall the system was developed focusing on maintaining Vitamin D – Calcium homeostasis that occurs mostly at the intestine while at the same time with a capacity to deliver a model antibiotic to the gut simultaneously**.**

References

[1] M.J. Glade, Vitamin D: health panacea or false prophet, Nutrition 29 (2013) 37-41.

[2] J. Hilger, A. Friedel, R. Herr, T. Rausch, F. Roos, D.A. Wahl, D.D. Pierroz, P. Weber, K. Hoffmann, A systematic review of vitamin D status in populations worldwide, Br. J. Nutr. 111 (2014) 23-45.

[3] L.A. Plum, H.F. DeLuca, Vitamin D, disease and therapeutic opportunities, Nat. Rev. Drug Disc. 9 (2010) 941-55.

[4] S.M. Jeon, E.A. Shin, Exploring vitamin D metabolism and function in cancer. Exp. Mol. Med. 50 (2018) 1-14.

[5] J. Feige, H. Salmhofer, C. Hecker, A.B. Kunz, M. Franzen, E. More, J. Sellner, Life-threatening vitamin D intoxication due to intake of ultra-high doses in multiple sclerosis: a note of caution, Mul. Scler. J. Exp. Transl. Clin. (Phila) 25 (2019) 1326-1328.

[6] K. Rajakumar, E.C. Reis, M.F. Holick, Dosing error with over-the-counter vitamin D supplement: a risk for vitamin D toxicity in infants, Clin. Pediatr. 52 (2013) 82-85.

[7] P. Borel, D. Caillaud, N.J. Cano, Vitamin D bioavailability: state of the art, Crit. Rev.FoodSci. Nutr. 55 (2015) 1193-1205.

[8] A.J. Hodgkinson, O.A.M. Wallace, M.C. Kruger, C. G. Prosser, Effect of the dietary delivery matrix on vitamin D3 bioavailability and bone mineralisation in vitamin-D3-deficient growing male rats, Br. J. Nutr. 119 (2018) 143-152.

[9] T.B. Drueke, E. Ritz, Treatment of secondary hyperparathyroidism in CKD patients with cinacalcet and/or vitamin D derivatives, Clin. J. Am. Soc. Nephrol. 4 (2009) 234-241.

[10] J.R. Wu-Wong, M. Nakane, G.D. Gagne, K.A. Brooks, W.T. Noonan, Comparison of the pharmacological effects of paricalcitol and doxercalciferol on the factors involved in mineral homeostasis, Int. J. Endocrinol. (2010) 621687.

[11] C. Leyssens, L, Verlinden, A. Verstuyf, The future of vitamin D analogs, Front. Physiol. 5 (2014) 122.

[12] V.K. Mauryaa, K. Bashirb, M. Aggarwal, Vitamin D microencapsulation and fortification: trends and technologies, J. Steroid Biochem. Mol. Biol. 196 (2020) 105489**.**

[13] R. Gupta, C. Behera, G. Paudwal, N. Rawat, A. Baldi, P.N. Gupta, Recent advances in formulation strategies for efficient delivery of vitamin D. AAPS Pharm. Sci. Tech. 20 (2018) 11.

[14] E. Glowka, J. Stasiak, J. Lulek, Drug delivery systems for vitamin D supplementation and therapy, Pharmaceutics. 11 (2019) 347.

[15] Y. Luo, T.Z. Eng, X. Wang, Q. Wang, Development of carboxymethyl chitosan hydrogel beads in alcohol-aqueous binary solvent for nutrient delivery applications, Food Hydrocoll. 31 (2013) 332-339.

[16] Y. Luo, Z. Teng, Q. Wang, Development of zein nanoparticles coated with carboxymethyl chitosan for encapsulation and controlled release of vitamin D3, J. Agric. Food Chem. 60 (2012) 836-843.

[17] B. Ozturk, S. Argin, M. Ozilgen, D.J. McClements, Nanoemulsion delivery systems for oil-soluble vitamins: influence of carrier oil type on lipid digestion and vitamin D3 bioaccessibility, Food chem. 187 (2015) 499-506.

[18] M. Guttoff, A.H. Saberi, D.J. McClements, Formation of vitamin D nanoemulsion-based delivery systems by spontaneous emulsification: factors affecting particle size and stability, Food Chem. 171 (2015) 117-122.

[19] C.Y. Hsu, P.W. Wang, A. Alalaiwe, Z.C. Lin, J.Y. Fang, Use of lipid nanocarriers to improve oral delivery of vitamins, Nutrients, 11 (2019) 68.

[20] C. Bothiraja, A. Pawar, G. Deshpande, Ex-vivo absorption study of a nanoparticle based novel drug delivery system of vitamin D3 (Arachitol NanoTM) using everted intestinal sac technique, J. Pharm. Investig. 46 (2016) 425-432.

[21] D.K. Mishra, R. Shandilya, P.K. Mishra, Lipid based nanocarriers: a translational perspective Nanomedicine: nanotechnology, Biolo. Med. 14 (2018) 2023-2050.

[22] G. Parisa, M.S. Soliman, Solid lipid nanoparticles and nanostructured lipid carriers as novel drug delivery systems: applications, advantages and disadvantages**,** Res. Pharm. Sci. 13 (2018) 288-303.

[23] S.G. Carvalho, V.H.S. Araujo, A.M. Santos, J.L. Duarte, A.L.P. Silvestre, B. Fonseca-Santos, J.C.O.Villanova, M. P. D. Gremião, Advances and challenges in nanocarriers and nanomedicines for veterinary application, Int. J. Pharm. 580 (2020) 1192147.

[24] B. Daglar, E. Ozgur, M.E. Corman, L. Uzun, G.B. Dem, Polymeric nanocarriers for expected nanomedicine: current challenges and future prospects, RSC Adv. 4 (2014) 48639-48659.

[25] S. Sharma, A. Verma, B.V. Teja, G. Pandey, N. Mittapelly, R. Trivedi, P.R. Mishra, An insight into functionalized calcium based inorganic nanomaterials in biomedicine: trends and transitions, Colloids Surf. B Biointerfaces 133 (2015) 120-139.

[26] N. Khazai, S.E. Judd, V. Tangpricha, Calcium and Vitamin D: Skeletal and Extra skeletal Health, Curr. Rheumatol. Rep. 10 (2008) 110-117.

[27] M.K. Kim, J.A. Lee, M.R. Jo, M.K. Kim, H.M. Kim, J.M. Oh, N.W. Song, S.J. Choi, Cytotoxicity, uptake behaviors, and oral absorption of food grade calcium carbonate nanomaterials, Nanomaterials. 5 (2015) 1938-1954.

[28] D. Render, T. Samuel, H. King, M. Vig, S. Jeelani, R.J. Babu, V. Rangari, Biomaterial-derived calcium carbonate nanoparticles for enteric drug delivery, J. Nanomater. (2016) 3170248.

[29] B.E. Nordin, Evolution of the calcium paradigm: the relation between vitamin D, serum calcium and calcium absorption, Nutrients. 2 (2010) 997-1004.

[30] S. Christakos, P. Dhawan, A. Porta, L.J. Mady, T. Seth, 2011. Vitamin D and intestinal calcium absorption, Mol. Cell. Endocrinol. 347 (2011) 25-29.

[31] R. Vieth, Vitamin D toxicity, policy, and science, J. Bone Miner. Res. 22 (2007) 64-68.

[32] J. lee, M.K. Kim, H.M. Kim, J.K. Lee, J. Jeong, Y.R. Kim, J.M. Oh, S.J. Choi, The fate of calcium carbonate nanoparticles administered by oral route: absorption and their interaction with biological matrices, Int. J. Nanomedicine 10 (2015) 2273-2293.

[33] D. Santhiya, H. Alajangi, F. Anjum, S. Murugavel, M. Ganguli, Bio-inspired synthesis of microporous bioactive glass-ceramic using CT-DNA as a template, J. Mater. Chem. B Mater. biolo. Med. 1 (2013) 6329-6338.

[34] F.F.O. Sousa, A. Luzardo-Alvarez, A. Perez-Estevez, R. Seoane-Prado, J. Blanco-Mendez, Development of a novel AMX-loaded PLGA/zein microsphere for root canal disinfection, Biomed. Mater. 5 (2010) 055008.

[35] C.H. Chang, Y.H. Lin, C.L. Yeh, Y.C. Chen, S.F. Chiou, Y.M. Hsu, Y.S. Chen, C.H. Wang, Nanoparticles incorporated in pH-sensitive hydrogels as amoxicillin delivery for eradication of Helicobacter pylori, Biomacromolecules. 11 (2009) 133-142.

[36] Y. Luo, Z. Teng, X. Wang, Q. Wang, Development of carboxymethyl chitosan hydrogel beads in alcohol-aqueous binary solvent for nutrient delivery applications, Food Hydrocoll. 31 (2013) 332-339.

[37] B. Tyliszczak, A. Drabczyk, S. Kudłacik-Kramarczyk, K. Bialik-Wąs, A. Sobczak-Kupiec, In vitro cytotoxicity of hydrogels based on chitosan and modified with gold nanoparticles. J. Polym. Res. 24 (2017), 153.

[38] S. Vijayakumar, S. Ganesan, In vitro cytotoxicity assay on gold nanoparticles with different stabilizing agents, J. Nanomater. (2012) 734398.

[39] E. Lee, H. Jeon, M. Lee, J. Ryu, C. Kang, S. Kim, J. Jung, Y. Kwon, Molecular origin of AuNPs-induced cytotoxicity and mechanistic study. Sci. Rep. 9 (2019) 2494.

[40] M. Calero, M. Chiappi, A. Lazaro-Carrillo, M.J. Rodríguez, F.J. Chichón, K. Crosbie-Staunton, A. Prina-Mello, Y. Volkov, A. Villanueva, J.L. Carrascosa, Characterization of interaction of magnetic nanoparticles with breast cancer cells, Int.J. Nanobiotechnology. Pharm. 13 (2015) 16.

[41] R.K. Mishra, M. Datt, A.K. Banthia, Synthesis and characterization of pectin/PVP hydrogel membranes for drug delivery system, AAPS Pharm. Sci. Tech. 9 (2008) 395-403.

[42] J. Wang, J.S. Chen, J.Y. Zong, D. Zhao, F. Li, R.X. Zhuo, S.X. Cheng, Calcium Carbonate/Carboxymethyl chitosan hybrid microspheres and nanospheres for drug delivery, J. Phys. Chem. C**,** 114 (2010) 18940-18945.

[43] Z. Xu, G. Liang, L. Jin, Z. Wang, C. Xing, Q. Jiang, Z. Zhang, Synthesis of sodium caseinate-calcium carbonate microspheres and their mineralization to bone-like apatite. J. Cryst. Growth 395 (2014) 116-122.

[44] P. Franco, E. Reverchon, I.D. Marco, 2019 Production of zein/antibiotic microparticles by supercritical antisolvent co-precipitation, J. Supercrit. Fluids 145 (2019) 31-38.

[45] L. Zhao, Y. Zhang, Y. Miao, L. Nie, Controlled synthesis, characterization and application of hydrophobic calcium carbonate nanoparticles in PVC, Powder Technol. 288 (2016) 184-190.

[46] Y. Chen, X. Ji, G. Zhao, X. Wang, Facile preparation of cubic calcium carbonate nanoparticles with hydrophobic properties via a carbonation route, Powder Technol. 200 (2010) 144-148.

[47] R. Singh, V. Luthra, R.S. Rawat, R.P. Tandon, Structural, dielectric and piezoelectric properties of $SrBi_2Nb_2O_9$ and $Sr_{0.8}Bi_2Nb_2O_9$ ceremics, Ceram. Int. 41 (2015) 4468-4478.

[48] J. Sargheini, A. Ataie, S.M. Salili , A.A. Hoseinion, One-step facile synthesis of $CaCO_3$ nanoparticles via mechano-chemical route, Powder Technol. 219 (2012) 72-77.

[49] R. Gopal, J.S. Park, C.H. Seo, Y. Park, Applications of circular dichroism for structural analysis of gelatin and antimicrobial peptides. Int. J. Mol. Sci. 13 (2012) 3229-3244.

[50] I.S. Raja, N.N. Fathima, A gelatin based antioxidant enriched biomaterial by grafting and saturation: towards sustained drug delivery from antioxidant matrix, Colloids Surf. B Biointerfaces 128 (2015) 537-543.

[51] R. Wetzel, E. Buder, H. Hermel, A. Hutter, Conformations of different gelatins in solutions and in films an analysis of circular dichroism (CD) measurements, Colloid Polym. Sci. 265 (1987) 1036-1045.

[52] R. Wustneck, R. Wetzel, E. Buder, H. Hermel, The modification of the triple helical structure of gelatin in aqueous solution I. The influence of anionic surfactants, pH-value, and temperature, Colloid Polym. Sci. 266 (1988) 1061-1067.

[53] D.I. Hitchcock, The isoelectric point of gelatin at 40° C, J. Gen. Physiol. 6 (1924) 457-462.

[54] Q. Xing, K. Yates, C. Vogt, Z. Qian, M.C. Frost, F. Zhao, Increasing mechanical strength of gelatin hydrogels by divalent metal ion removal. Sci. Rep. 4 (2014) 4706.

[55] T.J. FU, U.R. Abbott, C. Hatzos, Digestibility of food allergens and nonallergenic proteins in simulated gastric fluid and simulated intestinal fluids a comparative Study, J. Agric. Food Chem. 50 (2002) 7154-7160.

[56] S. Dash, P.N. Murthy, L. Nath, P. Chowdhury, Kinetic modeling on drug release from controlled drug delivery systems, Acta Pol. Pharm. aceutica-Drug Res. 67 (2010) 217-223.

Chapter 4

Pectin/PEG food grade hydrogel blend for the targeted oral co-delivery of nutrients

4.1. Introduction

There is always an increasing demand for ready to eat functional foods to promote health benefits with good quality, taste, and flavour. These functional foods carry added values beyond their mere nutritional values. The addition of such nutrients (minerals and vitamin) in food products has received much attention as it accompanies the same process of food consumption in our body.[1,2] It is noteworthy that introduction of such crucial nutrients is known for inducing physical and chemical vulnerabilities during food production conditions and to the digestion process resulting in detrimental effect on overall food properties. Hence, such functional food products are in need of advance technologies in order to avoid unwanted effects such as variation in food sensory properties and limiting the efficiency of nutrients.[3] Adapting pharmaceutical approaches are considered to be more attractive for the fabrication of food grade oral delivery vehicles for delivering nutrients at a controlled manner in order to prevent diseases and promote human health and well-being.[4-8] Such oral carriers are efficient in targeting and controlling the release of bioactive ingredients as they pass through the human gastrointestinal (GI) tract apart from protecting them.[9]

Among the various forms of oral vehicle, hydrogels made up of edible polymers are popular due to their biocompatibility and biodegradability.[8,10,11] Pectin, a type of edible polysaccharide can be easily fabricated as hydrogel.[12] It finds diverse food applications

as a source of soluble dietary fiber and can be successfully used as a gelling agent, stabilizer and fat replacer by food and beverage industries.[13,14] It also holds striking biomedical functions like decreasing blood fat, soothing pain, reducing the incidence of heart diseases, inhibiting lipase activity growth and metastasis of cancer cells as well as inducing their apoptosis.[15-17]

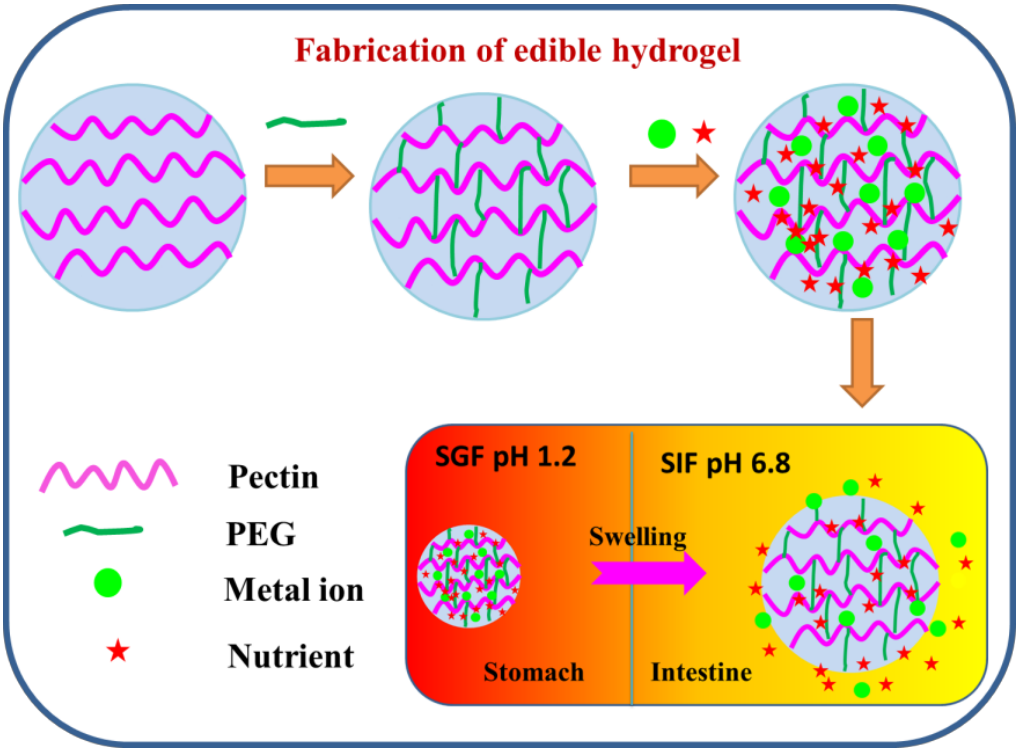

Fig 4.1: Schematic diagram of fabrication of edible hydrogel and release of nutrients in SGF and SIF

Also, pectin is resistant to proteases and amylase, which are active in the upper GI tract. On the other hand, they are digested by the microflora of the colon.[18] Due to these important properties, it is possible that pectin could function as a delivery vehicle to

escort a range of pharmaceutical and food bioactive compounds from the mouth to the colon.[19-21] From the literature, it is evident that so far, pectin based hydrogels were fabricated mostly after chemical modification or by chemical combination of pectin with other polymers involving complicated synthetic strategies.[22,23] Herein, we followed a simple methodology to fabricate pectin based hydrogel by using polyethylene glycol (PEG). PEG is one of the synthetic plasticizers which is approved by FDA and is used in combination with pectin for food packaging applications.[24,25]

In this study, edible pectin/PEG hydrogel (PP) was used for the first time to co-deliver nutrients. In detail, during the fabrication of PP hydrogel, Ca^{2+}, as well as vitamin D, was entrapped one after the other throughout the hydrogel matrix (PPCaD). Similarly, Fe^{2+}, as well as vitamin C, was added into the PP blend and set to form a hydrogel matrix (PPFeC). A Schematic diagram of fabrication of edible hydrogel and release of nutrients in SGF and SIF is shown in Fig. 4.1. It is pertinent to recall that vitamin D and calcium play important roles in bone mineralization.[26] Most importantly, calcium is actively absorbed from the small intestine in the presence of vitamin D. Thus, a diet containing both optimal vitamin D and calcium is important for proper mineralization of bone.[27] It is well known that iron deficiency is a common worldwide problem in which vitamin C enhances the availability and absorption of iron from the diet. Hence, food item containing iron and vitamin C is preferable for good health.[28.29] So obtained hydrogels (PPCaD and PPFeC) were thoroughly characterized by TGA and FTIR. The morphology of the hydrogels was viewed using Scanning electron microscopy (SEM). Detailed rheological studies were performed on as-fabricated hydrogels using rheometer. Further, hydrogels were subjected to *in-vitro* swelling studies in SGF at pH 1.2 as well as SIF at pH 6.8 and their corresponding degradability was also analyzed. During the swelling

studies at two different pH values, the release of vitamin D and vitamin C along with the corresponding metal ions were estimated.

4.2. Experimental and Characterization Details

4.2.1. Materials

Pectin (esterified 60 % to 70 %), Polyethylene glycol (PEG) 300 and 7-dehydrocholesterol (MW 384.64) were obtained from Sigma-Aldrich. Ferrous chloride ($FeCl_2$) (MW 162.78) and ascorbic acid (MW 176.13) were purchased from Central Drug House Pvt Ltd. Citric acid (MW 192.93) was obtained from Loba Chemie Pvt. Ltd. Calcium Chloride ($CaCl_2$) was purchased from Sisco research lab Pvt. Ltd. (SRL) Mumbai, India. Milli Q water was used for all the experimental work. All the chemicals were analytical reagent (AR) grade.

4.2.2. Methods

4.2.2.1. Preparation of pectin/PEG hydrogel (PP)

5% (w/v) Pectin solution was prepared in water under continuous stirring for 2 h until the solution becomes homogenous. 0.1 % (w/v) Citric acid was added into the prepared pectin solution for maintaining pH 3.5-3.8. After that 1 % PEG (v/v) was added as a cross-linker by maintaining the total volume, the solution was stirred well and placed in the water bath at 60 °C for 3 hours. Further, the samples were taken out from the water bath, cooled and cut into the equal size pellet 1 cm diameter × 1 cm thickness and dried at room temperature.

4.2.2.2. Preparation of PP hydrogel containing nutrients

Calcium and vitamin D (PPCaD)

As mentioned above, 5:1 Pectin/PEG solution was prepared by adjusting the pH 3.5-3.8 using citric acid. Thereafter, in order to entrap Ca^{2+} ions as well as vitamin D, 2 mg/mL of Ca^{2+} as 50 mM $CaCl_2$ solution and 5 μg/mL vitamin D (w/v) solution were added one after the other into the above pectin/PEG mixture by maintaining the final volume. The mixture was stirred well, poured into the test tube and kept in the water bath at 60 °C for 3 h.

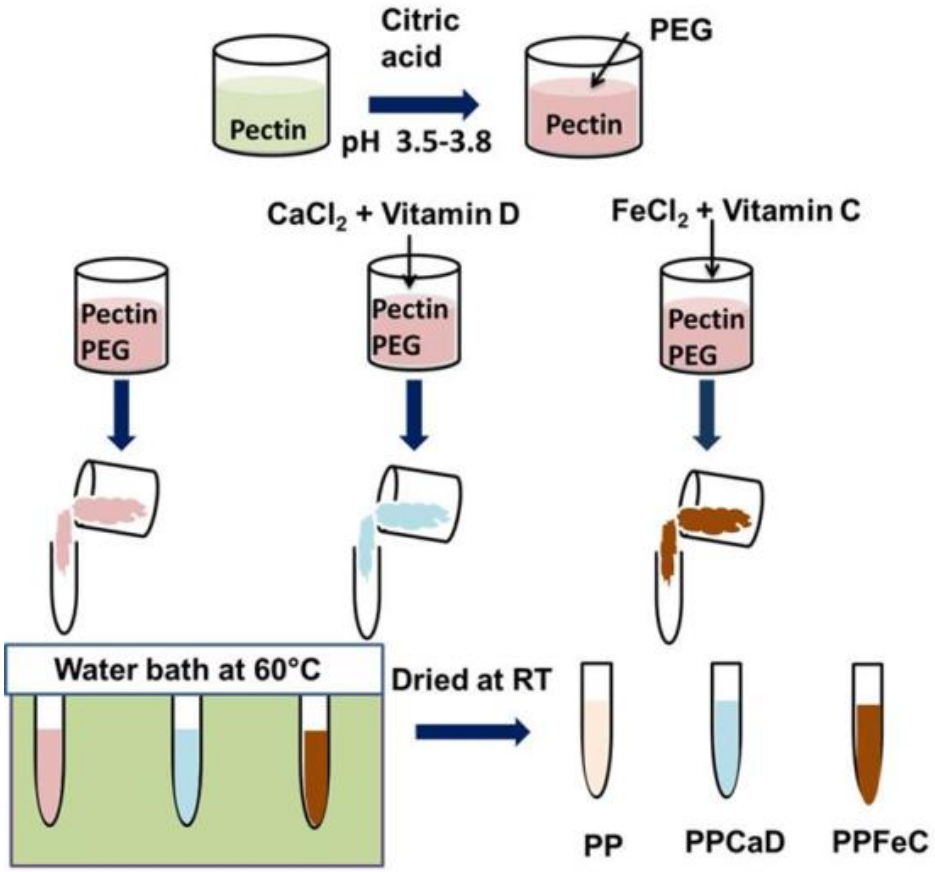

Fig. 4.2: Schematic illustration for the fabrication of various hydrogels PP, PPCaD and PPFeC containing nutraceuticals.

The resultant hydrogel sample was dried as described in the previous section (4.2.2.1). Similarly, pectin/PEG hydrogel containing Iron (2 mg/mL) with vitamin C (25 mg/mL)

(PPFeC) was also prepared by heating at 60 °C for 3 h. A Schematic illustration for the fabrication of various hydrogels PP, PPCaD and PPFeC containing nutraceuticals was shown in Fig. 4.2.

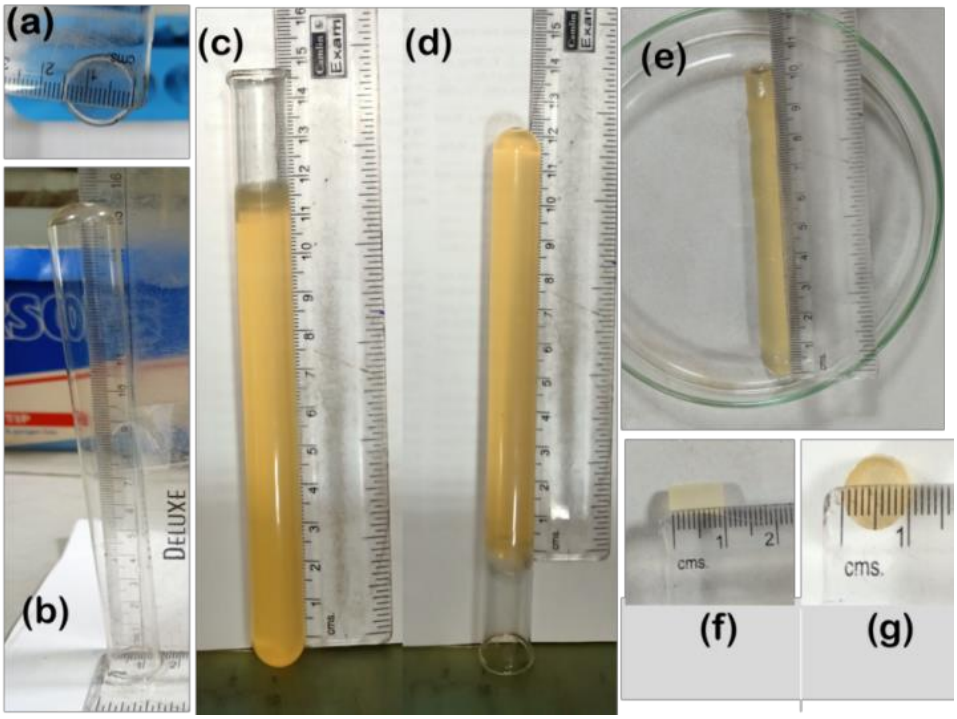

Fig. 4.3: (a) & (b) Diameter and length of empty test tube, (c) & (d) Test tube containing pectin hydrogel in wet condition, (e) Dried hydrogel, (f) & (g) height and diameter of the pellet.

During the fabrication PP, PPCaD and PPFeC, total volume was maintained as 20 mL in 25 mL test tube of 1.5 cm diameter × 15 cm height. In wet condition, the hydrogel occupies 12 cm height of the test tube and in dry condition dimension of as prepared hydrogel was observed as 1cm diameter × 10 cm height (Fig. 4.3). Herein, as per theoretical calculation, the chosen size of the hydrogel (1 cm diameter × 1 cm height) in the case of PPCaD and PPFeC contains 10 μg of vitamin D and 50 mg of vitamin C,

respectively, which are close to RDA values (10 μg per day and 45 mg/day for adults as per FAO and WHO).[30,31] The composition of hydrogel contents for 20 mL mixture was detailed in Table 4.1.

Table 4.1: Composition of Hydrogel

We maintained the size (1 cm diameter and 1 cm thickness). The hydrogel composition per 20 mL is given as follows:

S. No.	**Contents of PPCaD**	**Composition of PPCaD for 20 mL**
1.	Pectin	1000 mg
2.	PEG	0.2 mL
3.	Citric acid	20 mg
4.	Ca^{2+} ions as $CaCl_2$	40 mg
5.	Vitamin D	100 μg
S. No.	**Contents of PPFeC**	**Composition of PPFeC for 20 mL**
1.	Pectin	1000 mg
2.	PEG	0.2 mL
3.	Citric acid	20 mg
4.	Fe^{2+} ions as $FeCl_2$	40 mg
5.	Vitamin C	500 mg

4.2.3. Characterization of Hydrogels

The details of the FTIR spectra and TGA for the hydrogels samples are described in section 3.2.3.1 and 3.2.3.3 of chapter 3, respectively. For FTIR spectra, Attenuated Total Reflectance (ATR) mode was used and in TGA, Hydrogel samples were heated from room temperature to 600 °C to characterize the samples.

4.2.3.1. SEM

The morphology of the hydrogels was investigated by using Scanning Electron Microscope ZEISS MA 15. Samples were gold coated and observed at an accelerating voltage of 3 kV and 10000 magnification.

4.2.3.2. Rheological Properties

In order to find the gelling temperature of hydrogels, rheological measurements were performed in a rheometer (Anton Paar MCR 702, Austria) using a 50 mm plate and plate fixture, with a diameter of 25 mm. For this experiment, the required solutions were mixed in an ice bath and immediately transferred to the sample holder. Further, the sample holder was heated from 20 °C to 70 °C at the rate of 1 °C / min with 5 % shear strain and at 1 Hz frequency and corresponding viscoelastic properties were measured. The static, as well as dynamic rheological measurements of hydrogels, were determined using Anton Paar MCR 702, Austria. Herein, the shear viscosity was evaluated at various shear rates at 1 Hz frequency. Frequency sweep measurements were performed at the frequency range from 0.1 to 10 Hz at 0.1 % strain. Strain sweep (0 % to 100 %) of the hydrogel samples were also done at 1 Hz oscillation frequency.

4.2.3.3. Nutrient entrapment analysis

Percentage nutrient entrapment efficiency of the hydrogels PPCaD and PPFeC was estimated as per the procedure described by Hibbins *et al.*[32] For this, equal-sized hydrogel samples (1 cm dia. and 1 cm thick) were crushed, weighed and suspended in 10 mL of water for 24 hours. 5 mL sample was withdrawn and filtered using 0.5 μm injection filters. The filtered sample was used for the quantitative analysis of vitamin D and vitamin C using UV-visible spectroscopy (1800 Shimadzu spectrophotometer) and metal ion contents (Ca^{2+} and Fe^{2+}) by ICP-ES (Perkin-Elmer Optima 2000 DV Spectrometer) analysis. The procedure was conducted in triplicate and the entrapment efficiency of nutrients was determined according to the equation given below.[32]

$$\text{Nutrient entrapment efficiency (\%)} = \frac{\text{Actual nutrient content}}{\text{Theoretical nutrient content}} \times 100 \qquad (4.1)$$

4.2.3.4. Swelling and drug release studies

Swelling studies were performed initially using SGF for 3 h and the samples were washed in SIF. The washed samples were placed in SIF and swelling tests were continued for another 3 h. The SGF and SIF solutions were prepared as per the protocol described by Rosen et al.[33] and the corresponding details are given in annexure 1. Herein, tests were conducted at room temperature using hydrogel samples (size: 1 cm dia. × 1 cm thick). At regular intervals, samples were weighed and corresponding swelling ratios were calculated by using the following equation:

$$\text{Swelling ratio} = \frac{w_m}{w_d} \times 100\% \qquad (4.2)$$

where $W_m = W_s - W_d$ and W_s and W_d are the weights of the swollen sample and dried sample, respectively. Independently, experiments were conducted in duplicates for each reading and average data were plotted. To investigate the release study of vitamin D and vitamin C from PPCaD and PPFeC, respectively at the required intervals, the supernatant of the hydrogel samples were quantitatively analyzed using UV-Visible spectrophotometer (UV-1800 Shimadzu spectrophotometer). In the case of vitamin D, release from PPCaD was evaluated in SGF as well as SIF. The release profile of the drug was recorded for 6 h using UV-visible spectrophotometer at the wavelength of 281 nm as per the procedure described by Luo *et al*.[34] Similarly, vitamin C release from PPFeC was carried out using SGF as well as SIF for 6 h at regular time intervals using UV-visible spectrophotometer at the wavelength 261 nm as per the procedure described by Peng *et al*. [35] Likewise, the release profile of Ca^{2+} and Fe^{2+} from PPCaD and PPFeC, respectively, were measured using ICP-ES (Perkin-Elmer Optima 2000 DV Spectrometer).

4.2.3.5. *In-vitro* hydrogel degradation studies

The *in-vitro* degradability of hydrogels was monitored in SIF at 37 °C. A lyophilized hydrogel sample of size 1 cm thick × 1 cm dia. was accurately weighed and then immersed in 10 mL of SIF at different time points up to 24 h, with the medium being refreshed every 2 h. Samples were taken out at predetermined immersion time points, rinsed with deionized water, dried and finally weighed. The percentage of degradation was calculated from the dry mass before and after the immersion.[36] The degradation experiment was conducted in triplicates for all the samples and the average value was recorded.

4.2.3.6. Drug release kinetics

For further investigation of the release of vitamin D and vitamin C, zero order, first order, Higuchi and Peppas model were used to fit the released data from the sample PPCaD and PPFeC according to the following equations.[35]

Zero-order model: $$\frac{M_t}{M_\infty} = kt \quad (4.3)$$

First order model: $$\ln(1 - \frac{M_t}{M_\infty}) = -kt \quad (4.4)$$

Higuchi model: $$\frac{M_t}{M_\infty} = kt^{1/2} \quad (4.5)$$

Peppas model: $$\ln(\frac{M_t}{M_\infty}) = nlnt + \ln k \quad (4.6)$$

where, M_t is the cumulative amount of drug released until sampling time t, M_∞ is the cumulative total amount of drug released, M_t / M_∞ is the fraction of drug released at time t, *k* is a rate constant, and *n* is the diffusion exponent which indicates the drug release kinetics mechanism.

4.3. Results and Discussion

4.3.1. FTIR Analysis

Fig. 4.4(a) shows the FTIR spectra of PP, PPCaD and PPFeC. In the case of PP, peak at 3407 cm^{-1} is attributed to O-H stretching of pectin and PEG molecules. Peaks appeared at 1741 cm^{-1} and 1642 cm^{-1} are due to symmetric –C=O stretching and asymmetric stretching of $–COO^-$ of pectin, respectively. The peak at 1642 cm^{-1} is also due to –OH bending of both the polymer molecules. Two weak shoulders appeared at 1440 cm^{-1} and 1240 cm^{-1} are assigned to $–COO^-$ symmetric and $-CH_2$ stretching, respectively. Further, the shoulder ~1240 cm^{-1} also corresponds to the characteristic C-O-C vibration of PEG.

A sharp peak at 1024 cm^{-1} is due to the glycosidic linkage of pectin. In the case of PPCaD, a peak observed at 3339 cm^{-1} is attributed to -OH stretching of pectin/ PEG molecule and vitamin D. Herein, it is noteworthy that peaks of PP at 1741 cm^{-1} and 1642 cm^{-1} can be seen to appear as a small weak shoulder and a sharp intensified peak at 1740 cm^{-1} and 1643 cm^{-1} respectively. In addition, a weak shoulder observed at 1440 cm^{-1} of PP due to $–COO^-$ symmetric stretching is slightly shifted and reported at 1444 cm^{-1} for PPCaD.

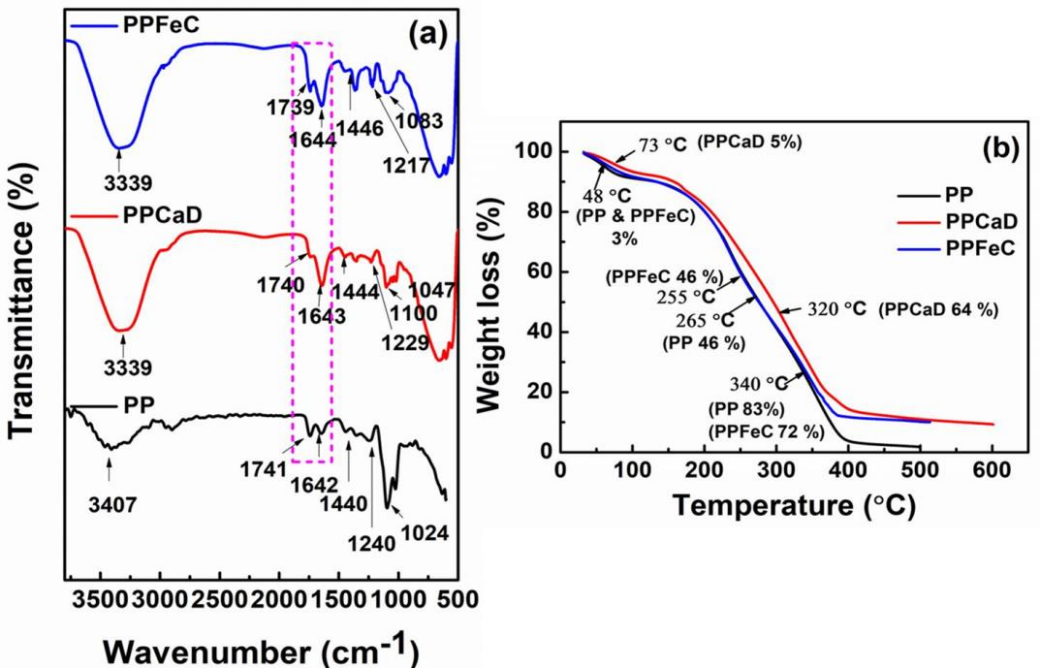

Fig. 4.4: (a) FTIR Spectra and (b) Thermogravimetric analysis of PP, PPCaD and PPFeC.

The observed changes in –C=O, $–COO^-$ and –OH peaks of PPCaD can be attributed to the interaction with the Ca^{2+} ions as well as with vitamin D molecules. Interestingly, in the case of PPFeC, peaks corresponding to –C=O symmetric stretching and $–COO^-$ asymmetric stretching was observed at 1739 cm^{-1} and 1644 cm^{-1}, respectively and are

intensified when compared to PP. Further, -COO^- symmetric stretching was slightly shifted compared to PP and reported at 1446 cm^{-1} in PPFeC. Pertinently in PPFeC, -C=O, –COO- and –OH group vibrations were observed to shift more significantly compared to PPCaD, indicating a strong interaction with iron ions along with vitamin C molecules. The above assigned peaks were in good agreement with pure individual polymers (data not shown) as well as with the literature.[24, 25,35]

4.3.2. TGA Analysis

Thermogravimetric analysis of all hydrogels is portrayed in Fig. 4.4(b). The degradation trends of the samples under study were noticed to be more or less similar. The initial weight loss of PP and PPFeC was shown to be 3 % at ~48 °C due to loss of water, while in the case of PPCaD, it was observed to be 5 % at 73 °C. Second decomposition (46 % weight loss) for the hydrogels PP and PPFeC were observed at 265 °C and 255 °C, respectively, due to depolymerization of pectin molecules. Final decomposition for the hydrogel PP and PPFeC was observed to be 83 % and 72 % at ~340 °C, respectively. It is noteworthy that in the case of PPCaD, only second decomposition (64 % weight loss) was noticed at 320°C. In general, the observed reduction in the % weight loss of the hydrogels after the addition of metal ions reveals the existence of thermal stability of the hydrogel samples (PPCaD and PPFeC) compared to the blank (PP).

4.3.3. SEM Analysis

SEM analysis revealed the surface morphology of the hydrogel samples under investigation PP, PPCaD were of rough in general and does not show much difference though there are additional contents Ca^{2+} and vitamin D (5 μg/mL) in PPCaD (Fig. 4.5

(a-b)). Interestingly, the SEM morphology of PPFeC (Fig.4.5 (c)) indicates its porous surface, probably due to the strongest crosslinking nature of Fe^{2+} along with the physical interaction of vitamin C in larger content (25 mg/mL) compared to PPCaD.

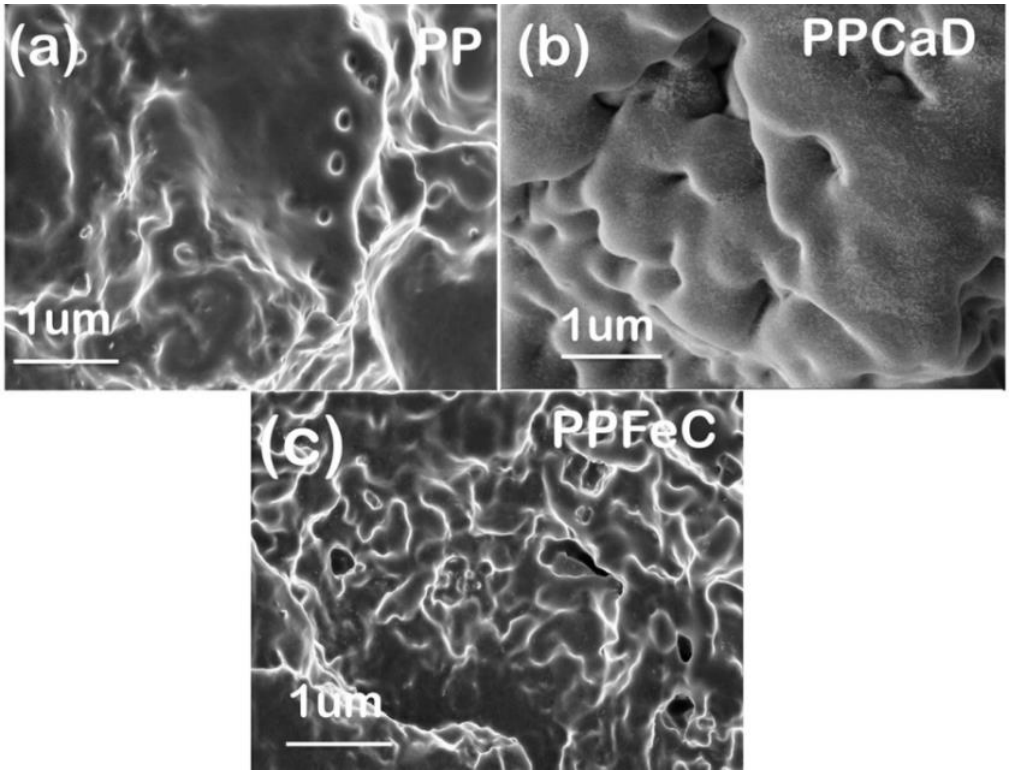

Fig. 4.5: SEM micrographs of PP, PPCaD and PPFeC.

4.3.4. Rheological properties

The temperature dependence of storage modulus (G′) and loss modulus (G″) for PPCaD and PPFeC were depicted in Fig. 4.6. From the figure, the gelation temperature of PPCaD was observed to be 32° C (Fig. 4.6(a)). After gelation temperature, G″ slightly

decreased compared to G′ upto ~ 60° C and there was a drastic increase in G′ as well as G″ after 60° C. Overall, G′ was greater than G″ indicating an increase in the elastic nature of the hydrogel sample. The reported elastic nature of the sample after the gelation temperature confirms the hydrogel formation, indicating the existence of crosslinking in the polymer matrix through the additives PEG, Ca^{2+} and vitamin D.[37]

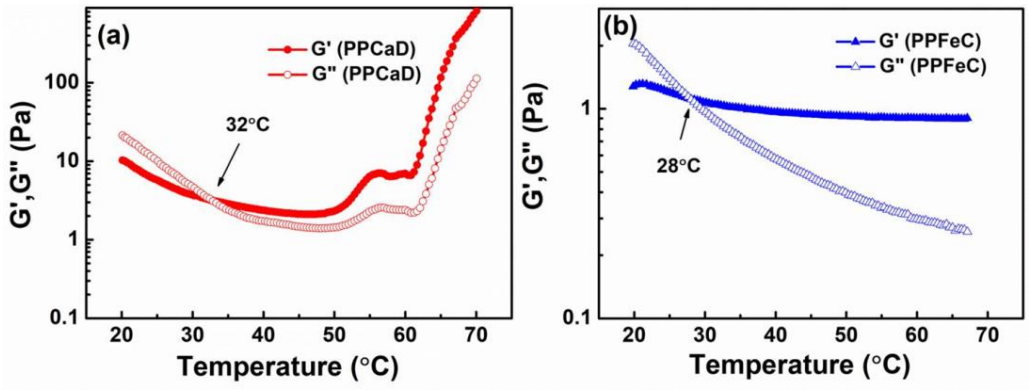

Fig. 4.6: Gel temperature of the hydrogel samples (a) PPCaD and (b) PPFeC.

Similarly, in the case of PPFeC (Fig. 4.6(b)), gelation temperature was reported at 28 °C. Further, below 28 °C, G″ was greater than G′ and a drastic decrease was found in the G″ while there was a slight decrease in G′. After gelation temperature, there was no change in the value of G′ from the temperature range of 28° C to 70° C indicating a rigid nature of the sample PPFeC compared to PPCaD. The observed rigid nature of PPFeC indicates strong electrostatic interaction between the polymer network and Fe^{2+} as revealed by FTIR (Fig. 4.4(a)). It is also worth recalling that the electron affinity of the Fe^{2+} (15.7 KJ/mol) is greater than Ca^{2+} (2.37 KJ/mol) and confirms strongest interactive nature of Fe^{2+} ions compared to Ca^{2+} ions with pectin molecules.[38] On the other hand, G″

drastically decreased with increase in temperature indicative of diminishing viscous nature of the sample. It is pertinent to recall that the gelation temperature of pectin-PEG (PP) was observed to be at 57° C (data not shown), which was greater than PPCaD and PPFeC. Hence, the possible interaction of PEG with pectin is only through weak physical forces like hydrogen bonding and Vander Waal's forces leading to higher gelation temperature for PP.

In the frequency sweep tests, storage moduli (Fig. 4.7(a)) of the hydrogel samples PP, PPCaD and PPFeC were significantly increased with the frequency range examined. The storage modulus of PPCaD sample was observed to be the highest in the magnitude compared to PPFeC and PP, indicating the highest elastic nature of the gel. Fig. 4.7(b) represents the tan δ of hydrogel samples as a function of the frequency. The magnitude of tan δ was found to be lesser than 1 for all hydrogel samples, confirming solid-like character of the hydrogel.[39] Here again, PPCaD and PPFeC showed better elastic character compared to PP. Fig. 4.7(c) shows the frequency dependence of the complex viscosity of the hydrogels. Generally, the complex viscosity of hydrogels decreased with an increase in applied frequency, indicating shear thinning behavior.[37] On a comparative basis, the order of the magnitude of the hydrogel complex viscosity was observed as follows: PPCaD >> PPFeC >PP. The observed highest complex viscosity of PPCaD reveals the closest association of pectin molecules only by Ca^{2+} ions, whereas a small amount of vitamin D (5 μg/mL) content of the hydrogel does not show any role. On the other hand, though the hydrogel PPFeC contains Fe^{2+} ions with the strongest electron affinity, the observed decrease in viscosity compared to PPCaD is mainly attributed to a large amount of vitamin C (25 mg/mL) content, which prevents the polymer association.[40]

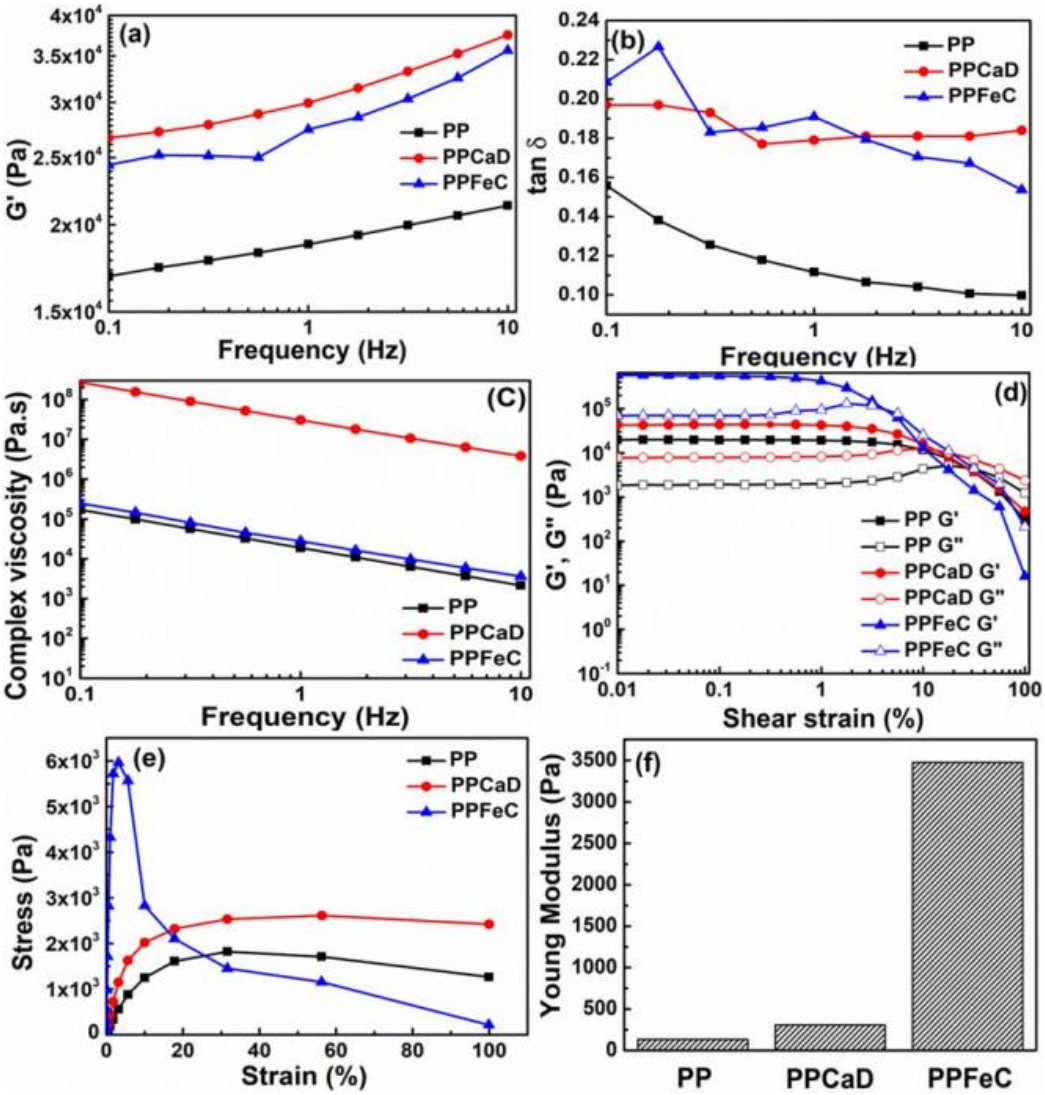

Fig. 4.7: Frequency dependence of (a) storage (G′), (b) tan δ and (c) complex viscosity (d) strain sweep in shear rheology at 1 Hz , (e) stress-strain curves (f) young modulus of various hydrogels.

In the case of PP, the observed lowest complex viscosity as a function of frequency is corroborating the weakest interaction between pectin and PEG molecules through hydrogen bonding and weak Vander Waal forces.[24] Fig. 4.7(d) shows a variation of G′ and G″ with respect to % shear strain for PP, PPCaD, and PPFeC. In detail, PP showed linearity of G′ and G″ from 0.01 % to ~ 1 % of strain values. On the other hand, in the

case of PPCaD and PPFeC, the linear region for G′ and G″ was found only upto ~ 0.5 % and ~ 0.1 %, respectively of strain value. The observed reduction in the magnitude of G′ and G″ for PPCaD and PPFeC in comparison to PP indicates destruction of the hydrogel network with an increase in the strain values due to addition of respective metal ions and vitamin molecules.[41] A significant difference in the stress-strain behaviour of the hydrogel samples was observed in Fig. 4.7(e). Stress-strain curves of PPCaD and PP indicates soft and weak nature of the hydrogel, whereas stress-strain behaviour of PPFeC reveals a comparatively harder nature. The corresponding Young's modulus (Fig. 4.7(f)) of the hydrogel samples was also calculated and the following trend was reported: PPFeC >> PPCaD > PP and thus confirms the elastic nature of PPCaD.

4.3.5. Nutrient entrapment efficiency

Entrapment efficiency of vitamin D and vitamin C from the hydrogel PPCaD and PPFeC was calculated as 99.1 % and 99.3 %, respectively. Additionally, metal ion contents of the hydrogels PPCaD and PPFeC were determined as 99.2 % for Ca and 99.6 % for Fe, respectively.

4.3.6. Swelling and drug release study

In order to determine the swelling behaviour, hydrogels were immersed for 3 h in the SGF at pH 1.2 followed by SIF at pH 6.8 for another 3 h (Fig. 4.8(a)). The highest swelling ratio was reported for PPCaD as 64 %, whereas 52 % for PPFeC and 41 % for PP was observed after 3 h in the SGF. Thereafter, the same pellet of all the hydrogels was placed in the SIF and swelling studies were continued at pH 6.8. In particular, at the end of 6 h, the swelling ratio of PPCaD, PPFeC, and PP was observed to be 130 %, 110 %

and 61 %, respectively. The highest swelling of PPCaD and PPFeC compared to PP revealed additional crosslinking of metal ions as well as vitamin molecules with the PP network. It is worth mentioning that PPCaD showed marginally higher swelling property compared to PPFeC due to its appreciable elastic nature, as revealed by rheological studies (Fig. 4.7(a)). Herein, the highest electron affinity of Fe^{2+} and non-covalent interaction of higher amount of vitamin C content with PP network hamper the swelling behavior of PPFeC by increasing its hardness (Fig. 4.7(e) and Fig. 4.7(f)). On the other hand, the observed lowest swelling property of pure PP network is associated with its soft nature due to the existence of very weak crosslinking forces between pectin and PEG, which could break easily as the water molecule diffuses in the polymer network and consequently disintegrate the network quickly.

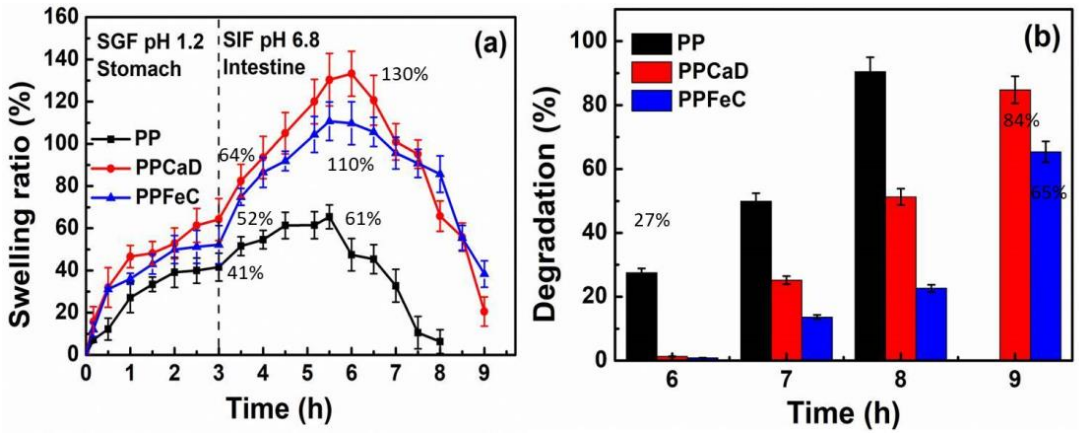

Fig. 4.8: (a) Swelling ratio of the hydrogels PP, PPCaD and PPFeC in SGF at pH 1.2 and in SIF at pH 6.8 (b) degradation behaviour in SIF at pH 6.8 for various hydrogels.

Additionally, during swelling experiments, the supernatant solutions at regular intervals were further subjected to determine the release of vitamin D and vitamin C. (Fig. 4.9(a))

as follows: In the case of PPFeC, the release of vitamin C was 5 % in 1 hour and increased as 11 % in 3 h at pH 1.2. In the case of PPCaD, the release of vitamin D was observed to be 10 % in 1 h and increased to 19 % in 3 h. When the same hydrogel pellet was placed into the SIF solution, 68 % of Vitamin C released from the sample PPFeC in 4 h whereas, 91 % was released in 6 h. Similarly, vitamin D released from the sample PPCaD was found to be 75 % and 95 % in 4 h and 6 h, respectively. It was concluded that in SGF, both drugs were released feebly while in SIF, the drugs were released at a higher amount. Herein, the release of vitamin D and vitamin C was influenced by the swelling behaviour of the hydrogels as well as crosslinking of the gel network.

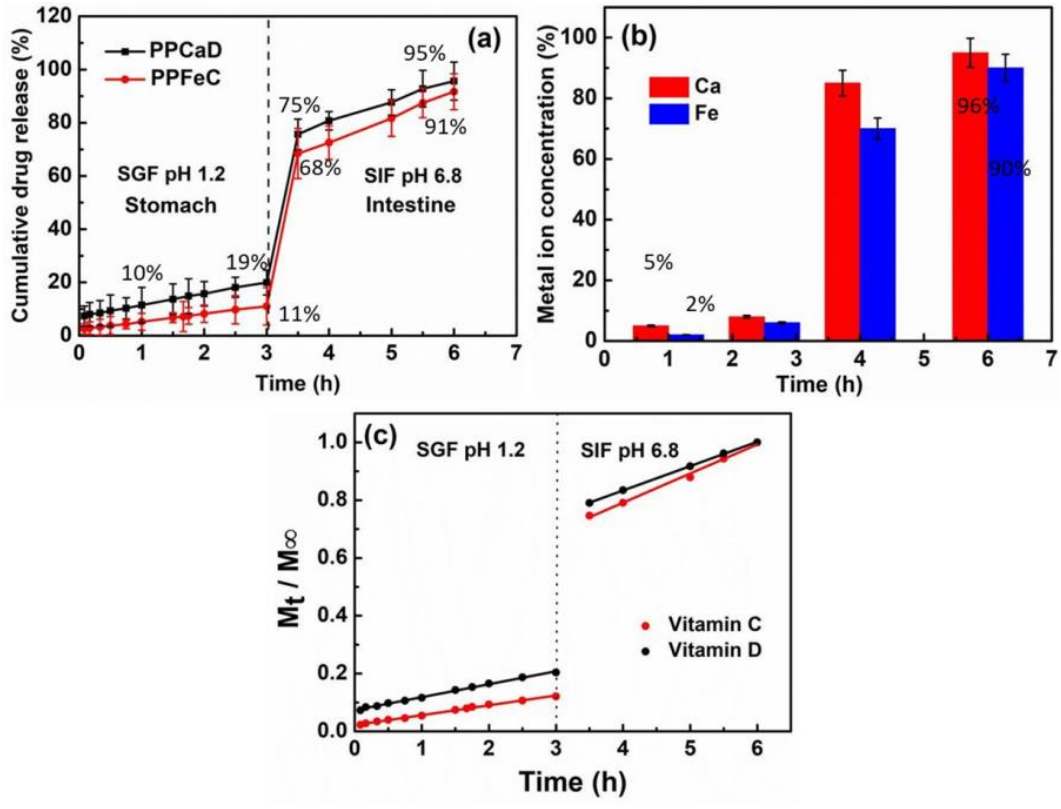

Fig. 4.9: (a) Cumulative release of (a) Vitamin D and vitamin C, (b) metal ion (Ca^{2+} / Fe^{2+}) from the hydrogel PPCaD and PPFeC in SGF (pH 1.2) and SIF (pH 6.8), respectively. (c) Release kinetics of vitamin D and vitamin C from PPCaD and PPFeC in SGF and SIF solutions, respectively.

In detail, in SGF due to the protonation of carboxylate anion of pectin molecules and the corresponding molecular association[42-44], nutrients are protected. On the other hand, the deprotonation of -COOH group on pectin in SIF (pH 6.8) leads to the loosening of pectin network due to the charge repulsion and resulting in a higher rate of vitamin release. The observed slight decrease in the drug release rate of PPFeC compared to PPCaD indicates the interaction of vitamin C molecules with pectin through physical forces in addition to the highest electron affinity of Fe^{2+}. Interestingly, it can be concluded that the lowest release of vitamin D and vitamin C in the SGF indicates the protection of the nutrients from the gastric environment for 3 h. Further, in the next 3 h due to the change in pH, a high swelling ratio of hydrogel samples under investigation was observed, followed by releasing of vitamin D and vitamin C. Moreover, From the ICP data (Fig. 4.9(b)), the metal ion concentration from the hydrogel was measured as 5 % for Ca^{2+} and 2 % for Fe^{2+} before 3 h. But in 4 h around 85 % Ca^{2+} and 70 % Fe^{2+} was released from the hydrogel matrix and finally, in the 6 h, Ca^{2+} and Fe^{2+} concentration were recorded as 96 % and 90 %, respectively.

4.3.7. Degradation studies

Degradation studies for all the samples were shown in fig. 4.8(b). It is pertinent to recall that hydrogel samples are intact in SGF. When hydrogels were placed into the SIF, no degradation was noticed for all the samples upto 5 h. Degradation for PP was 27 %, and for PPCaD as well as PPFeC was observed as ~1 % within 6 h. After 8 h the degradation of hydrogel PP was 90 %, while PPCaD and PPFeC hydrogel were 51 % and 22 %, respectively. In 9 h PP was completely degraded, whereas the degradation of PPCaD and PPFeC hydrogel was found to be 84 % and 65 %, respectively. These results are in good

agreement with swelling (Fig. 4.8(a)) and drug release (Fig. 4.9 (a)) behaviour of the hydrogel samples.

4.3.8. Release kinetics of the drug

The release kinetics of vitamin D and vitamin C from the hydrogel PPCaD and PPFeC in different release media such as SGF pH 1.2 as well as SIF pH 6.8 was shown in Fig. 4.9(c). It was noticed from the graph that a fractional amount (M_t / M_∞) of drug release was found to be occurring at a slow rate in SGF (pH 1.2), whereas it increased to a higher rate in SIF (pH 6.8) as explained in Section 4.3.6. Herein, various mathematical modelings were subjected to investigate the nutrient release mechanism from PPCaD and PPFeC in SGF and SIF, which help to optimize the design of a therapeutic device to yield information on the efficiency of various release models. [45] The Correlation coefficients (r^2) were obtained by the fitted experimental data from various models (given in equation) and their values are given in Table 4.2.

Table 4.2: Correlation coefficient (r^2) of different Models in SGF and SIF Solutions.

Model	**Vitamin D**		**Vitamin C**	
	SGF	**SIF**	**SGF**	**SIF**
Zero order	**0.9965**	**0.9996**	**0.9992**	**0.9981**
First order	0.9722	0.9565	0.9124	0.9781
Higuchi	0.9722	0.9858	0.8342	0.9771
Peppas	0.9608	0.9884	0.8941	0.9895

The highest value of r^2 was observed in case of zero-order model for both the samples vitamin D and vitamin C in both the medium SGF and SIF. The zero-order model was found to appropriate model for release mechanism based on the obtained r^2 values. Zero-order model indicates a disaggregation and slow release of drug in order to achieve prolonged action of drug in GI tract, which is an ideal method for the delivery of nutrients.[45]

4.4. Conclusion

In this study, nutrients Ca^{2+} along with vitamin D and Fe^{2+} along with vitamin C were entrapped in edible pectin based (PP) hydrogel matrices. The obtained edible hydrogel blends PPCaD and PPFeC were demonstrated to be efficient through *in-vitro* experiments in protecting nutrients at the harsh gastric environment and co-delivering the same in SIF in a controlled manner for 3 h following zero order kinetics. These interesting oral delivery vehicles fabricated by pharmaceutical approach could be easily incorporated into ready to eat functional foods in order to promote health benefits with good quality and are expected to overcome common human health problems.

References

[1] M.C. Braithwaite, C. Tyagi, L.K. Tomar, P. Kumar, Y.E. Choonara, V. Pillay, Nutraceutical-based therapeutics and formulation strategies augmenting their efficiency to complement modern medicine: an overview, J. Funct. Foods. 6 (2014) 82-99.

[2] R.C. Benshitrit, C.S. Levi, S.L. Tal, E. Shimonia, U. Lesmes, Development of oral food-grade delivery systems: current knowledge and future challenges, Food Funct. 3 (2012) 10-21.

[3] J.P. Gleeson, S.M. Ryan, D.J. Brayden, Oral delivery strategies for nutraceuticals: delivery vehicles and absorption enhancers, Trends Food Sci. Technol. 53 (2016) 90-10.

[4] L. Chen, G.E. Remondetto, M. Subirade, Food protein-based materials as nutraceutical delivery systems, Trends Food Sci. Technol. 17 (2006) 272–283.

[5] Y. Shoji, H. Nakashima, Nutraceutics and delivery systems, J. Drug Targeting. 12 (6) (2004) 385-391.

[6] N.E. Hughes, A.G Marangoni, A.J. Wright, M.A. Rogers, J.W.E. Rush, Potential food applications of edible oil organogels, Trends Food Sci. Technol. 20 (2009) 470-480.

[7] Z. Zhang, R. Zhang, E.A. Decker, D.J. Mc-Clements, Development of food-grade filled hydrogels for oral delivery of lipophilic active ingredients: pH-triggered release, Food Hydrocoll. 44 (2015) 345-352.

[8] M. Tsirigotis-Maniecka, R. Gancarz, A.W. Kazimiera, Polysaccharide hydrogel particles for enhanced delivery of hesperidin: fabrication, characterization and in vitro evaluation, Colloids Surf. A Physicochem. Eng. Asp. 532 (2017) 48-56.

[9] R.K. Ramanan, E.J. Rifna, R. Mahendran, Effect of concentration and temperature on the formation of wheat hydrogel and xerogel pattern, Colloids Surf. A Physicochem. Eng. Asp. 559 (2018) 385-391.

[10] A. Ali, S. Ahmed, Recent advances in edible polymer based hydrogels as a sustainable alternative to conventional polymers, J. Agric. Food Chem. 66 (2018) 6940-6967.

[11] L.S. Liu, J. Kost, F. Yan, R.C. Spiro, Hydrogels from biopolymer hybrid for biomedical, food, and functional food applications, Polymers 4 (2012) 997-1011.

[12] D.J. Mc-Clements, Recent progress in hydrogel delivery systems for improving nutraceutical bioavailability, Food Hydrocoll. 68 (2016) 238-245.

[13] C. Viebke, S. Al-Assafa, G.O. Phillips, Food hydrocolloids and health claims, Bioactive Carbohydr. dietary fibre. 4 (2014) 101-114.

[14] V.S. Kulkarni, K. D. Butte, S.S. Rathod, Natural polymers -a comprehensive Review, Int. J. Res. Pharma. Biomed. Sci. 3 (2012) 1597-1613.

[15] E.G. Maxwell, N.J. Belshaw, K.W. Waldron, V.J. Morris, Pectin- an emerging new bioactive food polysaccharide, Trends Food Sci. Technol. 24 (2012) 64-73.

[16] F. Naqash, F.A. Masoodi, S.A. Rather, S.M. Wani, A. Gani, Emerging concepts in the nutraceutical and functional properties of pectin-a review, Carbohydr. Polym., 15 (2017) 227-239.

[17] F. Munarin, M.C. Tanzi, P. Petrini, Advances in biomedical applications of pectin gels, Int. J. Biol. Macromol. 51 (2012) 681-689.

[18] L.S. Liu, M.L. Fishman, J. Kost, K.B. Hick, Pectin-based systems for colon-specific drug delivery via oral route, Biomaterials. 24 (2003) 3333-3343.

[19] V.R. Sinha, R. Kumria, Polysaccharides in colon-specific drug delivery, Int. J. Pharm. 224, (2001) 19-38.

[20] L.S. Liu, M.L. Fishman, K.B. Hicks, Pectin in controlled drug delivery – a review, Cellulose. 14 (2007) 15-24.

[21] N. Aqdas, N. Zill-i-Huma, A. Javeria, R. Ijaz, A. Mansha, N. Yaqoob, R. Iqbal, S. Tabasum, M. Zuber, K.M. Zia, Pectins functionalized biomaterials; a new viable approach for biomedical applications: a review, Int. J. Biol. Macromol. 101 (2017) 254-272.

[22] O. Munjeri, J.H. Collett, J.T. Fell, Hydrogel beads based on amidated pectins for colon-specific drug delivery: the role of chitosan in modifying drug release, J. Control. Release 46 (1997) 273-278.

[23] J. Jung, R.D. Arnold, L. Wicker, Pectin and charge modified pectin hydrogel beads as a colon-targeted drug delivery carrier, Colloids Surf. B Biointerfaces 104 (2013) 116-121.

[24] S. Seslija, A. Nesic, J. Ruzic, M.K. Krusic, S. Velickovic, R. Avolio, G. Santagata, M. Malinconico, Edible blend films of pectin and poly(ethylene glycol): preparation and physico-chemical evaluation, Food Hydrocoll. 77 (2018) 494-501.

[25] N. Bhattarai, H.R. Ramay, J. Gunn, PEG-grafted chitosan as an injectable thermosensitive hydrogel for sustain protein release, J. Control. Release 103 (2005) 609-624.

[26] M.F. Holick, Vitamin D: a millenium perspective, J. Cell. Biochem. 88 (2003) 296-307.

[27] N. Khazai, S.E. Judd, V. Tangpricha, Calcium and vitamin D: skeletal and extraskeletal health, Curr. Rheumatol. Rep. 10 (2008) 110-117.

[28] S.R. Lynch, Interaction of iron with other nutrients, Nutr. Rev. 55 (1997) 102-110.

[29] Y. Choa, J.T. Kimb, H.J. Park, Size-controlled self-aggregated N-acyl chitosan nanoparticles as a vitamin C carrier, Carbohydr. Polym. 88 (2012) 1087-1092.

[30] K.D. Sowell, C.L. Keen, J.Y. Uriu-Adams, Vitamin D and reproduction: from ametes to childhood, Healthcare 3 (2015) 1097-1120.

[31] S. Abbas, C.D. Wei, K. Hayat, X. Zhang, Ascorbic Acid: microencapsulation techniques and trends—a review, Food Rev. Int. 28 (2012) 343-374.

[32] A.R. Hibbins, P. Kumar, Y.E. Choonara, P.P.D. Kondiah, T. Marimuthu, L.C.D. Toit, V. Pillay, Design of a versatile pH-responsive hydrogel for potential oral delivery of gastric-sensitive bioactives, Polymers 9 (2017) 474-492.

[33] R.T. Rosen, R.D. Hiserodt, E.K. Fukuda, R.J, Ruiz, Z. Zhou, J. Lech, S.L. Rosen and T.G. Hartman, Determination of allicin, *S*-allylcysteine and volatile metabolites of garlic in breath, plasma or simulated gastric fluids, J. Nutr, 131 (2001) 968S-971S.

[34] Y. Luo, Z. Teng, X. Wang, Q. Wang, Development of carboxymethyl chitosan hydrogel beads in alcohol-aqueous binary solvent for nutrient delivery applications, Food Hydrocoll. 31 (2013) 332-339.

[35] H. Peng, S. Chen, M. Luo, F. Ning, X. Zhu, H. Xiong, Preparation and self-assembly mechanism of bovine serum albumin−citrus peel pectin conjugated hydrogel: a potential delivery system for vitamin C, J. Agric. Food Chem. 64 (2016) 7377-7384.

[36] E. Teodor, S.C. Litescu, C. Petcu, M. Mihalache, R. Somoghi, Nanostructured biomaterials with controlled properties synthesis and characterization, Nanoscale Res. Lett. 4 (2009) 544-549.

[37] H.R. Moreira, F. Munarin, R. Gentilini, L. Visai, P.L. Granja, M.C. Tanzi, P. Petrini, Injectable pectin hydrogels produced by internal gelation: pH dependence of gelling and rheological properties, Carbohydr. Polym. 103 (2014) 339-347.

[38] V.M.F. Lai, P.A.L Wong, C.Y. Lii, Effects of cation properties on sol-gel transition and gel properties of k-carrageenan, J. food sci. 65 (2000) 1332-1337.

[39] M. Alonso-Mougan, F. Meijide, A. Jover, E. Rodriguez-Nunez, J. Vazquez-Tato, Rheological behaviour of an amide pectin, J. Food Eng. 55 (2002) 123-129.

[40] A. Herp, T. Rickards, G. Matsumura, L.B. Jakosalem, W. Pigman, Depolymerisation of some polysaccharides and synthetic polymers by L-Ascorbic acid, Carbohydr. Res. 4 (1967) 63-71.

[41] R. Kocen, M. Gasik, A. Gantar S. Novak, Viscoelastic behaviour of hydrogel-based composites for tissue engineering under mechanical load, Biomed. Mater. 12 (2017) 025004.

[42] N. Ahmad, M.C.I.M. Amin, S.M. Mahali, I. Ismail, V.T.G. Chuang, Biocompatible and mucoadhesive bacterial cellulose-g-poly (acrylic acid) hydrogels for oral protein delivery, Mol. Pharmaceutics 11 (2014) 4130-4142.

[43] C.H. Chang, Y.H. Lin, C.L. Yeh, Y.C. Chen, S.F. Chiou, Y.M. Hsu, Y.S. Chen, C.C. Wang, Nanoparticles incorporated in pH-sensitive hydrogels as amoxicillin delivery for eradication of helicobacter pylori, Biomacromolecules 11 (2010) 133-142.

[44] M. Sadeghi, Pectin-Based Biodegradable Hydrogels with potential biomedical applications as drug delivery systems, J. Biomater. Nanobiotechnol. 2 (2011) 36-40.

[45] P. Costa, J.M.S. Lobo, Modeling and comparison of dissolution profiles. Eur. J. Pharm. Sci. 13 (2001) 123-133.

Chapter 5

In-situ mineralization of calcium carbonate in pectin based edible hydrogel for the delivery of protein at colon

5.1. Introduction

Oral route of drug administration is considered to be one of the simplest, cheap, suitable, convenient and safest routes.[1-3] Currently, protein therapeutics is the drug of choice for its incredible selectivity and ability to provide effective and potent action in almost every field of medicine.[4] In comparison with traditional therapeutic small molecules, proteins have greater potential to cure diseases with fewer side effects and can be highly specific with a complex set of functions.[5,6] In general, administering protein drugs orally is a challenging route when compared to other alternate routes due to their poor stability, susceptibility to proteolytic and chemical degradation as well as random physical unfolding and aggregation. Additionally, in oral administration of protein drugs, bioavailability and capability of protecting the protein molecule from the harsh conditions of the gastrointestinal (GI) tract are great challenges.[7-9] Hence, it becomes essential to construct an oral delivery system with very high bioavailability of protein molecules along with their protection from the harsh environment. Although, many delivery systems exist for oral delivery of protein; biodegradable hydrogels composed through proper selection of their building blocks along with appropriate cross-linking strategies are well appreciated.[10] Such hydrogels are well known to swell as well as hold a large amount of water and consequently maintain a three-dimensional network structure. These interesting properties of hydrogels have raised their utility as successful protein reservoirs and a

controlled delivery system for protein in the surrounding tissues or the systemic circulation over an extended period.[10-12]

Colon is considered to be the most suitable site to deliver protein drugs through the oral route since there is no protease present. Hence, for colon-specific oral delivery of protein drugs, it becomes essential to retain the vehicle intact as it reaches intestine from mouth not only to protect the loaded drug from proteolysis but also to release it instantly at the colon site.[13-15] Therefore, pectin-based drug delivery vehicles are considered to be more suitable for oral administration, especially for colon-specific protein delivery systems due to their pH sensitivity as well as film-forming ability.[16] Even though numerous attempts have been made till now to establish successful pectin based protein delivery system, it only becomes effective in the case of water-insoluble drugs, such as anti-inflammatory drugs for lower bowel diseases compared to the delivery of protein drugs.[17] It is also noteworthy that as far as our knowledge, pectin based hydrogels reported in the literature for colon-specific protein delivery, are less in number. In addition, till date reported protein carriers were synthesized mostly after the chemical modification or by the chemical combination of pectin with other polymers involving complicated synthetic strategies.[17-19]

In this investigation, a simple methodology was followed to prepare edible pectin based hydrogel using polyethylene glycol (PEG). It is worth to recall that the polymer PEG is one among a very few synthetic polymers which is approved by the FDA for biomedical application due to its good plasticizing, nontoxic and food grade property.[2] Further, calcium carbonate ($CaCO_3$) particles were *in-situ* mineralized in pectin/PEG blend matrix to protect the protein and control its delivery at the colon site. Herein, BSA loading was carried out soon after the *in-situ* formation of $CaCO_3$ particles in the

polymer blend matrix by mixing a required amount of BSA solution and the mixture was gently heat treated to set as a hydrogel. So obtained hydrogel was thoroughly characterized along with appropriate blank samples by standard characterization techniques such as X-ray diffraction (XRD), Thermogravimetric analysis (TGA) and Fourier transform infrared spectroscopy (FTIR). The mineralization of micron-sized $CaCO_3$ particles in the pectin based hydrogels was confirmed using microscopic techniques, Scanning electron microscopy (SEM) and Transmission electron microscopy (TEM). Rheological studies on prepared pectin based hydrogels were carried out using rheometer.

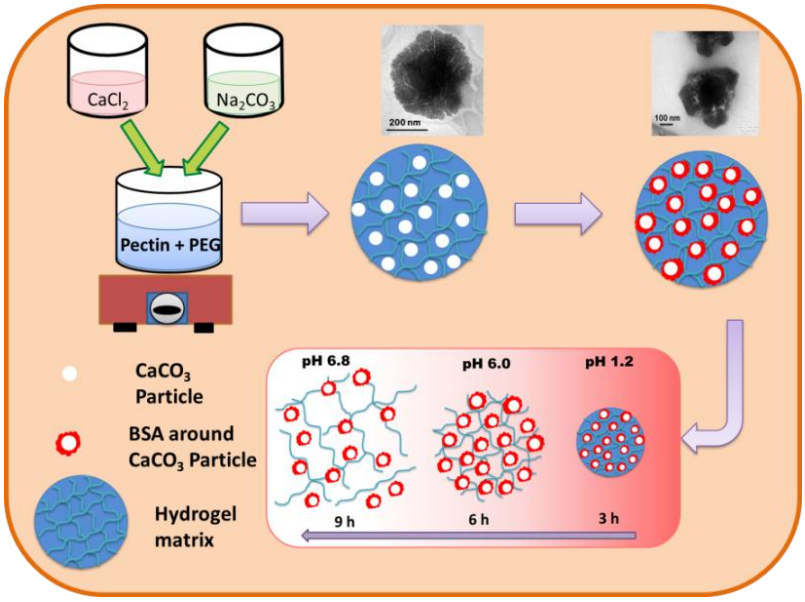

Fig. 5.1: Schematic diagram *in-situ* mineralized $CaCO_3$ nanoparticles in hydrogel matrix and their release in different pH conditions

Further, hydrogels were subjected to *in-vitro* swelling studies in simulated gastric fluid (SGF at pH 1.2) as well as simulated intestinal fluid (SIF) of two different pH values (pH 6.0 and pH 6.8) and the corresponding dispersion of hydrogel components

were also monitored (Fig. 5.1). During the swelling studies at three different pH values, the corresponding release of BSA was estimated. Finally, the conformational stability of the released BSA was also analyzed by SDS-PAGE and CD spectropolarimetry.

5.2. Experimental Section

5.2.1. Materials

For the preparation of the hydrogel, pectin (esterified 55 % to 70 %) and polyethylene glycol (300) (PEG) were purchased from Sigma-Aldrich. Additionally, the precursors used for the synthesis of $CaCO_3$ particles; calcium chloride and sodium carbonate were obtained from Sisco Research Lab. Pvt. Ltd. (SRL), Mumbai, India and Qualigens Fine Chemicals, Mumbai, India, respectively. The model protein BSA used in this study was procured from Sigma-Aldrich. Milli-Q water was used for all the experimental work and all other reagents used in this study were of analytical reagent (AR) grade of high purity.

5.2.2. Method

Fabrication of hydrogel blend matrix

A homogenous transparent solution of pectin 4 % (w/v) was prepared in water at neutral pH (≈ pH 7) by continuous stirring for 2 h followed by the dropwise addition of PEG (pectin/PEG weight ratio (4:1)) with constant stirring. After the addition of PEG into the pectin solution, gelation of pectin/PEG mixture was noticed. Herein, the total gel volume was maintained as 25 mL. The obtained gel was transferred in a test tube and heated in a water bath at 55 - 60 °C for 3 h. The obtained pectin- PEG hydrogel blend (PP) was taken out from the water bath and allowed to cool down to

the room temperature. After that lyophilization was carried out for 16 h and the gel was cut into equal sized pieces (1 cm dia. and 1 cm thick) and stored under dry conditions. Mineralization of *in-situ* $CaCO_3$ particles into PP blend matrix: Soon after the gelation of pectin-PEG blend, precursor solutions namely calcium chloride (50 mM) and sodium carbonate (50 mM) in 1:1 ratio, were added dropwise one after the other in such a way that total volume of the gel content was maintained as 25 mL and set as a hydrogel (PPC) by following the similar steps as mentioned above. BSA loading into PP and PPC blends: 0.3 mg/mL BSA solution was added dropwise into PP as well as PPC gel blends, heated and lyophilized. The resulting hydrogels were named as PPB and PPCB, respectively. A Schematic illustration for the synthesis of various pectin based hydrogels was shown in Fig. 5.2.

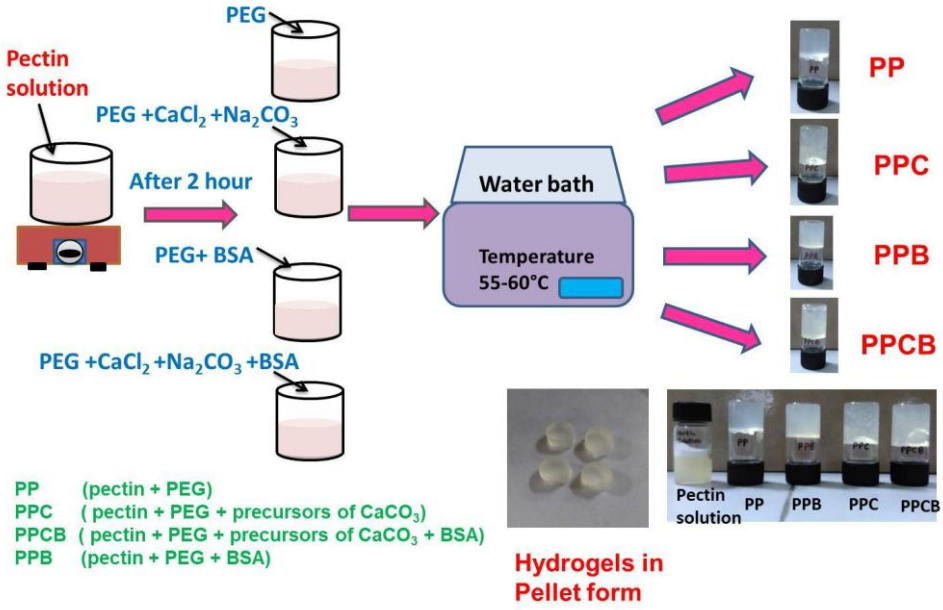

Fig. 5.2: Schematic illustration for the synthesis of various pectin based hydrogels

5.2.3. Characterization of hydrogels

The details of the Fourier Transform Infrared spectroscopy (FTIR), Thermogravimetric analysis (TGA) used in this chapter are already described in the section 3.2.3.1 and 3.2.3.3 of chapter 3 and section 4.2.3 of chapter 4. The details of X-ray diffraction (XRD) analysis and Scanning Electron Microscopy (SEM) are described in 3.2.3.2 and 4.2.3.1 in chapter 3 and chapter 4, respectively. In SEM analysis 5 kV accelerating voltage was used to record the data for this chapter. Hydrogels (PPC and PPCB) were also subjected to Energy Dispersive X-Ray Analysis (EDX) operated at 20 kV using (ZESIS EVO MA15) in order to investigate the presence of calcium ions in the hydrogel systems (PPC and PPCB). The characterization technique to execute the $CaCO_3$ particle size measurements of hydrogels in this chapter are same as discussed in section 3.2.3.6 of chapter 3. For the hydrogel samples 1 cm dia. and 1 cm thick sized hydrogel sample was carefully dispersed in water by vortexing and the resultant solution was subjected to particle size analysis. The particle size was determined using the refractive index of water (1.33) and $CaCO_3$ (1.59). Further, the characterization technique used for the rheological studies in this chapter for the hydrogel samples (PP, PPC, PPCB and PPB) are also described in section 4.2.3.2 of chapter 4.

5.2.3.1. Transmission Electron Microscopy (TEM)

The morphology of *in-situ* mineralized $CaCO_3$ particles in the hydrogel matrix was characterized using TEM (Tecnai G2 200 KV HRTEM SEI HOLLAND).

To analyze the samples by FTIR, TGA, XRD, SEM and TEM equal sized hydrogel pieces (1 cm dia. and 1 cm thick) were crushed and used for analysis.

5.2.3.2. BSA entrapment analysis

Percentage BSA entrapment efficiency in the hydrogels PPB and PPCB was estimated as per the procedure discussed in the section 4.2.3.4 of chapter 4.

5.2.3.3. Swelling and BSA release studies

The swelling studies on the various hydrogels of size (1 cm dia. and 1 cm thick) were carried out by immersing into SGF at pH 1.2 for 3 h. After 3 h, the samples were washed and transferred in SIF at pH 6.0 and the swelling experiment was continued in the same way for the next 3 h. Further, swelling studies were also carried on the same samples for another 3 h after washing in SIF solution at pH 6.8. Simultaneously, the released BSA during swelling was subjected to quantitative analysis as described by Ahmad *et al.*[22]. Additionally, dynamic swelling studies on the various hydrogel samples were performed alternatively (1 h in each solution) by immersing the hydrogel samples in SGF at pH 1.2, SIF at pH 6.0 and SIF at pH 6.8. The same procedure was repeated up to 9 h (in total for every 3 h for the hydrogel samples). In all these studies, the swelling ratio of the samples was determined gravimetrically.[22,23]

5.2.3.4. *In-vitro* hydrogel dispersion studies

The *in-vitro* dispersion of the prepared hydrogels (PP, PPC, PPCB and PPB) was examined using SIF (pH 6.8) at 37 °C. The detail of the dispersion procedure is used, as mentioned in section 4.2.3.5 of chapter 4. The percentage of dispersion was calculated from the dry weight before and after the immersion.[24]

5.2.3.5. Studies on conformational stability of released BSA from the hydrogel samples

SDS-PAGE Analysis and CD spectropolarimetry

The primary structural stability of released BSA from the various hydrogel samples (PPB and PPCB) was analyzed using sodium dodecyl sulfate-polyacrylamide gel electrophoresis (SDS-PAGE). The amount of released BSA from the hydrogel samples was analyzed, as explained in the swelling studies (Section 5.2.3.3). Herein, 200 μL were drawn from the release medium and the concentration of BSA was determined using the Bradford reagent and further adjusted to 10 μg/mL using corresponding release medium using 4 % stacking and 10 % resolving gel (Mini-PROTEAN Tetra Cell: Bio-Rad Laboratories, Germany) as described by Ahmad *et al.*[22] The stability of the secondary structure of BSA released from the hydrogels (PPB and PPCB) was confirmed by CD spectropolarimetry. The detail of the instrument for CD spectra of the protein samples at 25 °C was mentioned in section 3.2.2.2 of chapter 3.

5.3. Result and Discussion

5.3.1. Structural characterization

The hydrogel PP (Fig. 5.3(a)) indicated a broad band centered at 3407 cm^{-1} due to O-H stretching. Interestingly, sharp peaks of pure pectin (Fig. 5.3(a)) observed at 1747 cm^{-1} and 1635 cm^{-1} due to esterified -C=O and -COO^- asymmetric stretching appeared at 1741 cm^{-1} and 1646 cm^{-1} respectively in PP. It is noteworthy that peak at 1446 cm^{-1} corresponding to -COO^- symmetric stretching of pure pectin were reported at lower

wavenumber as 1440 cm^{-1}. Further, the characteristic peak of PEG due to C-O-C stretching in PP was shifted by 10 cm^{-1} lower wavenumber from 1250 cm^{-1} of pure PEG (Fig. 5.3(a)), confirming the presence of PEG in the hydrogel PP.[20] In general, the observed changes in these reported characteristic wavenumbers of PP compared to pure components could be attributed to the existence of inter as well as intramolecular physical forces including ionic, hydrogen bonding and hydrophobic between pectin and PEG molecules.[25,26] Herein, the observed FTIR data on pure pectin is in good agreement with the literature.[27,28]

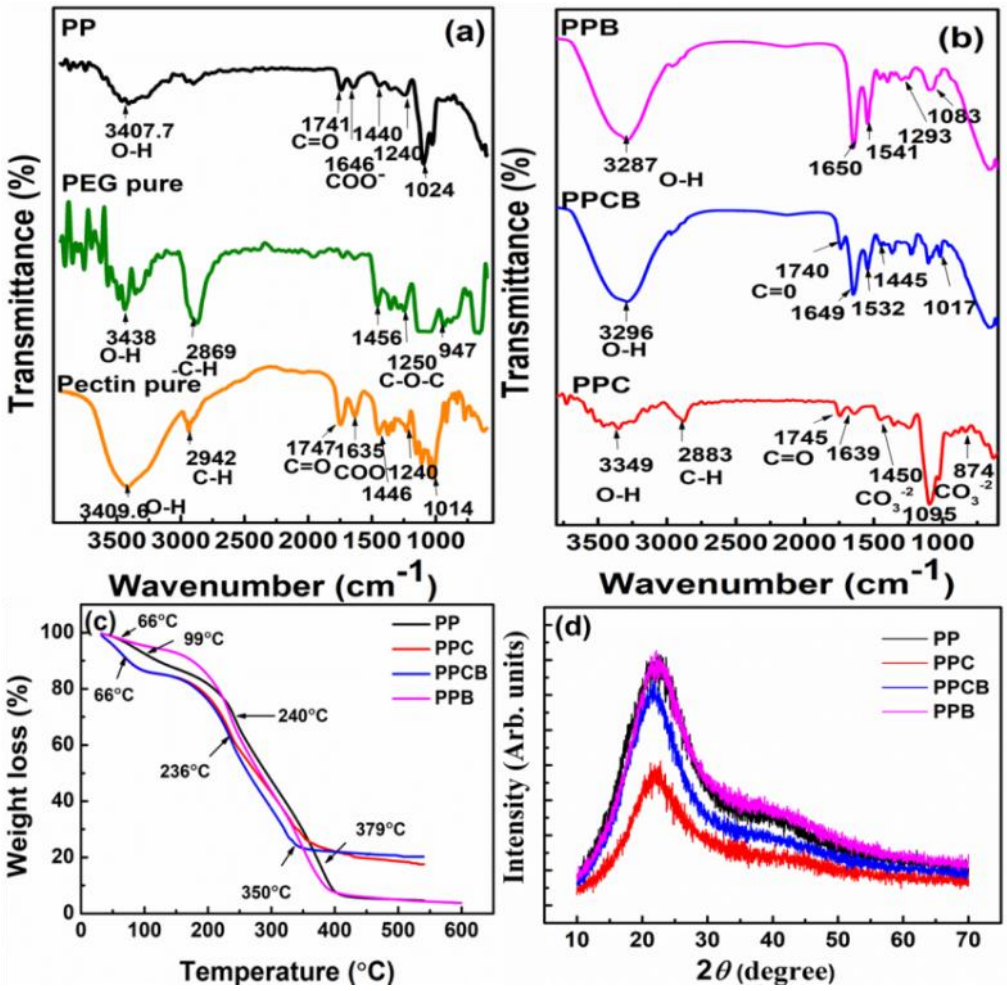

Fig. 5.3: (a) and (b) FTIR spectra, (c) Thermogravimetric analysis and (d) XRD patterns of various pectin based hydrogels

The FTIR spectra of PPB, PPC and PPCB are depicted in Fig. 5.3(b). In the case of PPB and PPCB, the observed broad peak at 3287 cm^{-1} and 3296 cm^{-1} are not only due to –OH stretching of the pectin and PEG molecules but also refers to asymmetric – NH_2 stretching of BSA molecules. Similarly, a sharp peak observed at 1650 cm^{-1} might be an overlapping peak due to esterified -C=O and asymmetric $-COO^-$ stretching of pectin as well as due to –C=O stretching of secondary amide groups (amide I) of BSA.

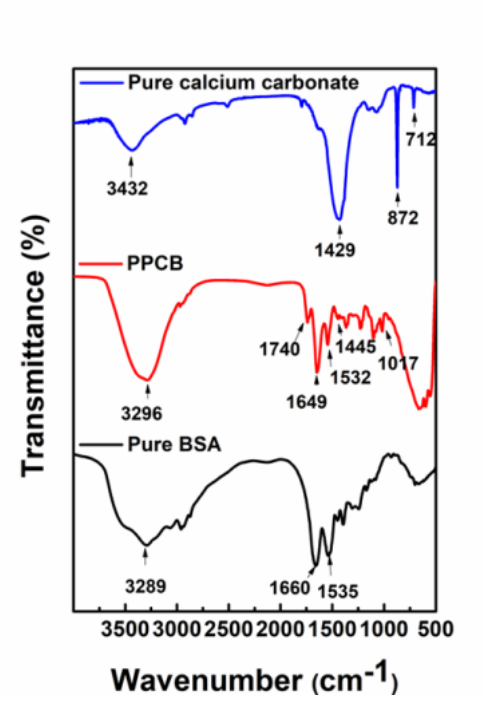

Fig. 5.4: FTIR spectra of Pure BSA, PPCB and pure $CaCO_3$

The unique peak appeared at 1541 cm^{-1} is due to bending vibrations of the N—H bond (amide II) of BSA and evidencing the presence of BSA content in the hydrogels PPB and PPCB. It is to be highlighted that in the case of PP, the peak observed at 1741 cm^{-1} (Fig. 5.3(a)) due to esterified -C=O of pectin, has disappeared in PPB. The

observation confirmed the covalent interaction between BSA and pectin and the participation of the BSA molecule throughout the PPB hydrogel matrix.[28] On the other hand, esterified -C=O of pectin peak 1741 cm^{-1} reappeared in PPCB. Further, it is to be noted that in PPB and PPCB the amide I and amide II bands due to BSA were shifted and appeared at lower wavenumbers (PPB: 1650 cm^{-1} and 1541 cm^{-1} and PPCB: 1649 cm^{-1} and 1532 cm^{-1}) compared to pure BSA (Fig. 5.4) (1660 cm^{-1} and 1535 cm^{-1}). These observations indicate only physical interactions in the hydrogel matrix. Interestingly, in the case of hydrogels PPC and PPCB Fig. 5.3(b), the appearance of the new weak shoulders at 1740 cm^{-1}, 1445 cm^{-1} and 874 cm^{-1} compared to the FTIR spectra of PP and PPB hydrogels, confirmed the formation of inorganic carbonate molecules.[29-31] The FTIR spectrum of pure calcium carbonate is shown in (Fig. 5.4). The appearance of esterified -C=O of pectin peak in the case of PPCB reveals the interaction of BSA only with mineralized $CaCO_3$.

Thermogravimetric analysis data on various pectin based hydrogels under study were depicted in Fig. 5.3(c). In the case of the hydrogel (PP), initially, 7.42 % weight loss was observed at 99 °C due to the loss of surface water. Interestingly, after incorporation of *in-situ* $CaCO_3$ particles (PPC) and BSA (PPB) as well as both $CaCO_3$ and BSA (PPCB), 8 % weight loss was detected for PPC and PPCB, while only 3 % weight loss for PPB at 66 °C. Further, ~30 % weight loss for PP and PPB while 40 % weight loss for PPC and PPCB at around 240 °C was observed due to depolymerization of pectin chains. The maximum weight loss was observed as 85 % and 78% for the sample PP and PPB at 379 °C and 350 °C, respectively. The reported final weight loss of PP and PPB was approximately 95 % at 540 °C indicated the existence of 4 % non-degradable contents. Interestingly, in the case of PPC and

PPCB, the maximum weight loss was observed as 83 % and 80 %, respectively, which indicated the existence of 17 % and 20 % non-degradable residue. The reported higher residual content of PPC and PPCB as compare to PP and PPB at 540 °C was due to the existence of inorganic $CaCO_3$ particles into the hydrogel matrix.

As prepared pectin based hydrogel blends (PP, PPC, PPCB, and PPB) were subjected to XRD analysis and results were displayed in Fig. 5.3(d). It was observed that the XRD pattern of the various hydrogels understudy was similar. Only a broad peak at 2θ degree values ranging from 15° to 30° was observed in the diffraction pattern of the hydrogels. The observed broad peak might be due to the glass substrate used during the XRD measurement. It is clear from the XRD data that $CaCO_3$ was present as amorphous within the pectin/ PEG hydrogel blend.

5.3.2. Morphological observation

Hydrogel blend PP possessed (Fig. 5.5(a)) rough morphology. On the other hand, the SEM picture of PPB (Fig. 5.5(d)) showed relatively smooth morphology compared to PP. Interestingly, the morphology of hydrogels PPC (Fig. 5.3(b)) and PPCB (Fig. 5.5(c)) indicated the presence of micro-sized particles. EDX (inset of Fig. 5.5(b)) analysis of the particles confirmed the existence of calcium in the particles. Once again, the existence of $CaCO_3$ particles was confirmed to be present in the hydrogel blend PPC with a particle size of 200 nm as determined by TEM micrographs (Fig. 5.6(a) and 5.6(b)). TEM SAED pattern (inset Fig. 5.6(a)) confirmed the amorphous nature of $CaCO_3$ particles, as indicated by XRD (Fig. 5.3(d)). Further, in the presence of BSA in PPCB, (Fig. 5.6(b) and 5.6(c)), the size of $CaCO_3$ particles was noticed to increase from 200 nm to 400 nm, which might be due to the accumulation of BSA molecules around the calcium-based particles as clearly displayed in Fig. 5.6(d).

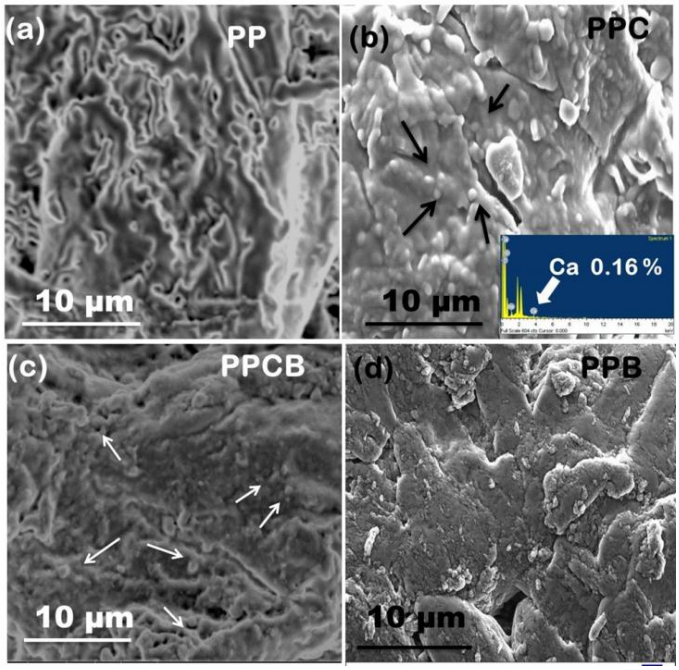

Fig. 5.5: SEM micrographs of various pectin based hydrogels (a) PP (mag 10000) (b) PPC inset shows EDX for Ca (mag 10000) (c) PPCB (mag 10000) (d) PPB (mag 10000)

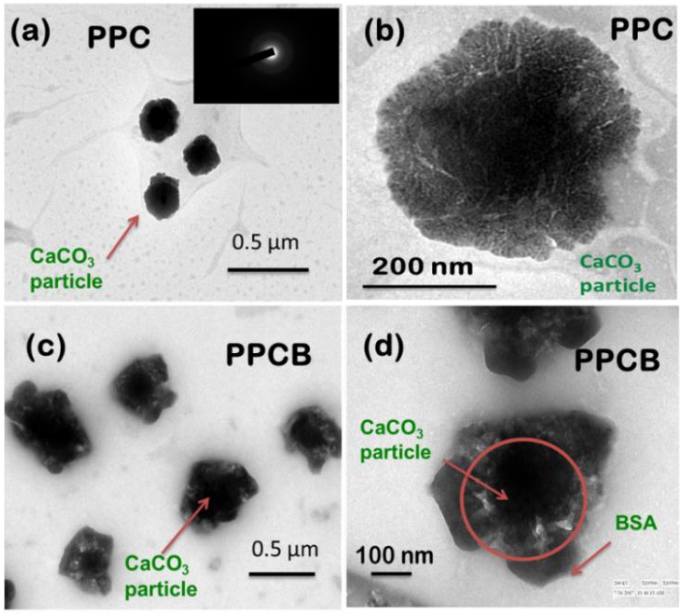

Fig. 5.6: TEM images (a) PPC (inset shows SAED pattern), (b) and (c) magnified TEM image of a single $CaCO_3$ particle and PPCB respectively, (d) $CaCO_3$ particle surrounded by BSA

5.3.3. Particle size analysis

$CaCO_3$ particle size distribution analysis was carried out on PPC and PPCB hydrogels using Malvern zetasizer after careful dissolution in water. The results revealed that PPC and PPCB consisted of monodispersed $CaCO_3$ particles of Z average (d. nm) 321 nm and 420 nm, respectively (Fig. 5.7 and Fig. 5.8).

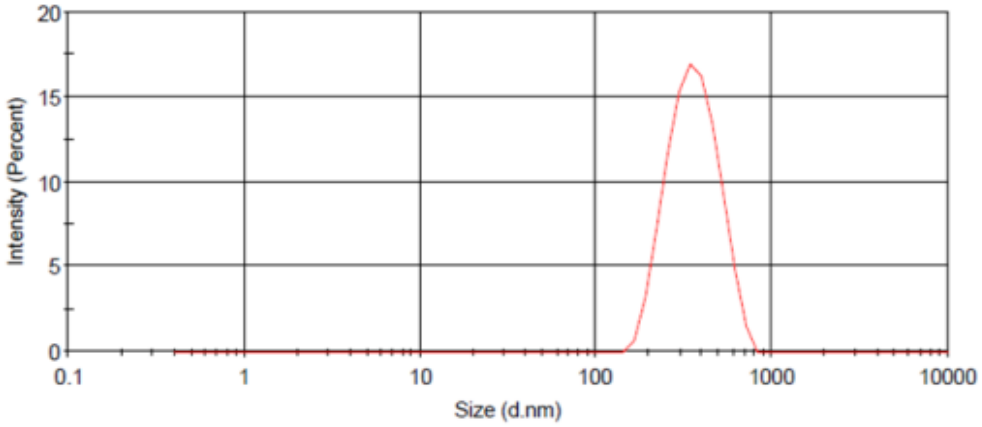

Fig. 5.7: Particle size distribution of $CaCO_3$ in PPC hydrogel with Z-average (d.nm) 321 nm

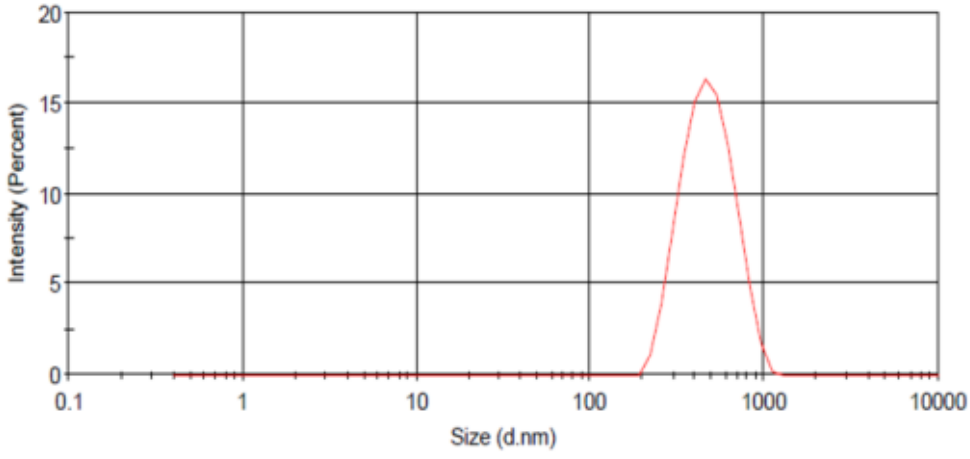

Fig. 5.8: Particle size distribution of $CaCO_3$ in PPCB hydrogel with Z-average (d.nm) 420 nm

The Z average particle size of $CaCO_3$ in PPC and PPCB was of hydrodynamic radius and not comparable with TEM analysis (Fig. 5.6(b) and 5.6(d)), where $CaCO_3$ particle sizes were observed to be 200 nm in PPC and 400 nm in PPCB.

5.3.4. Rheological studies

5.3.4.1 Gelling temperature

Fig. 5.9(a) to 5.9(d) showed the temperature dependence of the storage modulus G′ and the loss modulus G″ for the PP, PPC, PPCB and PPB at a frequency of 1 Hz. In the case of PP (Fig. 5.9(a)), the gelling temperature was reported at 57 °C. In the first region of G′-G″ crossover (below 57 °C), the magnitude of G′ was lower than G″ and decreased as the temperature increased indicating the common viscoelastic behaviour of liquid due to the presence of surrounding water content of the hydrogel.

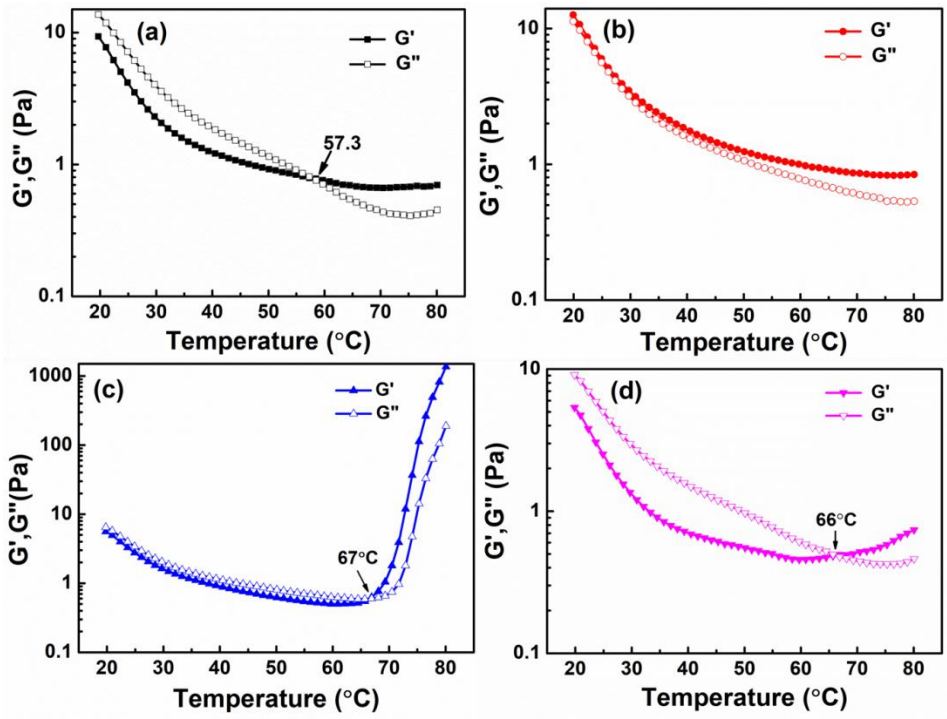

Fig. 5.9: Gel temperature of the hydrogel samples (a) PP, (b) PPC, (c) PPCB and (d) PPB

On the other hand, a slight increase in G′ and decrease in G″ was observed in the second region (above 57 °C) indicated an elastic gel network was formed between pectin and PEG molecules. The observed network formation is due to the removal of surrounding water molecules, which increases intermolecular hydrogen bonding by enhancing the polymer molecular association.[32] In the case of PPCB and PPB, gelation temperature was observed at 67 °C and 66 °C, respectively, with similar features as PP. It is noteworthy that the incorporation of BSA molecules increased the gelling temperature of PPB and PPCB due to the interaction of BSA molecules with pectin in addition to pectin– PEG interaction, as evidenced by FTIR (Fig. 5.3(a) 5.3(b). Whereas, in the case of PPC, there was no clear cut crossover between G′ and G″ indicating the existence of semisolid like structure, which might be due to the formation of $CaCO_3$ particles, which was expected to hinder polymer molecular associations and hence gelation.[32-34]

5.3.4.2. Small amplitude oscillatory shear

In general, the observed graph pattern of viscosity as a function of shear rate indicated (Fig. 5.10(a)) shear thinning behaviour of hydrogels (PP, PPC, PPCB, and PPB) with pseudo-plastic character.[35] Herein, PPC yielded very high viscosity confirms the hindrance in the formation of pectin- PEG association within the system due to the presence of $CaCO_3$ particles. Interestingly, PPCB overcame such hindrance in pectin-PEG association due to the presence of BSA molecules compared to PPC. It is also noteworthy that for the hydrogel systems PP and PPB, viscosity as a function of shear rate was reported to be the lowest indicating tight molecular associations.[36] The frequency sweep tests conducted on the pectin based hydrogels using oscillatory shear were portrayed in Fig. 5.10(b) to 5.10(d). As shown in Fig. 5.10(b) and 5.10(c), in

general, both elastic (storage) and viscous modulus (loss) of PP and PPB were observed to be greater than PPC and PPCB systems.

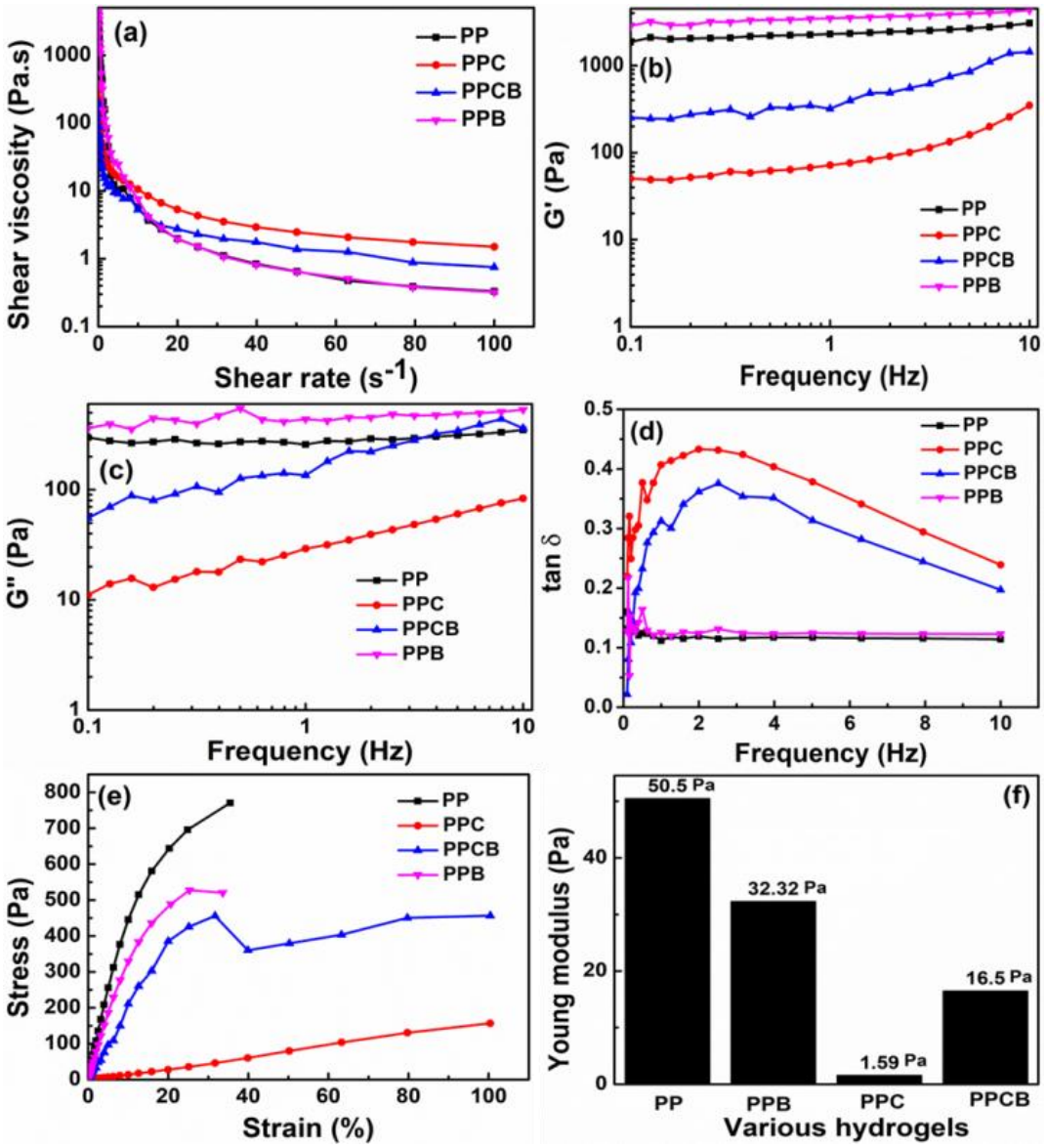

Fig. 5.10: (a) Viscosity variation (b) G′, (c) G″, (d) tan δ (e) strain sweep at 1 Hz and (f) young modulus of various hydrogels by rheological studies

In addition, the elastic and viscous modulus of PP and PPB were not sensitive to change from the low-frequency to the high-frequency region once again confirm the

close association of the polymer molecules. On the other hand, in the case of PPC and PPCB, strong frequency dependence of both G′ and G″ were observed with increasing vibrational frequency evidencing a tangled network system supported by a weak network system. From the loss factor (tan δ = G″/G′) illustrated in Fig. 5.10(d)), an increase of tan δ is evidenced for PPC and PPCB at lower frequency range (0 to 3 Hz), indicating the viscoelastic nature of the materials. The observation implies that at lower frequency range, the polymer network has sufficient time to reorganize and results in an increase of tan δ.

In contrast, at higher frequencies (>3Hz), the decrease in loss factor indicates, a lack of time for the required rearrangement of the polymer and results in the material stiffening. The observed interesting rheological behaviour in PPC and PPCB elucidated the dynamic nature of the hydrogel.[37] The reported dynamic nature of the hydrogel can help to predict spreading and covering properties at the target site to release BSA.[38-39] On the other hand, the loss tangent of PP and PPB showed independent behaviour with increasing frequency.

The stress-strain curves of various hydrogel blends obtained at 1 Hz were displayed in Fig. 5.10(e). The shape of stress-strain curves of PP and PPB indicate their hard and strong category due to strong non-covalent interactions. Whereas, the stress-strain curve of PPC shows the soft nature of the hydrogel, indicating disruptions of polymer network system due to the presence of $CaCO_3$ particles. Interestingly, the stress-strain behaviour of PPCB shows relatively hard and tough behaviour compared to PPC and also regains the polymer network formation due to the presence of BSA. Changes in Young's modulus (Fig. 5.10(f)) of the corresponding stress-strain curves further confirm the above observations.

5.3.5. Swelling studies on various hydrogels

In this investigation, *in-vitro* swelling experiments were carried out at different pH conditions mimicking those of the stomach (using SGF pH 1.2), intestine (using SIF, pH 6.0) and of the colon (using SIF pH 6.8) and results were shown in Fig. 5.11(a) and 5.11(b). Interestingly, the observed swelling ratio of the hydrogels (PP, PPB, PPC, and PPCB) was found to be below 50 % up to 3 h in SGF at pH 1.2 (Fig. 5.11(a)). This could be attributed to the protonation of $–COO^-$ group on pectin molecule as -COOH, leading to the close association of the polymer molecules.[22,23,40] On the other hand, when hydrogel samples were placed into the SIF solution at pH 6.0, it is noteworthy that the swelling of hydrogels was taking place. In general, the observed swelling in SIF solution was due to the deprotonation of -COOH group on pectin, leading to the charge repulsion resulting in the dissociation of the polymer molecules. Interestingly, among all hydrogels understudy, PPB showed the highest swelling ratio (130 % to 148 %) and the lowest swelling ratio was observed for the hydrogel PPC (87 %) and PPCB (89 %). It is pertinent to recall that the zeta potential of BSA above pH 5.0 is negative.[41,42] Hence, the highest negative charge density on PPB (data not shown) compared to other hydrogel samples led to its highest swelling (130 % to 148 %). The lowest swelling ratio of PPC indicated partial neutralization of negative charges of PP by positively charged $CaCO_3$ particles at pH 6.0. Herein, the isoelectric point of $CaCO_3$ is around pH 7.0.[43] It is also noteworthy that PPCB showed comparatively almost similar swelling ratio as PPC up to 6 h. It is worth recalling that after the 6^{th} hour the hydrogel samples were carefully taken out, washed with SIF solution at pH 6.8 and continued for swelling studies for another 3 h. Interestingly, allhydrogel samples were started degrading in SIF at pH 6.8, indicating instability of

the hydrogel matrix due to higher anion-anion charge repulsion at pH 6.8 (Fig. 5.11(a)).

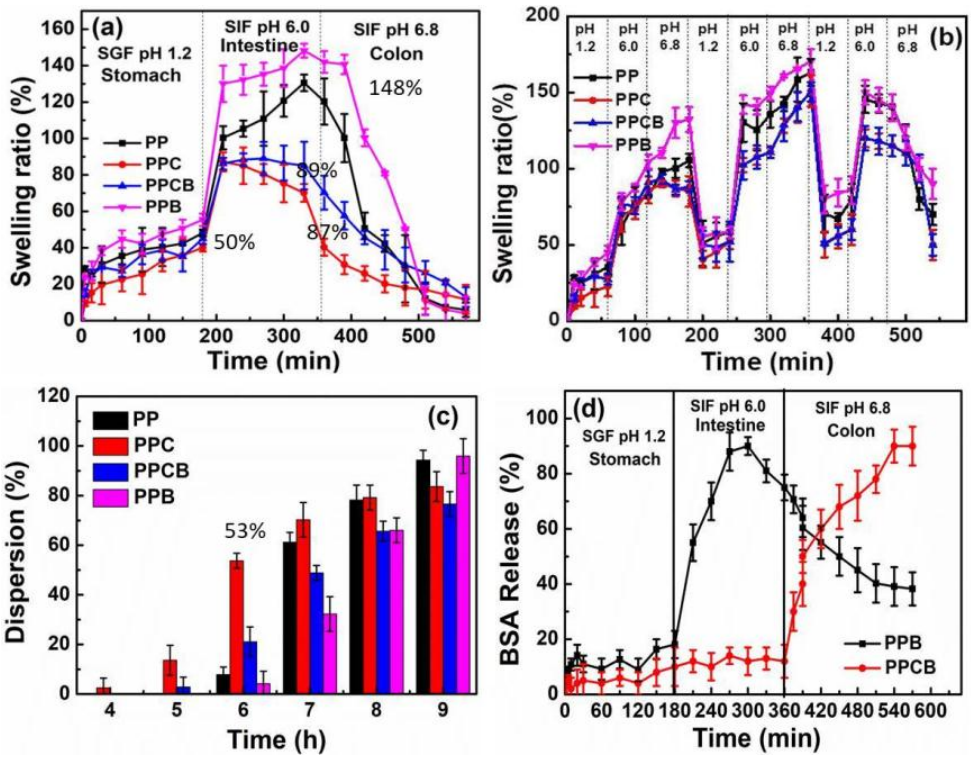

Fig. 5.11: (a) Swelling ratio as a function of time,(b) switch on- off swelling as a function of time, (c) Dispersion behaviour of the hydrogel samples and (d) BSA release of various hydrogels in SGF at pH 1.2, SIF at pH 6.0 and SIF at pH 6.8

In order to test swelling as well as the deswelling behavior of hydrogel blend, the samples were initially dipped in SGF at pH 1.2 for an hour, after that the samples were continued to swell in SIF at pH 6.0 up to 2 h, finally in SIF at pH 6.8 for 3 h. The similar procedure was repeated up to the 9th h and results were portrayed in Fig. 5.11(b). The feeble swelling of the hydrogel samples was observed up to 1 h at pH 1.2 and the deswelling of the hydrogel samples were noticed after 4 h as well as at the 7th h of the experiment. At pH 6.0 and pH 6.8, swelling behaviour of the hydrogels was as similar as observed in Fig. 5.11(b). Here again, the sample dispersion was noticed

after 8 h in SIF at pH 6.8. The purpose of this swelling de-swelling was to understand the function of the hydrogel in the controlled release of the protein at various pH conditions of the stomach, small intestine and colon and their behaviour with time.[22,40]

5.3.6. *In-vitro* hydrogel dispersion studies

The dispersion results (Fig. 5.11(c)) of the hydrogels under investigation showed integrity up to 5 h. At 6 h, the dispersion of PPC was noticed as 53 %, whereas, in other hydrogels, very slight dispersion was noticed. On the other hand, after 6 h dispersion of hydrogels PP, PPCB and PPB were observed to increase drastically up to 9 h along with PPC (PP: 7 % to 94 %, PPCB: 21 % to 76 %, PPB: 4 % to 95 %, PPC: 53 % to 83 %). It is noteworthy that the disappearance of the samples was visualized at 9 h. This proved that the hydrogels were dispersed completely and suitable for oral delivery applications.

5.3.7. BSA release profile

The BSA encapsulation efficiency of the hydrogels PPB and PPCB were determined as 98.2 % and 97.6 %, respectively and BSA release profiles were determined based on the observed encapsulation efficiency. Initially, BSA release profile from the hydrogels PPB and PPCB was investigated in SGF at pH 1.2 for 3 h. The protein release (Fig. 5.11(d)) was observed to be feeble for the initial 3 h from PPB and PPCB likely due to the lowest swelling of hydrogels at acidic pH 1.2, as observed in the swelling studies (Fig. 5.11(a)). After 3 h, the hydrogel samples were transferred to SIF at pH 6.0 and BSA release was monitored from 3 h to 6 h. Similarly, BSA release studies were continued in SIF at pH 6.8 for another 3 h. Interestingly, BSA burst release detected from the hydrogel PPB was 90 % in 5 h. On the other hand, the

amount of protein release was observed from PPCB was only 12 % in 5 h. It is pertinent to recall that the highest swelling percentage of PPB (Fig. 5.11(a) 130 % to 148 %) was taken place from 3 h 30 min to 5 h 30 min and at the same duration the lowest swelling ratio of PPCB was observed (86 % to 89 %), which was in line with the BSA release in SIF at pH 6.0. Interestingly, after 7 h, the release of BSA from PPB was showing a steady decline due to the burst release at pH 6.0. In contrast, the protein release from PPCB after 6 h increased gradually and reached the maximum to 90 % in 9 h, indicating the controlled release of BSA at pH 6.8. Herein, it is important to highlight that the observed highest release of BSA after 9 h was due to the interaction of loaded BSA with the $CaCO_3$ particles. It is evident from the observed *in-vitro* BSA release result that the hydrogel PPCB can be promising drug carrier for controlled release of protein selectively at the colon site compare to PPB, which released protein in a burst release mode at the intestinal pH 6.0.

5.3.8. Conformational Stability analysis of BSA

The released BSA from hydrogel PPB (Fig. 5.12(a)) and PPCB (Fig. 5.12(b)) was subjected to SDS-PAGE analysis in order to investigate the loaded protein structural integrity. It is noteworthy that, BSA released for 4 h from PPB (L3) indicated degradation in the protein structure compared to the control (L2) and might be attributed to the unfavorable conditions of SGF as well as SIF. On the other hand, the primary structure of released BSA was retained (L4 and L5) after 4 h due to the mild pH conditions (pH 6.0 and pH 6.8). Interestingly, the protein release was not observed up to 6 h (L2 to L4) and it was noticed only at 9 h (L5) from PPCB. The absence of protein bands from L2 to L4 might be due to the feeble protein content. Importantly, the released protein drug at 9 h (L5) was noticed to retain its primary structure

compared to the control (L2) (Fig. 5.12(a)). Further, the CD signatures of released BSA (200-250 nm) and (250-350 nm) were retained up to 9 h from PPCB in comparison with control (Fig. 5.12(c) & 5.12(d)), suggesting that hydrogels preserved the secondary as well as tertiary structure of BSA during the loading as well as release process.

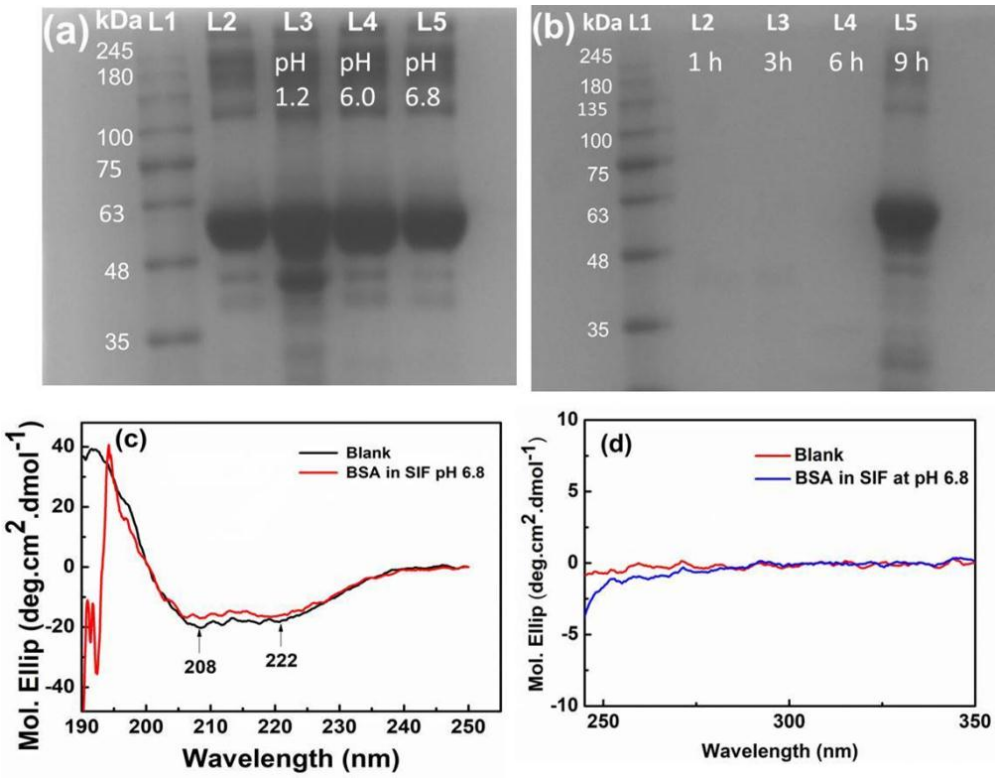

Fig. 5.12: SDS-PAGE Analysis on the released BSA from (a) PPB (L2 : Blank, L3: in SGF pH 1.2, L4: SIF pH 6.0 and L5: SIF pH 6.8) and (b) PPCB (L2 and L3 SGF at 1h and 3 h, respectively, L4: SIF at pH 6.0 for 6 h and L5: SIF pH 6.8 for 9 h), Circular Dichroism spectra of blank and released BSA from PPCB in SIF at pH 6.8 (c) far UV and (d) near UV

5.3.9. Hydrogel Fabrication Mechanism

A schematic diagram indicating the fabrication mechanism of the pectin/ PEG-based hydrogel blends is shown in Fig. 5.13(a) to 5.13(c). The hydrogel samples (PP, PPC, PPCB, and PPB) were fabricated approximately at neutral pH. It is relevant to recall

that the pKa value of pectin is 3.5.[44] Hence, at pH 7.0, pectin is negatively charged. As per FTIR studies (Fig. 5.3(a) and 5.3(b)), the interaction between pectin and PEG is possible only through inter as well as intramolecular physical forces (Fig. 5.13(a)).

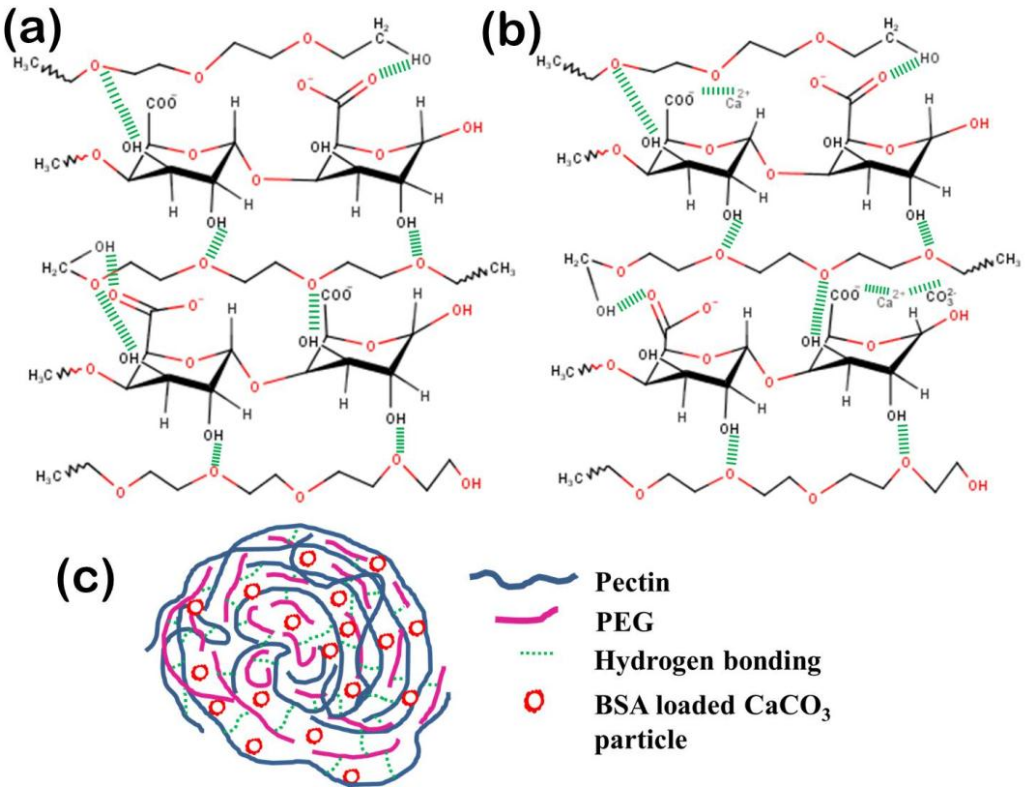

Fig. 5.13: A schematic diagram indicating fabrication mechanism of PP, PPC and PPCB hydrogel blend

The added BSA molecules interacted with pectin/PEG blend through covalent interaction with pectin and participated throughout the PPB hydrogel matrix. During the fabrication of PPC, incorporated calcium ions can be electrostatically attracted towards negatively charged $–COO^-$ group of pectin or occupied the voids of the polymer blend. Consecutively, added carbonate ions can also electrostatically interact with calcium ions already present in the blend and lead to the mineralization of $CaCO_3$

microparticles (Fig. 5.13(b)). In the case of PPCB (Fig. 5.13(c)), the interaction of added BSA molecules were mostly with the mineralized $CaCO_3$ microparticles as confirmed by FTIR (Fig. 5.3(a) and 5.3(b)) and TEM (Fig. 5.6(g) and 5.6(h)) analysis. The preferred interaction of BSA with $CaCO_3$ in PPCB is inclined to electrostatic attraction of feebly positively charged $CaCO_3$ surface (IEP of $CaCO_3$ pH 7.5).[44,45] The interaction of loaded BSA on the mineralized $CaCO_3$ surface makes the hydrogel to release BSA in a controlled manner at the colon site (Fig. 5.11(d)).

5.4. Conclusion

In summary, we have successfully fabricated BSA containing *in-situ* $CaCO_3$ mineralized pectin based novel pectin/ PEG hydrogel blend (PPCB). FTIR spectra of the hydrogel samples revealed the pectin/ PEG molecular interaction was through hydrogen bonding. TEM micrographs of the obtained hydrogel exhibited accumulation of loaded BSA molecules, around the mineralized $CaCO_3$ microparticles. *In-vitro* BSA release studies showed that the presence of micro-particles throughout the hydrogel matrix not only protected BSA but also released it in a controlled manner at the colon site. Rheological studies by frequency sweep of as prepared hydrogel before as well as after BSA loading showed dynamic nature. The observed interesting dynamic property of the hydrogel PPCB is expected to promote spreading and covering of the vehicle at the colon site. Herein, *In-vitro* protein drug release experiments were successfully demonstrated the release of the model drug BSA at the colon site and were shown to retain its conformational stability up to 9 h.

References

[1] A.M. Hillery, A.W. Lloyd, J. Swarbrick, Drug delivery and targeting for pharmacists and pharmaceutical. In Vincent H.L., Lee Johnny and J. Yang (Eds.). Oral drug delivery, New York: Taylor & Francis e-Library, 2005, pp. 131-167.

[2] L.M. Ensign, R. Cone, J. Hanes, Oral drug delivery with polymeric nanoparticles: the gastrointestinal mucus barriers, Adv. Drug Deliv. Rev. 64 (2012) 557-570.

[3] H. Chen, R. Langer, Oral particulate delivery: status and future trends, Adv. Drug Deliv. Rev. 34 (1998) 339-350.

[4] H.A.D. Lagasse, A. Alexaki, V.L. Simhadri, N.H. Katagiri, W. Jankowski, Z.E. Sauna, C.K. Sarfaty, Recent advances in (therapeutic protein) drug development, F1000 Res. 6 (2017) 113-117.

[5] S. Frokjaer, D.D. Otzen, Protein drug stability: a formulation challenge, Nat. Rev. Drug Disc. 4 (2005) 298-306.

[6] L. Benjamin, J.B. Quentin, D.E. Golan, Protein therapeutics: a summary and pharmacological classification, Nat. Rev. Drug Disc. 7 (2008) 21-39.

[7] M. Mariko, A.P. Nicholas, Is the oral route possible for peptide and protein drug delivery? Drug Discov. Today 11 (2006) 905-910.

[8] S. Rick, Oral protein and peptide drug delivery. In: W. Binghe, S. Teruna, S. Richard, editors. Drug delivery: principles and applications, New Jersey: Wiley Interscience, 2006, pp. 189.

[9] G. Michael, I.G. Orellana, Challenges for the oral delivery of macromolecules, Nat. Rev. Drug Disc. 2 (2003) 289-295.

[10] V. Tina, C. Roberta, E.H. Wim, Hydrogels for protein delivery, Chem. Rev. 112 (2012) 2853-2888.

[11] R. Singh, S. Singh, L.W James, Past, present, and future technologies for oral delivery of therapeutic proteins, J. Pharm. Sci. 97 (2008) 2497-2523.

[12] S.K.H. Gulrez, S.A. Assaf, G.O. Phillips, Hydrogels: methods of preparation, characterisation and applications: progress in molecular and environmental bioengineering-from analysis and modelling to technology applications, Rijeka: In Tech, 2011, pp. 117-151.

[13] V.R. Sinha, R. Kumria, Polysaccharides in colon-specific drug delivery, Int. J. Pharm. 224 (2001) 19-38.

[14] T.F. Vandamme, A. Lenourry, C. Charrueau, J.C. Chaumeil, The use of polysaccharides to target drugs to the colon, Carbohydr. Polym. 48 (2002) 219-231.

[15] J.A. Fix, Oral controlled release technology for peptides: status and future prospects, Pharm. Res. 13 (1996) 1760-1763.

[16] A. Noreen, Z.I.H. Nazli, J. Akram, I. Rasul, A. Mansha, N. Yaqoob, R. Iqbal, S. Tabasum, M. Zuber, K.M. Zia, Pectins functionalized biomaterials; a new viable approach for biomedical applications: a review, Int. J. Biol. Macromol. 101 (2017) 254-272.

[17] L.L. Shu, M.L. Fishmana, K. Joseph, B.H. Kevin, Pectin-based systems for colon-specific drug delivery via oral route, Biomaterials 24 (2003) 3333-3343.

[18] F. Munarin, M.C. Tanzi, P. Petrini, Advances in biomedical applications of pectin gels, Int. J. Biol. Macromol. 51 (2012) 681-689.

[19] P. Sriamornsak, Investigation of pectin as a carrier for oral delivery of proteins using calcium pectinate gel beads, Int. J. Pharm. 169 (1998) 213-220.

[20] N. Bhattarai, H.R. Ramay, J. Gunn, PEG-grafted chitosan as an injectable thermosensitive hydrogel for sustain protein release, J. Control. Release 103 (2005) 609-624.

[21] A.R. Hibbins, P. Kumar, Y.E. Choonara, P.P.D. Kondiah, T. Marimuthu, L.C.D. Toit, V. Pillay, Design of a versatile pH-responsive hydrogel for potential oral delivery of gastric-sensitive bioactives, Polymers 9 (2017) 474-492.

[22] N. Ahmad, M.C.I.M. Amin, S.M. Mahali, I. Ismail, V.T.G. Chuang, Biocompatible and mucoadhesive bacterial cellulose-g-poly (acrylic acid) hydrogels for oral protein delivery, Mol. Pharm. 11 (2014) 4130-4142.

[23] C.H. Chang, Y.H. Lin, C.L. Yeh, Y.C. Chen, S.F. Chiou, Y.M. Hsu, Y.S. Chen, C.C. Wang, Nanoparticles incorporated in pH-sensitive hydrogels as amoxicillin delivery for eradication of helicobacter pylori, Biomacromolecules 11 (2010) 133-142.

[24] E. Teodor, S.C. Litescu, C. Petcu, M. Mihalache, R. Somoghi, Nanostructured biomaterials with controlled properties synthesis and characterization, Nanoscale Res. Lett. 4 (2009) 544-549.

[25] K. Varaprasad, G.M. Raghavendra, T. Jayaramudu, M.M. Yallapu, R. Sadiku, A mini review on hydrogels classification and recent developments in miscellaneous applications, Mater. Sci. Eng. C 79 (2017) 958–971.

[26] S. Seslija, A. Nesic, J. Ruzic, M.K. Krusic, S. Velickovic, R. Avolio, G. Santagata, M. Malinconico, Edible blend films of pectin and poly(ethylene

glycol): preparation and physico-chemical evaluation, Food Hydrocoll. 77 (2018) 494-501.

[27] S.Y. Chan, W.S. Choo, D.J. Young, X.J. Loh, Thixotropic supramolecular pectin-poly (ethylene glycol) methacrylate (PEGMA) hydrogels, Polymers 8 (2016) 404-416.

[28] H. Peng, S. Chen, M. Luo, N. Fangjian, X. Zhu, H. Xiong, Preparation and self-assembly mechanism of bovine serum albumin-citrus peel conjugated hydrogel: a potential delivery system for vitamin C, J. Agric. Food Chem. 64 (2016) 7377-7384.

[29] C. Wang, P. Xiao, J. Zhao, X. Zhao, Y. Liu, Z. Wang, Biomimetic synthesis of hydrophobic $CaCO_3$ nanoparticles via a carbonation route, Powder Technol. 170 (2006) 31-35.

[30] M. Xie, M. Olderoy, J.P. Andreassen, S.M. Selbach, B. L. Strand, P. Sikorski, Alginate-controlled formation of nanoscale $CaCO_3$ and hydroxyapatite mineral phase within hydrogel networks, Acta Biomater. 6 (2010) 3665-3675.

[31] W. Fang, H. Zhang, J. Yin, B. Yang, Y. Zhang, J. Li, F. Yao, Hydroxyapatite crystal formation in the presence of polysaccharide, Cryst. Growth Des. 16 (2016) 1247-1255.

[32] Y. F. Tang, Y. M. Du, X. W. Hu, X. W. Shi, J. F. Kennedy, Rheological characterisation of a novel thermosensitive chitosan/poly(vinyl alcohol) blend hydrogel, Carbohydr. Polym. 67 (2007) 491-499.

[33] C. Lofgren, P. Walkenstro, A. M. Hermansson, Microstructure and rheological behavior of pure and mixed pectin gels, Biomacromolecules 3 (2002**)** 1144-1153.

[34] H. R. Moreira, F. Munarin, R. Gentilini, L. Visai, P. L. Granja, M. C. Tanzi, P. Petrini, Injectable pectin hydrogels produced by internal gelation: pH dependence of gelling and rheological properties, Carbohydr. Polym. 103 (2014) 339-347.

[35] X. Hua, K.Wang, R. Yang, J. Kang, J. Zhang, Rheological properties of natural low-methoxyl pectin extracted from sunflower head, Food Hydrocoll. 44 (2015) 122-128.

[36] G.P. Andrews, D.S. Jones, Rheological characterization of bioadhesive binary polymeric systems designed as platforms for drug delivery implants, Biomacromolecules 7 (2006) 899-906.

[37] A. Gantar, N. Drnovsek, P. Casuso, A.P.S. Vicente, J. Rodriguez, D. Dupin, S. Novak, I. Loinaz, Injectable and self-healing dynamic hydrogel containing bioactive glass nanoparticles as a potential biomaterial for bone regeneration, RSC Adv. 6 (2016) 69156-69166.

[38] M. Ozyazıcı, M. Fırlak, S.T. Tanrıverdı, S. Rençber, S.Y. Karavana and M.V. Kahraman, Bioadhesive gel and hydrogel systems for buccal delivery of ketoprofen: preparation and *In vitro* evaluation studies, Am. J. Drug Deliv. Ther. 2 (2015) 078-091.

[39] Q. Chai, Y. Jiao and X. Yu, Hydrogels for biomedical applications: their characteristics and the mechanisms behind them, Gels 3 (2017) 6.

[40] M. Sadeghi, Pectin-based biodegradable hydrogels with potential biomedical applications as drug delivery systems, J. Biomater. Nanobiotechnol. 2 (2011) 36-40.

[41] S. Salgin, U. Salgin, S. Bahadir, Zeta potential and isoelectric point of biomolecules: the effect of ion type and types of ionic strengths, Int. J. Electrochem. Sci. 7 (2012) 12404-12414.

[42] H.T.M. Phan, S. Bartelt- Hunt, K.B. Rodenhausen, M. Schubert, J.C. Bartz, Investigation of bovine serum albumin (BSA) attachment onto self-assembled monolayers (SAMs) using combinational quartz crystal microbalance with dissipation (QCM-D) and spectroscopic ellipsometry (SE), PLOS ONE 10 (2015) e0141282.

[43] A.M. Silva, F.L.S. Cruz, R.M.F. Lima, M.C. Teixeira, V.A. Leao, Manganese and limestone interactions during mine water treatment, J. Hazardous Mater. 181 (2010) 514-520.

[44] P. Opanasopit, A. Apirakaramwong, T. Ngawhirunpat, T. Rojanarata, U. Ruktanonchai, Development and characterization of pectinate micro/nanoparticles for gene delivery, AAPS Pharm. Sci. Tech. 9 (2008) 67-74.

[45] J. Plank, G. Bassioni, Adsorption of carboxylate anions on a $CaCO_3$ surface, Z. Naturforschung 62 (2007) 1277-1284.

Future work

- Calcium based oral drug carriers are being proven as an efficient delivery systems and hence much work has to be done with more efforts to meet current challenges.
- Despite several challenges in the fabrication of targeted calcium based oral carriers; they have much more potential to reach the market with probabilities of improved outcomes as they are likely to face fewer regulatory hurdles in comparison to newly designed organic or inorganic materials.
- In future calcium based oral carriers will be having much more advance applications in medicine comparison to any other delivery system due to their cost effectiveness, biodegradability and ability to encapsulate various kinds of molecules like proteins, dyes, drugs and oligonucleotides.
- Polymer based edible coating over calcium based carriers shows their high potential functionality by protecting them against the loss of nutrients that will not only enhances their usefulness by upgrading the physical stability in *in-vivo* system but also increases their encapsulation efficiency.
- The practicability of designing dosage forms that are acceptable to humans and efficacious needs for calcium based drug carriers to be further explored in *in-vivo* systems.

LIST OF PUBLICATIONS

- **Meenakshi Gautam** and Deenan Santhiya, Pectin/PEG food grade hydrogel blend for the targeted oral co-delivery of nutrients, **Colloids and Surface A: physicochemical and engineering aspects, (SCI indexed) 577 (2019) 637-644. (Impact factor: 3.99)**
- **Meenakshi Gautam** and Deenan Santhiya, *In-situ* mineralization of calcium carbonate in pectin based edible hydrogel for the delivery of protein at colon, **Journal of drug delivery science and technology, (SCI indexed) 53 (2019) 101137 (Impact factor: 2.73)**
- **Meenakshi Gautam,** Deenan Santhiya and Namit Dey, Zein coated calcium carbonate nanoparticles for the targeted controlled release of model antibiotic and nutrient across the intestine, **Material Today Communication, (SCI indexed) 25 (2020) 101394 (Impact factor: 2.67)**

Conferences Proceedings

- **Meenakshi Gautam**, Deenan Santhiya, Different Template Based $CaCO_3$ nanoparticles, **International conference** on technologically advanced Materials & Asian Meeting on Ferroelectricity, held at University of Delhi, India during 7-11 Nov 2016.
- **Meenakshi Gautam**, Deenan Santhiya**,** *In situ* Mineralization of $CaCO_3$ nanoparticles in Pectin Based Hydrogel System for Oral Drug Delivery Applications, **International conference** on Advance in polymer Science &Technology, Organized by Indian Institure of Technology, Delhi, India during 23-25 Nov 2017.

- **Meenakshi Gautam**, Deenan Santhiya**,** Rheological Studies on Pectin Based Edible Hydrogels for Oral Delivery, **International conference** of nanotechnology: ideas, Innovation and initiatives-2017, held at Indian Institute of Technology, Roorkee, india during 06-08 December 2017.
- **Meenakshi Gautam**, Deenan Santhiya, Pectin Based edible hydrogel for Nutrient Delivery, 6th **International conference** on technical textile and nonwovens, held at Indian Institute of Technology, Delhi, India during 6-8 Dec 2018.

Annexure 1

The composition of the Simulated Gastric Fluid (SGF) and Simulated Intestinal Fluid (SIF) solutions are given below:

SGF preparation: 2 g NaCl and 3.2 g pepsin were dissolved in 500 ml distilled water then 3 ml concentrated HCl was added to it and made upto 1litre. The solution was adjusted to pH 1.2.

SIF preparation: 6.8 g monobasic potassium phosphate (KH_2PO_4) was dissolved in 650 ml of distilled water. 190 ml of 0.2 N NaOH was added. 1 g of pancreatin mixture was added to the solution. The pH of the solution was adjusted to pH 6 by adding 0.2 N NaOH. Make up the solution to the 1000 ml mark.